НАЦІОНАЛЬНА АКАДЕМІЯ НАУК УКРАЇНИ
ІНСТИТУТ ОРГАНІЧНОЇ ХІМІЇ НАН УКРАЇНИ
НАЦІОНАЛЬНИЙ ФАРМАЦЕВТИЧНИЙ УНІВЕРСИТЕТ

Рік заснування – 1966

ЖУРНАЛ ОРГАНІЧНОЇ ТА ФАРМАЦЕВТИЧНОЇ ХІМІЇ

JOURNAL OF ORGANIC AND PHARMACEUTICAL CHEMISTRY

2025 — том 23, випуск 4 (92)

Харків
НФаУ

У журналі розглянуто проблеми синтезу й аналізу органічних та елементоорганічних сполук, аналогів природних сполук і лікарських субстанцій, наведено результати фізико-хімічних досліджень у вищезазначених напрямах.

Для працівників науково-дослідних установ, вищих навчальних закладів та фахівців хімічного, фармацевтичного, біологічного, медичного і сільськогосподарського профілів.

«Журнал органічної та фармацевтичної хімії» внесено до затвердженого МОН України Переліку наукових фахових видань України (категорія «Б») для опублікування результатів дисертаційних робіт за спеціальністю 102 – Хімія та 226 – Фармація, промислова фармація (наказ МОН України від 28.12.2019 р. № 1643); індексовано в наукометричних базах даних: Chemical Abstracts (CAS), Index Copernicus; внесено до каталогів та пошукових систем: Directory of Open Access Journals (DOAJ), Bielefeld Academic Search Engine (BASE), Directory of Open Access scholarly Resources (ROAD), PKP Index, Ulrich's periodicals, Worldcat, НБУ ім. В. І. Вернадського і УРЖ «Джерело».

Затверджено до друку вченою радою Інституту органічної хімії НАН України, протокол № 1 від 05.01.2026 р.

Затверджено до друку вченою радою Національного фармацевтичного університету, протокол № 10 від 24.12.2025 р.

Адреса для листування: 61002, м. Харків, вул. Григорія Сковороди, 53, Національний фармацевтичний університет, редакція «Журналу органічної та фармацевтичної хімії». E-mail: publish@nuph.edu.ua, orgpharm-journal@nuph.edu.ua. Сайт: http://ophcj.nuph.edu.ua

Рішення Національної ради України з питань телебачення і радіомовлення № 1911 (протокол № 17 від 30.05.2024 р.) «Про заяви Національного фармацевтичного університету, м. Харків, щодо реєстрації суб'єкта у сфері друкованих медіа» (ідентифікатор медіа R30-05024)

Підписано до друку 07.01.2026 р. Формат 60 × 84 1/8.

Папір офсетний. Друк ризо. Умовн. друк. арк. 9,3. Обліков.-вид. арк. 10,76. Тираж 50 прим.

Редакторка — О. Ю. Гурко. Комп'ютерне верстання — О. М. Білинська

«Журнал органічної та фармацевтичної хімії». Том 23, випуск 4 (92), 2025

ISSN 2308-8303 (Print)

ISSN 2518-1548 (Online)

Journal of Organic and Pharmaceutical Chemistry

Original Research

OPEN ACCESS
Freely available online on
http://ophcj.nuph.edu.ua

UDC 615.074:615.28:543.42

A. S. Koptielov[1], V. I. Plyska[2], O. V. Bevz[1], O. V. Rudakova[3], N. Yu. Bevz[1], Ya. I. Studenyak[2]

[1] National University of Pharmacy of the Ministry of Health of Ukraine,
53 Hryhorii Skovoroda str., 61002 Kharkiv, Ukraine
[2] State University "Uzhhorod National University", 3 Narodna Square, 88000 Uzhhorod, Ukraine
[3] The Professional College of the National University of Pharmacy of the Ministry of Health of Ukraine,
18 Zaikivska str., 61140 Kharkiv, Ukraine

The Potentiometric Quantification of Chondroitin Sodium Sulfate Using Ion-Selective Electrodes

Abstract

Chondroitin sodium sulfate is an anionic polysaccharide widely used in pharmaceutical practice as an active ingredient of mono- and multicomponent medicinal products, and its quantitative determination is an essential stage of the quality control. It has been found that the application of potentiometric titration with ion-selective electrodes can increase the accuracy and objectivity of the quantitative analysis, which is of great importance for ensuring the quality and safety of medicines.

The aim of the study was to develop and validate a potentiometric method for the quantitative determination of chondroitin sodium sulfate in the substance and in a combined medicinal product in the form of the sachet powder.

The study objects were chondroitin sodium sulfate substance and a combined medicinal product containing chondroitin sodium sulfate in combination with D-glucosamine sodium sulfate, methylsulfonylmethane, sodium hyaluronate, ascorbic and citric acids, and sorbitol. The conditions of the potentiometric titration with 0.001 M solution of cetylpyridinium chloride were studied using an ion-selective electrode based on cetylpyridinium ionic associates with some lipophilic anions. The titrant was standardized using sodium dodecyl sulfate as a primary standard, as well as the substance itself. The equivalence point was determined from the titration curve and its mathematically processed forms (differential curve, first derivative, and Gran functions). It has been found that the plasticized membrane ion-selective electrodes based on cetylpyridinium associates with dodecyl sulfate and tetraphenylborate anions are characterized by a stable near-Nernstian response in the operating range of cetylpyridinium concentrations of 10^{-3}–10^{-6} mol L^{-1}. The analytical characteristics of the electrodes remained stable for at least 30 consecutive titrations. The selectivity of the reaction between chondroitin sodium sulfate and cetylpyridinium chloride was found, ensuring a clear determination of the equivalence point even in the presence of other mixture components. The influence of pH on the titration results was evaluated; it was shown that in the pH range of 4–8 the shape of titration curves and potential values remained constant, confirming the robustness of the method. The accuracy, precision, linearity (within 80–120 % of the nominal content of the analyte), and the reproducibility of the method were characterized.

It has been experimentally demonstrated that the potentiometric method proposed is accurate, selective, and reproducible for the quantitative determination of chondroitin sodium sulfate both in pure form and in combined medicinal products. The results obtained confirm the analytical suitability of the method developed and the prospects of its implementation in the pharmaceutical analysis practice for the quality control of substances and combined medicinal products of small-scale and industrial production.

Keywords: chondroitin sodium sulfate; potentiometry; quality control; method validation; pharmaceutical analysis; small-scale production

А. С. Коптєлов[1], В. І. Плиска[2], О. В. Бевз[1], О. В. Рудакова[3], Н. Ю. Бевз[1], Я. І. Студеняк[2]

[1] Національний фармацевтичний університет Міністерства охорони здоров'я України, вул. Григорія Сковороди, 53, м. Харків, 61002, Україна
[2] ДВНЗ «Ужгородський національний університет», пл. Народна, 3, м. Ужгород, 88000, Україна
[3] Фаховий коледж Національного фармацевтичного університету Міністерства охорони здоров'я України, вул. Заїківська, 18, Харків, 61140, Україна

Потенціометричне кількісне визначення хондроїтин натрію сульфату з використанням іон-селективних електродів

Анотація

Хондроїтин натрію сульфат є аніонним полісахаридом, який широко застосовують у фармацевтичній практиці як активний інгредієнт моно- та багатокомпонентних лікарських засобів і кількісне визначення якого є важливим етапом

контролю якості. З'ясовано, що застосування потенціометричного титрування з іон-селективними електродами дозволяє підвищити точність і об'єктивність кількісного аналізу, що має важливе значення для забезпечення якості та безпеки лікарських засобів.

Метою роботи були розробка та валідація методики кількісного потенціометричного визначення хондроїтин натрію сульфату в субстанції та у складі комбінованого лікарського засобу у формі порошку в саше-пакетах.

Об'єктами дослідження були субстанція хондроїтин натрію сульфату та комбінований лікарський засіб, що містить хондроїтин натрію сульфат у поєднанні з D-глюкозаміну натрію сульфатом, метилсульфонілметаном, натрію гіалуронатом, аскорбіновою та лимонною кислотами, а також сорбітолом. Розглянуто умови потенціометричного титрування 0,001 М розчином цетилпіридинію хлориду з використанням іон-селективного електрода на основі іонних асоціатів цетилпіридинію з деякими ліпофільними аніонами. Стандартизацію титранту здійснювали із застосуванням додецилсульфату натрію як первинного стандарту, а також із використанням субстанції. Точку еквівалентності визначали за кривою титрування та її математично обробленими формами (диференційна крива, перша похідна та функції Грана). З'ясовано, що досліджувані пластифіковані мембранні іон-селективні електроди на основі асоціатів цетилпіридинію з додецилсульфат- та тетрафенілборат-аніонами характеризуються стабільним відгуком, близьким до нернстівського, у робочому діапазоні концентрацій цетилпіридинію 10^{-3}–10^{-6} моль $л^{-1}$. Аналітичні характеристики електродів залишалися стабільними протягом щонайменше 30 послідовних титрувань. Виявлено селективність реакції між хондроїтин натрію сульфатом та цетилпіридинію хлоридом, що забезпечує чітке визначення точки еквівалентності навіть у присутності інших компонентів суміші. Оцінено вплив pH середовища на результати титрування; з'ясовано, що в діапазоні pH 4–8 форма кривих титрування та значення потенціалу залишаються сталими, що підтверджує робастність методики. Схарактеризовано точність, прецизійність, лінійність (у межах 80–120 % від номінального вмісту аналіту) та відтворюваність методики.

Експериментально продемонстровано, що запропонована потенціометрична методика є точною, селективною та відтворюваною для кількісного визначення хондроїтин натрію сульфату як у чистому вигляді, так і у складі комбінованих лікарських засобів. Отримані результати підтверджують аналітичну придатність розробленої методики й перспективність її впровадження в практику фармацевтичного аналізу для контролю якості субстанцій і комбінованих лікарських засобів малосерійного та промислового виробництва.

Ключові слова: хондроїтин натрій сульфат; титрування; контроль якості; валідація методу; фармацевтичний аналіз; малосерійне виробництво

Citation: Koptielov, A. S.; Plyska, V. I.; Bevz, O. V.; Rudakova, O. V.; Bevz, N. Yu.; Studenyak, Ya. I. The Potentiometric Quantification of Chondroitin Sodium Sulfate Using Ion-Selective Electrodes. *Journal of Organic and Pharmaceutical Chemistry* **2025**, *23* (4), 3–11.
https://doi.org/10.24959/ophcj.25.350114
Received: *4 September 2025*; **Revised:** *2 November 2025*; **Accepted:** *10 November 2025*

Funding: The authors received no specific funding for this work.
Conflict of interests: The authors have no conflict of interests to declare.

■ Introduction

Chondroitin sodium sulfate (CS) is a sulfated glycosaminoglycan widely used in pharmaceutical practice as an active pharmaceutical ingredient in both mono- and combination medicinal products for the treatment of degenerative disorders of the musculoskeletal system, particularly osteoarthritis. The pharmacological activity of CS largely depends on its structural characteristics, degree of sulfation, and molecular weight, which necessitates a strict quality control at all stages of the drug production [1].

In recent years, the pharmaceutical market has shown a growing number of combined products containing CS together with glucosamine, methylsulfonylmethane, ascorbic acid, and other biologically active components. Such combinations are aimed at enhancing the anti-inflammatory and chondroprotective effects of these preparations [2]. Therefore, a medicinal product in the form of powder in sachets was selected as the object of this study. Its composition includes glucosamine sodium sulfate (1500 mg), chondroitin sodium sulfate (500 mg), methylsulfonylmethane (400 mg), vitamin C (80 mg), sodium hyaluronate (30 mg), and excipients, such as sorbitol and citric acid [3].

At the same time, the multicomponent composition significantly complicates the pharmaceutical quality control since the presence of polyelectrolytes and surfactants may affect the selectivity and accuracy of the quantitative determination of CS. Recent studies indicate the substantial variability in the qualitative and quantitative composition of chondroitin sodium sulfate, especially in combined medicinal products where impurities of other polysaccharides or excipients may be present [4]. In this regard, the implementation of reliable, selective, and reproducible analytical methods capable of providing an objective quantitative determination of chondroitin sodium

ISSN 2308-8303 (Print) / 2518-1548 (Online)

sulfate in multicomponent systems is an urgent task.

Scientific studies confirm that pharmacopoeial methods may be insufficiently sensitive for the detection and quantitative assessment of combined medicinal products of industrial and small-scale production, which necessitates the development and introduction of new analytical approaches [5].

The ability of chondroitin sodium sulfate to form poorly soluble complexes with cetylpyridinium chloride (CPC) is used for the quantitative analysis of CS in the substance. Indicator-based and photometric titration methods regulated by leading pharmacopoeias consist of two stages: the titration with 4.000 g L^{-1} CPC solution with the visual or instrumental endpoint detection, or the photometric titration with 1.000 g L^{-1} CPC solution [6, 7]. The non-indicator photometric-turbidimetric titration using Mettler-Toledo phototrodes is also widely applied [8, 9].

The disadvantages of these methods include the practical impossibility of performing titration in the presence of certain colored substances and colloidal systems, which usually leads to a significant increase in the analytical uncertainty. For example, it has been reported [10] that this method provides satisfactory results for the determination of CS in chewable tablets only when the effect of the excipient xanthan gum is compensated by adding the same amount to the standard CS solution as contained in the tablets. Similar problems associated with the titration of CS with CPC solutions using the photometric endpoint detection were reported by other authors [11, 12], which partly motivated the present study.

When developing a titrimetric method, it is essential to evaluate validation characteristics, including the method uncertainty, which depends on the titrant standardization approach (primary or secondary) and, in some cases, on the laboratory temperature, burette accuracy, purity of reference standards, and other factors.

In this way, we aimed to develop and validate a potentiometric method for the quantitative determination of chondroitin sodium sulfate in the substance and in a combined medicinal product in the form of the sachet powder.

■ Materials and methods

Reagents and Materials. The study objects included sodium chondroitin sulfate (Bioiberica, S.A.U., R.M. Barcelona, Spain, batch F0932, 100.0% API content, loss on drying – 6.3%) and a novel combined pharmaceutical powder formulation in sachets, containing, in addition to sodium chondroitin sulfate, sodium glucosamine sulfate (Shandong Xiwang Sugar Industry, China, batch XWAC003), ascorbic acid (SD LUWEI Pharmaceutical Co. Ltd, China, batch 201404197), methylsulfonylmethane (Shijiazhuang Jirong Pharmaceutical, China, batch 101-1303006), sodium hyaluronate (Nippon Rica, Japan, batch 5992-143), sorbitol (Evonic Industries, Germany, batch 2111240201), and citric acid monohydrate (Shandong Ensing Industry Co., Ltd, China, batch 3MT2504023).

For titration, cetylpyridinium chloride (CPC) solutions with concentrations of 0.001–0.01 M were used. Sodium dodecyl sulfate (SDS, analytical grade) served as the primary standard for the titrant standardization. All solutions were prepared using purified water.

Equipment. Potentiometric titrations were conducted at 20 ± 5 °C using a cetylpyridinium-selective indicator electrode, with potential readings recorded by a Radelkis OP-208/1 potentiometer equipped with an analog-to-digital converter (ADC ADA-1406, HOLIT DataSystems, Ukraine) under constant stirring on a magnetic stirrer. The measurement scheme: Ag, AgCl/KCl sat./Test solution // Membrane // 10^{-3} M CPC/AgCl, Ag.

Standardization of 0.001 M CPC solution. A 0.2884 g sample of SDS (288.38 g mol^{-1}) was dissolved in distilled water, and the solution was diluted to the volume of 1000 mL in a volumetric flask at 20 °C. Then, 1.0 mL of the resulting 0.01000 M solution or 10.0 mL of the diluted 0.00100 M solution was transferred to a titration cell equipped with the ion-selective electrode, a reference electrode, and a magnetic stirrer. 20–40 mL of water was added, and the solution was titrated with 0.0010 M CPC in 0.5 mL increments, while recording the potential changes of the indicator system. The CPC concentration was calculated as the mean of at least two titrations using the formula:

$$C(\text{CPC}) = C(\text{SDS}) \times \frac{V(\text{SDS})}{V(\text{CPC})} \; [mol\ L^{-1}]$$

Preparation of titration solutions. 0.100 g of sodium chondroitin sulfate or an equivalent amount of the pharmaceutical powder (corresponding to 0.100 g of sodium chondroitin sulfate) was placed in a 100 mL volumetric flask, dissolved in 50 mL of water, and diluted to the volume with water.

The pH of the solution was adjusted to 4.0 using 0.01 M sodium hydroxide. 2.0 mL of this solution was transferred to a titration cell, 20–40 mL of water was added, and the titration was performed potentiometrically with 0.001 M CPC. 1 mL of 0.001 M CPC is equivalent to 0.35 mg of CS.

Potentiometric Titration Conditions. Standard 0.001 M or 0.01 M CPC solutions were added in 0.5 mL increments, and the potential changes (E, mV) were recorded, or the titration was continued until a predetermined potential of the indicator system was reached. Testing the response of the ion-selective electrodes to the cetylpyridinium cation demonstrated the near-Nernstian behavior for a monovalent cation (58 ± ± 3 mV/pC) in the CPC concentration range from 10^{-3} to 10^{-6} mol L^{-1}.

Systematic titration errors were minimized by the primary standardization of the titrant and careful determination of the titration endpoint of the test sample, maintaining a temperature of 20 ± 5 °C and using ISO Class A volumetric glassware [13].

Determination of the CS content. The content of chondroitin sulfate in the substance and pharmaceutical preparation was calculated using the formula:

$$X = \frac{V \cdot K \cdot T \cdot V_{v.fl.} \cdot 100\ (m_{av})}{m_n \cdot V_{pip.}}$$

where: V – is the volume of 0.001 M CPC solution used for titration, mL;
K – is the titration correction factor;
T – is the mass of the analyte equivalent to 1 mL of the titrant of the nominal concentration;
m – is the mass of the sample, g;
m_{av} – is the average sample mass, g.

Data processing. The statistical analysis of the results was performed according to the State Pharmacopoeia of Ukraine (SPhU) 5.3.N.1 "Statistical Analysis of Chemical Experiment Results" [13] using Microsoft Excel. The analysis included calculation of the mean of three determinations, the standard deviation of the mean, and the relative standard deviation. No additional statistical methods were applied as the study had an analytical focus.

■ Results and discussion

The development of a potentiometric titrimetric method for the quantitative determination of CS in a mixture with D-glucosamine sodium sulfate, methylsulfonylmethane, ascorbic acid, sodium hyaluronate, citric acid, and sorbitol involved the following steps:

- the selection of an ion-selective electrode;
- the determination of optimal conditions for the potentiometric titration;
- the standardization of the CPC solution;
- testing the method for the quantitative determination of chondroitin sodium sulfate in the presence of other mixture components;
- the determination of the quantitative content of chondroitin sodium sulfate in the combined medicinal product using the titrimetric method proposed.

Cetylpyridinium chloride belongs to the group of cationic surfactants and is widely used for the potentiometric titration of anionic surfactants. Sodium chondroitin sulfate, due to the presence of carboxyl and sulfate groups in its structure, is a negatively charged polysaccharide. This feature ensures its interaction with CPC cations and provides selectivity of the titrimetric reaction and the determination of the titration end-point using a CPC-selective electrode [14].

The development of the potentiometric titrimetric method for the quantitative determination of sodium chondroitin sulfate in the mixture using the CPC solution began with the selection of an ion-selective electrode. According to the described modified method [15], an ionic associate [16] was obtained by the interaction of aqueous 0.01 M solutions of cetylpyridinium chloride with sodium dodecyl sulfate or sodium tetraphenylborate in the ratio of 1:1. Upon the formation of the corresponding ionic associates, ion-selective membranes were prepared using polyvinyl chloride grade 6602 and Fluka. The PVC electrodes contained approximately 1% of the associate and 73 ± 3% of a plasticizer, which was one of the phthalic acid diesters (octyl, nonyl) or *o*-nitrophenyl octyl ether.

The stability of the prepared ion-selective electrodes based on CPC ionic associates with dodecyl sulfate and tetraphenylborate [17], plasticized with phthalates or *o*-nitrophenyl octyl ether, was tested over 30 consecutive titrations (over the period of 6 months). No significant differences were observed in the titration volume when potentiometrically determining the titration endpoint.

To select the optimal titration conditions, the behavior of potentiometric systems with different electrodes was studied, including the method

ISSN 2308-8303 (Print) / 2518-1548 (Online)

selectivity, the effect of pH, linearity, and reproducibility of the method on the substance, model mixture, medicinal product, and placebo.

During the potentiometric titration of CS with 0.001 M or 0.01 M CPC solutions, a typical titration curve was observed. Two examples for different electrodes are shown in **Figure 1**, presenting one of the differential dependencies. On the titration curve with 0.001 M CPC solution, a titration jump of more than 60 mV was observed. This allows reliable determination of the titration end-point with the minimal influence from the nature of the ion-selective electrode (**Figure 1**).

Due to the asymmetry of titration curves for reactions with stoichiometry different from 1:1 and the frequent heterogeneity of monomer units of natural polyelectrolytes, an important issue arises regarding the correct determination of the equivalence point and the calculation of analytical results. To clarify the uncertainty of such analysis, the behavior of titrimetric systems and methods for processing/calculating titration results were experimentally studied over the period of two years. First of all, the method for the titrant standardization was selected, and the use of sodium dodecyl sulfate as a primary standard proved to be the most appropriate, with control of the results performed using the CS substance standard.

Figure 2 presents the typical data obtained during the titrant standardization using SDS and CS, along with the corresponding methods for processing the experimental data.

As can be seen from the dependences, the titration jump for CS is significantly smaller compared to that for SDS; however, it allows the determination of CS at concentrations in the titrated solution ranging from 0.02 to 10 mg mL^{-1} at the corresponding titrant concentration (with a titer of 0.35–3.50 mg mL^{-1}).

The titrant (CPC) volume corresponding to the equivalence point was determined using various approaches, namely: the titration to a constant potential corresponding to the equivalence point (E_end), processing of EMF dependences f(t) by the Gran method, and the calculation of derivatives (**Figure 2**). It has been found that the most reliable method in terms of selectivity and accuracy is titration to a predetermined E_end value previously determined based on the standardization data and the CS substance titration. Due to the asymmetry of the chondroitin titration curve caused by interaction coefficients differing from unity, this approach makes it possible to obtain reliable results.

During the titrant (CPC) standardization using SDS, any of the listed methods for determining the titration end-point may be applied, which, in contrast to the CS titration, yield practically identical results (**Figure 2***B*). It should be noted that differential processing of curves is sensitive to the titrant portion volume interval ΔV_{CPC} introduced during the titration and, accordingly, may be characterized by higher uncertainty.

The presence of foreign interferents forming more stable/less soluble ionic associates with cetylpyridinium leads, under conventional titration conditions, to positive systematic errors in the determination of chondroitin sulfate. However, when

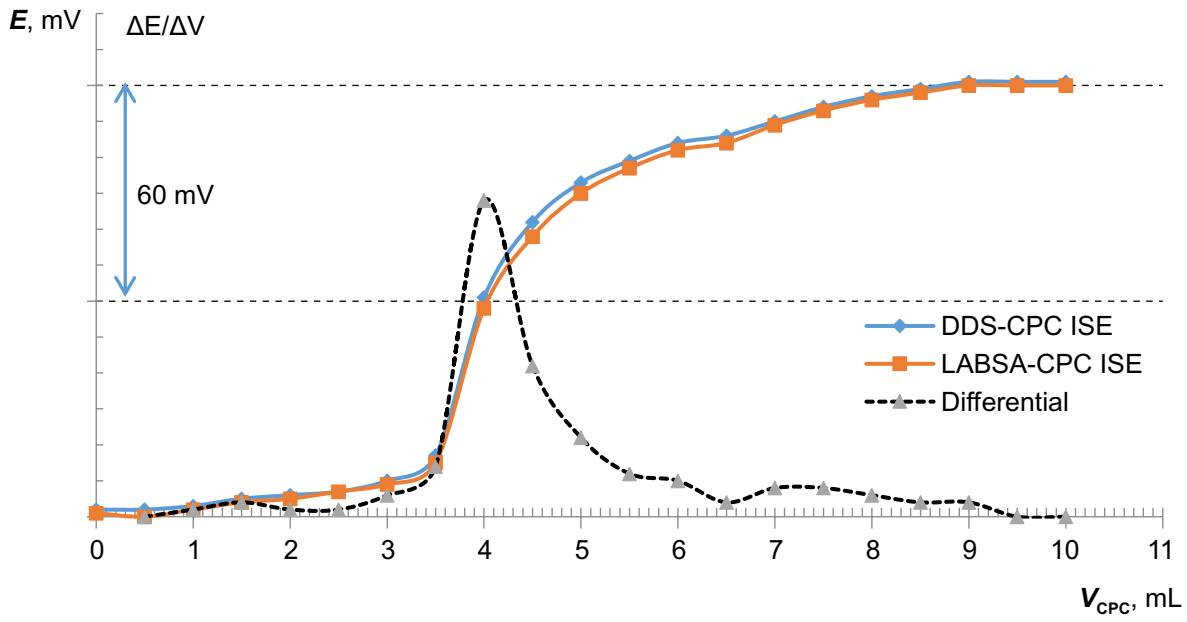

Figure 1. Original (classical) and differential titration curves of the chondroitin sodium sulfate sample titrated with 0.01 M CPC solution using two different ion-selective electrodes

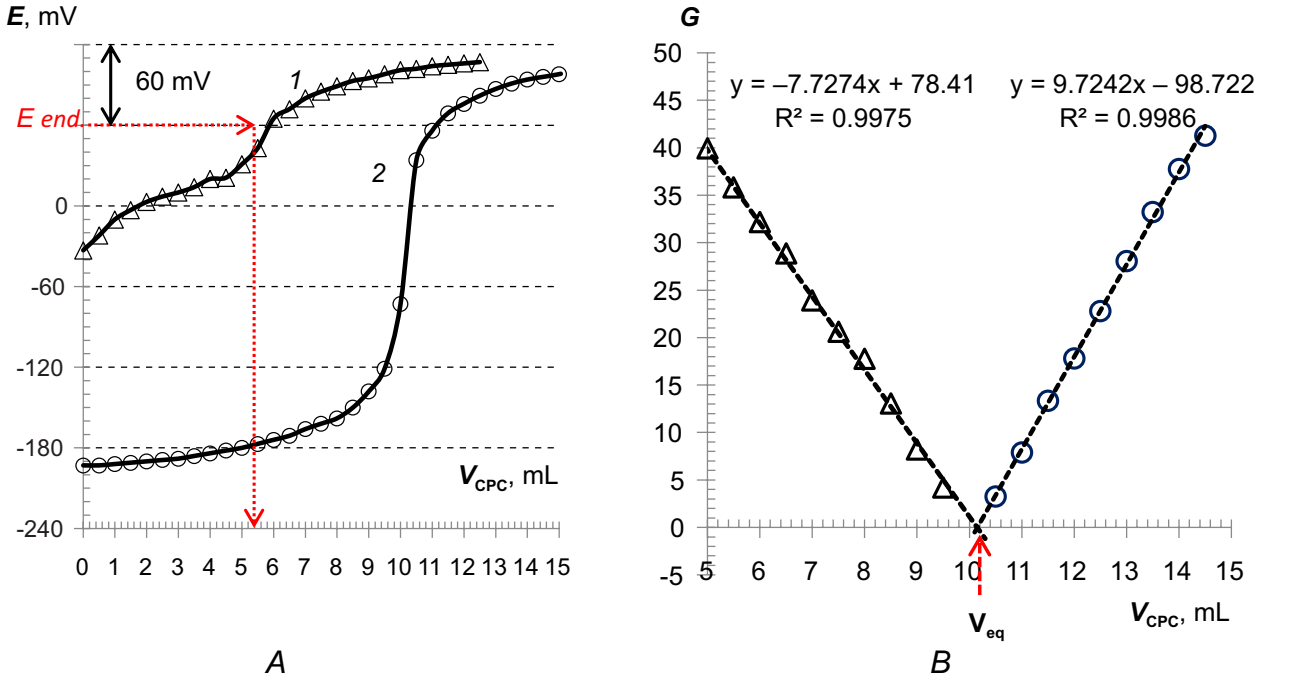

Figure 2. Potentiometric titration curves obtained with 0.001 M CPC solution for the standard SDS solution (2) and the chondroitin sodium sulfate substance solution (1) using a TPhB–CPC electrode (*A*), and processing of the SDS titration curve by the Gran method (*B*): $G = (V_{total} + V_{CPC}) \times 10^{(k \pm E)S^{-1}}$

this effect is taken into account by constructing differential curves, such influences can be partially considered and compensated (**Figure 3**). Nevertheless, it should be taken into account that the differential form indicates the inflection point of the titration curve, which does not coincide with the equivalence point when the titration stoichiometry differs from 1:1. This will play a certain role when titrating minimal amounts of CS.

If the titration is performed in the presence of foreign polyelectrolytes forming less stable/more soluble ionic associates, such as hyaluronate, the systematic error can be eliminated by the titration to a specific potential corresponding to the equivalence point of the chondroitin–cetylpyridinium interaction reaction (**Figure 4**).

Thus, when titrating CS in the presence of foreign interferents, for example, hyaluronic acid, reliable results are obtained only when the

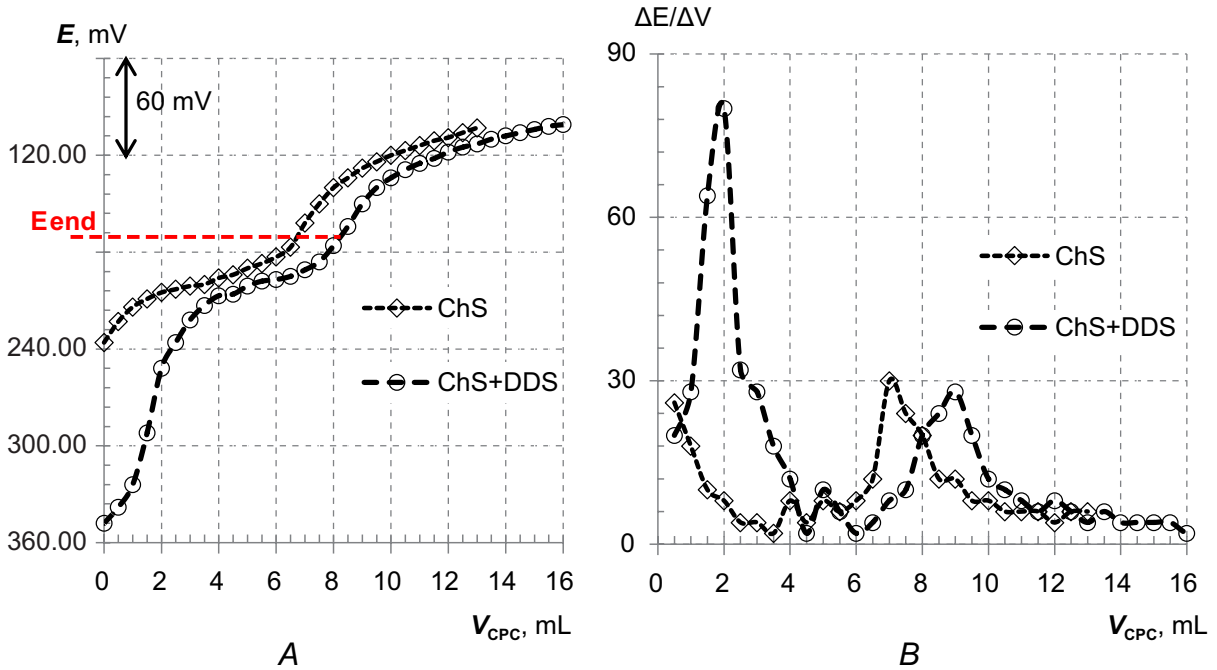

Figure 3. Titration curves obtained with 0.001 M CPC solution: *A*) glucosamine (ChS) and a mixture of glucosamine with sodium dodecyl sulfate (SDS); *B*) corresponding differential dependences

ISSN 2308-8303 (Print) / 2518-1548 (Online)

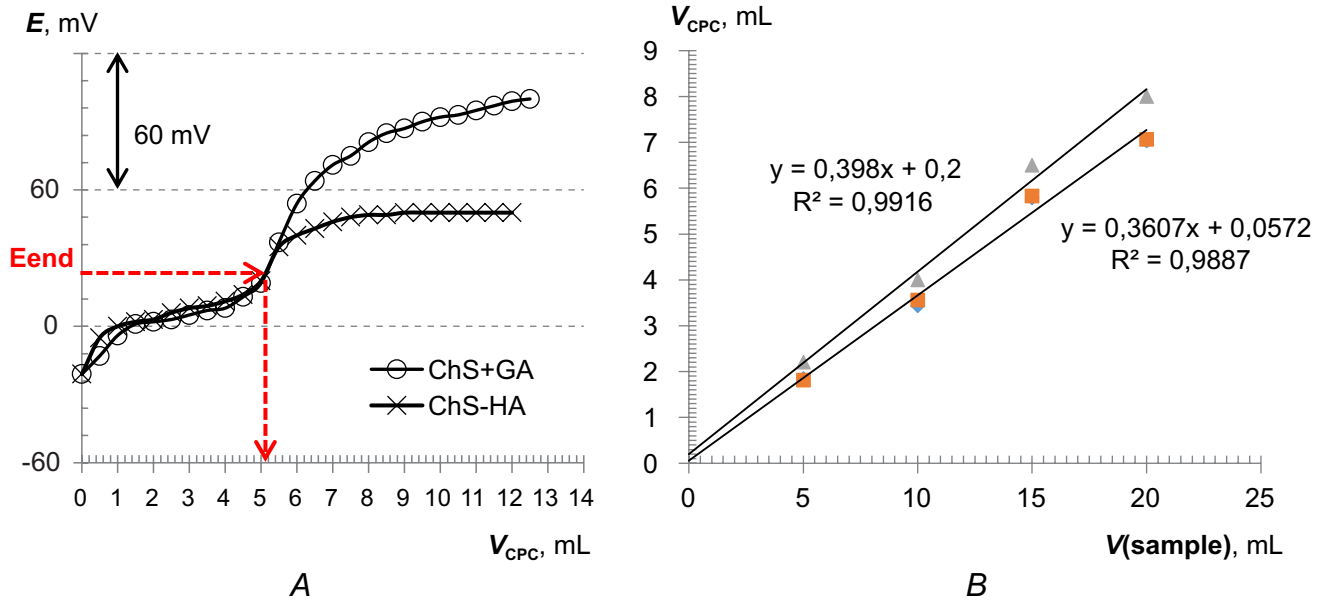

Figure 4. Titration curves of chondroitin sulfate obtained with 0.001 M CPC solution in the presence of an eight-fold excess of glucosamine and, respectively, a ten-fold excess of sodium hyaluronate (*A*), and plots of the titrant volume versus the sample volume using different methods for the end-point determination (*B*)

titration is performed to a constant potential value (E_{end}).

The titration to a constant E_{end} value is convenient for automation of titration using autotitrators. The Gran function applied to the data obtained after the equivalence point does not allow correct results to be obtained in the presence of anionic interferents capable of interacting with CPC to form ionic associates of lower stability/higher solubility compared to CPC–CS associates. Taking into account the stability of CS ionic associates compared to SDS associates, and under satisfactory performance of the ion-selective indicator electrode, the titration end-point potential (E_{end}) can be selected based on the end-point potential of the SDS titration with CPC solutions, which in the case of 0.001 M titrant solution will be 60–70 mV more positive.

The linearity of the method was studied by titrating different sample volumes of the chondroitin sodium sulfate solution with different data processing approaches (**Figure 4***B*). The linearity of the quantitative potentiometric determination of chondroitin sodium sulfate in the mixture was studied within ± 5% acceptance limits relative to the nominal concentration of the active compound in the range from 80% to 120% according to the method, and a calibration plot in normalized coordinates was constructed (**Table 1**) [13].

The study of the dependence of the electroanalytical properties of the ion-selective electrode on the solution acidity showed that the electrode response and the shape of titration curves remained constant within the pH range of 4–8.

Table 1. Validated method parameters

Parameter	Result
Number of determinations	27 (9 × 3 aliquots)
Concentration range	80–120% (80.0–120.0 mg)
a	0.200
b	0.398
r^2	0.9916 Complies
Mean value of Z%	100.09
The lack of statistically significant the systematic error: δ ≤ 1.89	0.5523 ≤ 1.89 Complies
The practical insignificance of the systematic error: δ ≤ 1.0667	0.09 ≤ 1.0667 Complies
The overall conclusion on precision and accuracy	Complies

The study of dependence of the electroanalytical properties of the ion-selective electrode on the medium acidity demonstrated that in the pH range of 4–8, the electrode response and the shape of potentiometric titration curves remained stable. The results obtained indicate the absence of a significant pH effect on the course of the titrimetric reaction, confirming the robustness of the method developed and the possibility of its application over a wide range of analytical conditions.

The results of the quantitative determination of chondroitin sodium sulfate in the substance and in the combined medicinal product are presented in **Table 2**.

It was found that the actual content of the active substance agreed with the declared value. The relative standard deviation (RSD) did not exceed 3.0% in any determination, meeting the

Table 2. The results of the CS determination in the substance and the medicinal product

Test object	Declared content	Found content	SD	RSD	Conclusion
Substance	100.0 %	100.13 %	0.2628	0.26	Complies
Medicinal product	500.0 mg	500.36 mg	1.3106	0.26	Complies

pharmacopoeial requirements for analytical methods. The data obtained confirm the accuracy and practical applicability of the method proposed for the quality control of finished medicinal products.

The approach proposed can be integrated into routine quality control without the use of expensive equipment, which makes it attractive for laboratories of small and medium-sized pharmaceutical enterprises.

■ Conclusions

A potentiometric method for the quantitative determination of chondroitin sodium sulfate using a cetylpyridinium-selective electrode has been developed and validated. The method is characterized by the simple sample preparation and the total analysis time of no more than 15–20 min per sample.

The effect of other active pharmaceutical ingredients and excipients of the medicinal product has been studied, and it has been shown they do not to have a statistically significant effect on the analytical results ($p > 0.05$), confirming the specificity of the method.

The method is characterized by linearity, accuracy, and reproducibility, complying with the pharmacopoeial requirements and ICH recommendations.

The results obtained allow recommending the application of the method developed not only in scientific research, but also in practical activities of large pharmaceutical enterprises and pharmacies engaged in small-scale production, including control of the incoming raw material and finished medicinal products of chondroitin sodium sulfate of both small-scale and industrial manufacture.

■ References

1. Shen, Q.; Guo, Y.; Wang, K.; Zhang, C.; Ma, Y. A Review of Chondroitin Sulfate's Preparation, Properties, Functions, and Applications. *Molecules* **2023**, *28* (20), 7093. https://doi.org/10.3390/molecules28207093.
2. Li, H.; Zeng, C.; Wei, J.; Yang, T.; Gao, S. G.; Li, Y. S.; Lei, G. H. Associations between Dietary Antioxidants Intake and Radiographic Knee Osteoarthritis. *Clin. Rheumatol.* **2016**, *35* (6), 1585–1592. https://doi.org/10.1007/s10067-016-3177-1.
3. Koptielov, A. S.; Deyneka, A. S.; Bevz, N. Yu.; Kuchtenko, O. S. Vyznachennia farmakotekhnolohichnykh pokaznykiv aktyvnykh farmatsevtychnykh inhrediientiv pry rozrobtsi khondroprotektornoho likarskoho zasobu [Determination of pharmacotechnological indicators of active pharmaceutical ingredients during the development of a chondroprotective drug, *in Ukrainian*]. *Health* 2024, *1*, 13. https://doi.org/10.32782/health-2024.1.13.
4. Restaino, O. F.; Finamore, R.; Diana, P.; et al. Evaluation of commercial chondroitin sulfate samples. *Carbohydr. Polym.* **2019**, *222*, 114998. https://doi.org/10.1016/j.carbpol.2019.114998.
5. Patil, R. N.; Deore, B. L.; Gurav, D. G. Analytical method development and validation. *Indian Journal of Pharmacy and Drug Studies* **2024**, *3* (4), 1–7.
6. *European Pharmacopoeia*, 11th ed.; Council of Europe: Strasbourg, 2023. 4370 p.
7. *State Pharmacopoeia of Ukraine.* 2nd ed. Vol. 3. State Enterprise "Ukrainian Scientific Pharmacopoeial Center for Quality of Medicines". Kharkiv; 2014. 732 p.
8. Caro, C. A. D. Analysis of Dietary Supplements: Turbidimetric Titration of Chondroitin Sulfate. *UserCom Anal. Chem.* **2005**, No. 10, Publication ME 51724437 (access https://www.researchgate.net/publication/311517550_Analysis_of_dietary_supplements_Turbidimetric_titration_of_chondroitin_sulfate_UserCom_Analytical_Chemistry_No_10_Mettler-Toledo_Publication_ME-51724437_September_2005).
9. Metrohm Application Note AN-T-083. Turbidimetric Titration of Chondroitin Sulfate. https://www.metrohm.com/en/applications/application-notes/aa-t-001-100/an-t-083.html (accessed 2025-06-17).
10. Liang, Z.; Bonneville, C.; Senez, T.; Henderson, T. Development and Validation of a Photometric Titration Method for the Quantitation of Sodium Chondroitin Sulfate in Cosequin® DS Chewable Tablet. *J. Pharm. Biomed. Anal.* **2002**, *28* (2), 245–249. https://doi.org/10.1016/S0731-7085(01)00563-5.
11. Burns, D. T.; Walker, M. J.; Mussell, C. Chondroitin Sulfate: A Critical Review of Generic and Specific Problems in Its Characterization and Determination. *J. AOAC Int.* **2018**, *101* (1), 196–202. https://doi.org/10.5740/jaoacint.17-0213.
12. Restaino, O. F.; Schiraldi, C. Chondroitin Sulfate: Are the Purity and the Structural Features Well Assessed? *Carbohydr. Polym.* **2022**, *292*, 119690. https://doi.org/10.1016/j.carbpol.2022.119690.
13. *State Pharmacopoeia of Ukraine. 2nd ed., Suppl. 7, Vol. 2. Kharkiv: State Enterprise "Ukrainian Scientific Pharmacopoeial Center for Quality of Medicines*. Kharkiv; 2024. 242 p.
14. (a) Khaled, E.; Aboul-Enein, H. Y. Surfactants. In *Environmental Analysis by Electrochemical Sensors and Biosensors*; Elsevier, 2015; pp 905–930. (b) Müller, W.; Déjugnat, C.; Zemb, T.; Dufrêche, J.-F.; Diat, O. How Do Anions Affect Self-Assembly and Solubility of Cetylpyridinium Surfactants in Water. *The Journal of Physical Chemistry B* **2013,** *117* (5), 1345–1356. https://doi.org/10.1021/jp3093622.
15. Fizer, O.; Fizer, M.; Sidey, V.; Studenyak, Y. Predicting the end point potential break values: a case of potentiometric titration of lipophilic anions with cetylpyridinium chloride. *Microchem. J.* **2021**, *160*, 105758. https://doi.org/10.1016/j.microc.2020.105758.

ISSN 2308-8303 (Print) / 2518-1548 (Online)

16. Hajduković, M.; Samardžić, M.; Galović, O.; Széchenyi, A.; Sak-Bosnar, M. A Functionalized Nanomaterial-Based Solid-State Cationic-Surfactant-Selective Sensor. *Sens. Actuators B Chem.* **2017**, *251*, 795–803. https://doi.org/10.1016/j.snb.2017.05.067.
17. Fizer, O.; Fizer, M.; Filep, M.; Studenyak, Y.; Mariychuk, R. Deciphering the Structural and Functional Peculiarities of Cetylpyridinium Tetraphenylborate. *J. Mol. Liq.* **2025**, 127858. https://doi.org/10.1016/j.molliq.2025.127858.

Information about the authors:
Andrii S. Koptielov, PhD student, Department of Pharmaceutical Chemistry, National University of Pharmacy of the Ministry of Health of Ukraine; https://orcid.org/0000-0001-7512-7426.
Vitaliia I. Plyska, PhD student, Department of Analytical Chemistry, Uzhhorod National University, https://orcid.org/0000-0003-3937-7086.
Olena V. Bevz (*corresponding author*), PhD in Pharmacy, Associate Professor, Department of Pharmaceutical Chemistry, National University of Pharmacy of the Ministry of Health of Ukraine; https://orcid.org/0000-0002-7695-3612;
e-mail for correspondence: bevz.helen@gmail.com.
Olha V. Rudakova, PhD in Pharmacy, Lecturer at the Cyclic Committee of Pharmaceutical Chemistry and Pharmacognosy, Professional College of National University of Pharmacy of the Ministry of Health of Ukraine; https://orcid.org/0000-0003-4216-0590.
Nataliia Yu. Bevz, PhD in Pharmacy, Associate Professor, Department of Pharmaceutical Chemistry, National University of Pharmacy of the Ministry of Health of Ukraine; http://orcid.org/0000-0002-7259-8908.
Yaroslav I. Studenyak, PhD in Chemistry, Associate Professor, Head of Department of Analytical Chemistry, Uzhhorod National University; https://orcid.org/0000-0002-8970-2222.

Journal of Organic and Pharmaceutical Chemistry

Original Research

OPEN ACCESS
Freely available online on
http://ophcj.nuph.edu.ua

UDC 54.04+547.562.4+615.011

O. I. Kalchenko[1], A. B. Drapailo[1], S. O. Cherenok[1], A. I. Selikhova[1], P. López-Cornejo[2], V. I. Kalchenko[1]

[1] Institute of Organic Chemistry of the National Academy of Sciences of Ukraine, 5, Academik Kukhar str., 02094 Kyiv, Ukraine
[2] Departamento de Química Física, Facultad de Química, Universidad de Sevilla, c/ Prof. García González 1, 41012 Sevilla, Spain

The Complexation of Water-Soluble Calix[4]Arene-Phosphine Oxides With Antiviral Drugs

Abstract

The complexation of tetrahydroxycalix[4]arene-methyldimethylphosphine oxide (**CMPO**), tetrahydroxythiacalix[4]arene-methyldimethylphosphine oxide (**TCMPO**), and tetrapropoxycalix[4]arene-methyldiethylphosphine oxide (**CEPO**) with active pharmaceutical ingredients of antiviral drugs Remdesivir, Nevirapine, Vesatolimod, Bictegravir, Emtricitabine, and Tenofovir in the water medium was studied using the RP HPLC method. By analyzing the dependence of the drug capacity values on the concentration of calixarenes in the chromatographic mobile phase, the stability constants (K_A = 1100 – 12000 M^{-1}) of the complexes formed were determined. Quantum-chemical calculations show that the antiviral drugs form supramolecular *exo*-complexes with the calixarene-phosphine oxide molecules. These complexes can be stabilized by intermolecular hydrogen bonds between the proton acceptor P=O groups and the proton donor groups of antiviral drugs.

Keywords: calixarenes; antiviral drugs; supramolecular complexes; chromatography; molecular modeling

О. І. Кальченко[1], А. Б. Драпайло[1], С. О. Черенок[1], А. І. Селіхова[1], П. Лопес-Корнехо[2], В. І. Кальченко[1]

[1] Інститут органічної хімії НАН України, 02094, м. Київ, вул. Академіка Кухаря, 5, Україна
[2] Севільський університет, Хімічний факультет, Відділення фізичної хімії, 41012, м. Севілья, вул. Професора Гарсія Гонзалес, 1, Іспанія

Комплексоутворення водорозчинних калікс[4]арен-фосфіноксидів з антивірусними препаратами

Анотація

Методом ОФ ВЕРХ досліджено комплексоутворення тетрагідроксикалікс[4]арен-метилдиметилфосфіноксиду (**CMPO**), тетрагідрокситіакалікс[4]арен-метилдиметилфосфіноксиду (**TCMPO**) та тетрапропоксикалікс[4]арен-метилдіетилфосфіноксиду (**CEPO**) з активними фармацевтичними інгредієнтами антивірусних препаратів Ремдесивір, Невірапін, Весатолімод, Біктегравір, Емтрицитабін та Тенофовір у водному середовищі. Аналізом залежності значень хроматогофічної ємності препарату від концентрації каліксарену в рухомій фазі визначено константи стійкості утворених супрамолекулярних комплексів (K_A = 1100 – 12000 M^{-1}). Квантово-хімічними розрахунками показано, що каліксаренфосфіноксиди утворюють з дослідженими препаратами супрамолекулярні *екзо*комплекси. Ці комплекси можуть бути стабілізовані міжмолекулярними водневими зв'язками протоноакцепторних P=O груп каліксаренів з протонодорними угрупованнями антивірусних препаратів.

Ключові слова: каліксарени; антивірусні препарати; супрамолекулярні комплекси; хроматографія; молекулярне моделювання

Citation: Kalchenko, O. I.; Drapailo, A. B.; Cherenok, S. O.; Selikhova, A. I.; López-Cornejo, P.; Kalchenko V. I. The Complexation of Water-Soluble Calix[4]Arene-Phosphine Oxides With Antiviral Drugs *Journal of Organic and Pharmaceutical Chemistry* **2025**, *23* (4), 12 – 21.
https://doi.org/10.24959/ophcj.25.342282
Received: *29 August 2025*; **Revised:** *30 October 2025*; **Accepted:** *7 November 2025*

Funding: This work was supported by the National Academy of Sciences of Ukraine (grant No 0120U104649), and by the Ministerio de Ciencia, Innovación y Universidades (PID2023-151642OB-I00) and the European Union (Feder Funds).
Conflict of interests: The authors have no conflict of interests to declare.

ISSN 2308-8303 (Print) / 2518-1548 (Online)

■ Introduction

Antiviral drugs are widely used to prevent and treat many infectious diseases [1, 2]. However, such drugs may have low bioavailability and cause side effects [3, 4]. Therefore, in some cases, they are used as prodrugs or as supramolecular complexes with cyclodextrins. Calixarenes [5, 6] and their self-assembled supramolecular aggregates [7], which form host-guest supramolecular complexes with the active pharmaceutical ingredients (APIs) of drugs, are considered promising objects in the design of the drug delivery vectors [8–15]. Advantages of calixarene vectors include low cytotoxicity [16–20] and the absence of immune reactions [21].

Among a variety of water-soluble calixarenes, their sulfonic acid derivatives are the best-studied vectors [22]. They form supramolecular complexes with known pharmaceutical ingredients – 3-phenyl-1*H*[1]benzofuro[3,2-*c*]pyrazole (tyrosine kinase III inhibitor) [23], Carvediol (management of hypertension) [24], Paclitaxel (ovarian, breast, lung and colon cancer treatment) [25], Tramadol (analgesic) [26], Irinotecan (colon cancer treatment) [27], Nifedipine (calcium channel blocker) [28], Tenofovir (antiviral drug) [29].

Water-soluble cup-shaped calixarenes functionalized on the upper or lower rim of the macrocycle with hydrophilic organophosphorus groups are also used to create drug delivery systems.

Phosphorus-containing calixarenes are characterized by a high biological activity and low cytotoxicity [30]. The calixarene and thiacalixarene-phosphonic acids effectively and selectively inhibit ATP-hydrolase systems of smooth muscle cells [31] and therapeutically important phosphatases of various origins [32].

It has been shown that the lower-rim calixarene-diphosphoric acid, which forms supramolecular complexes with water-insoluble APIs in aqueous solutions, is appropriate for the drug formulation and delivery [33]. This acid also activates the transfer of polyarginine cell-penetrating peptides across biological membranes [34].

The upper rim modification of the calix[4]arene platform by hydrophilic phosphonic acid groups yields water-soluble derivatives that form supramolecular complexes with AFIs of antiviral drugs Tenofovir and Emtricitabine [35].

Micellar alkoxycalixarene-hydroxymethylene-bisphosphonic acids form nanoscale supramolecular complexes with fluorescently labeled polylysine and HIV-1 nucleocapsid due to electrostatic interactions. Such nanocomplexes cross biological membranes and deliver the therapeutically important proteins into cells [36].

In this article, within a context of further research on the drug formulation and delivery, the host-guest complexation of the tetrahydroxycalix[4]arene-methyldimethylphosphine oxide (**CMPO**), tetrahydroxythiacalix[4]arene-methyldimethylphosphine oxide (**TCMPO**), and tetrapropoxycalix[4]arene-methyldiethylphosphine oxide (**CEPO**) hosts with active pharmaceutical ingredients of antiviral drug guests Remdesivir, Nevirapine, Vesatolimod, Bictegravir, Emtricitabine and Tenofovir (**Figure 1**) in the water medium was studied using RP HPLC and molecular modeling methods.

Due to biologically friendly properties of a phosphorus atom, a number of drugs for medicinal purposes have been created on the basis of natural and synthetic organophosphorus compounds [37]. Highly polar $Me_2P{=}O$ or $Et_2P{=}O$ groups are currently used in medicinal chemistry to improve the water solubility of API molecules, optimize their pharmacokinetic profile [38–40], and create new drugs for medicine [41–43]. It should be noted in the context of the drug design that the proton-accepting property of the oxygen atom of dimethylphosphine oxide derivatives exceeds the proton-accepting property of the oxygen atoms of phosphates, phosphonates, sulfones, and carbonyl compounds [44].

The presence of hydrophilic proton-accepting $Me_2P{=}O$ and $Et_2P{=}O$ groups on the upper rim of **CMPO**, **TCMPO**, and **CEPO** is capable of increasing the water solubility of the calixarenes. On the other hand, these groups can stabilize supramolecular host-guest complexes by forming intermolecular hydrogen bonds P=O···H-X (X = O, N) with amine, amide, hydroxyl, and other groups of the antiviral drugs.

■ Materials and methods

Reagents and Materials

Remdesivir, Nevirapine, Vesatolimod, Bictegravir, Emtricitabine, and Tenofovir were purchased from Sigma-Aldrich (St. Louis, MO, USA) or Abcam (Cambridge, UK) or obtained from UOSLAB (Kyiv, Ukraine). The cone shaped tetrapropoxycalixarene-diethylphosphine oxide **CEPO** was synthesized according to the method [45].

The solvents for the synthesis of **CMPO** and **TCMPO** were purified using standard techniques [46]. The reactions were conducted under a dry

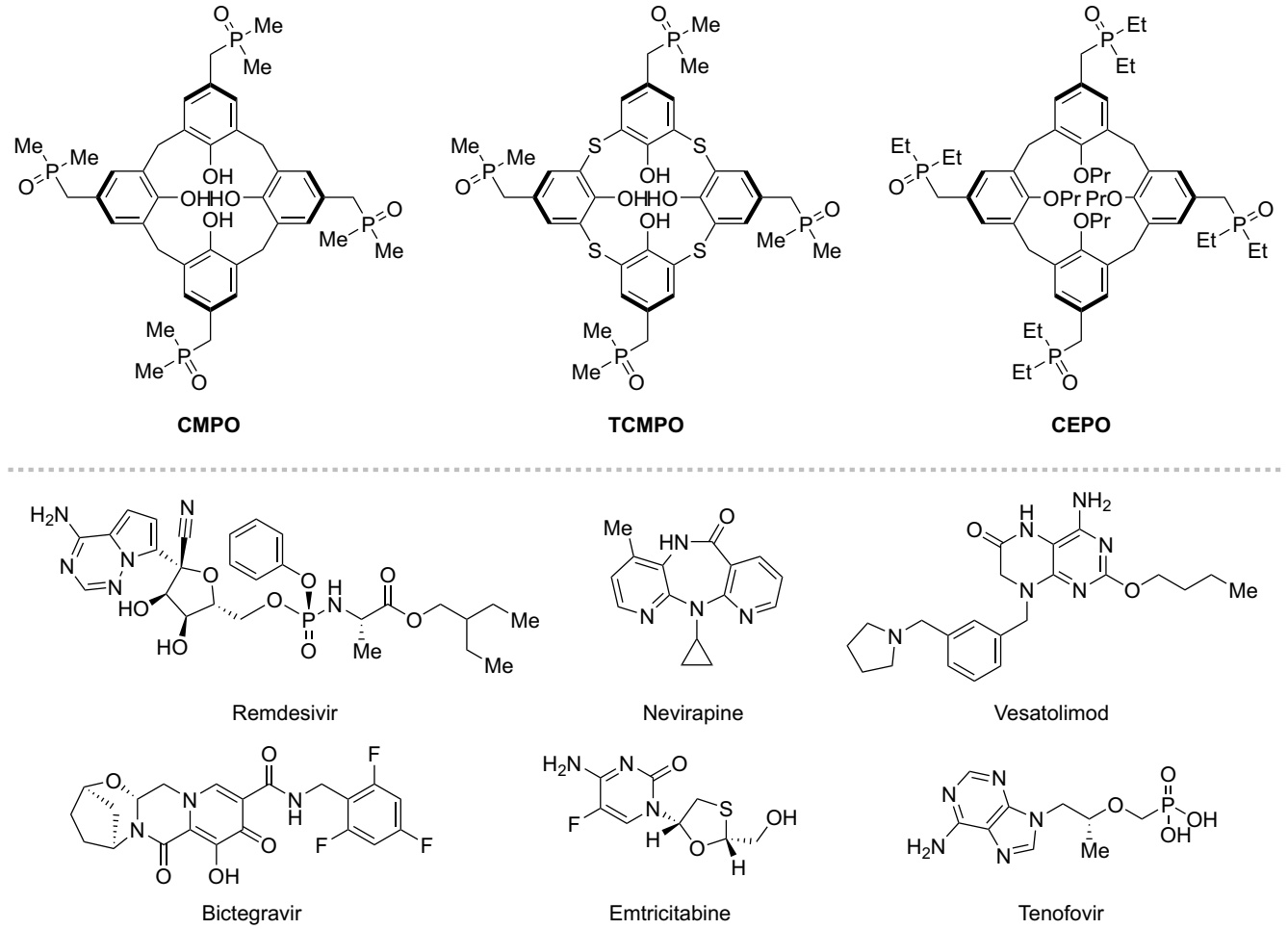

Figure 1. The water soluble calixarene-phosphine oxide hosts **CMPO, TCMPO, CEPO**, and antiviral drug guests Remdesivir, Nevirapine, Vesatolimod, Bictegravir Emtricitabine and Tenofovir

argon atmosphere, using anhydrous solvents. Chemical glassware was dried at 150 °C under vacuum. Melting points were determined using a Boetius apparatus. NMR spectra ^{1}H (300 MHz), ^{31}P (81 MHz) were recorded using a Varian VXR-300 spectrometer. Chemical shifts are reported relative to tetramethylsilane (^{1}H) used as an internal standard, or relative to H_3PO_4 (85%) (^{31}P) as an external standard.

CMPO and **TCMPO** were synthesized by the Arbuzov reaction of the corresponding tetrachloromethyltetrahydroxy(thia)calixarenes **1,2** with the trimethylsilyl ester of dimethylphosphinic acid in CH_2Cl_2 solution at 25 °C for 24 hours (**Scheme 1**).

CMPO and **TCMPO** are solid compounds that are readily soluble in water, DMSO and DMF and insoluble in nonpolar solvents. The structure of the calixarenes was confirmed by the ^{1}H, ^{31}P NMR spectra (*SI File*, **Figures S1**, **S2**, **S3**, **S4**).

A conical conformation of **CMPO** was confirmed by the presence of two wide signals of the AB spin system of axial (3.77 ppm) and equatorial (5.01 ppm) protons of methylene linkers broadened due to slow in NMR time scale rotation of benzene fragments around Ar-CH_2-Ar bonds in ^{1}H NMR spectrum recorded in DMSO-d_6 solution [47]. The ^{1}H NMR spectrum of **CMPO** also contains signals of CH_3 groups (1.32 ppm, d, $^{2}J_{HP}$ = 15 Hz), CH_2P groups (2.88 ppm, d, $^{2}J_{HP}$ = 15 Hz), ArH groups (6.94 ppm, s) and a wide signal of OH groups (9.61 ppm) (*SI File*, **Figure S1**).

The ^{1}H NMR spectrum of **TCMPO** contains signals of CH_3 groups (1.25 ppm, d, $^{2}J_{HP}$ = 15 Hz), CH_2P groups (2.98 ppm, d, $^{2}J_{HP}$ = 15 Hz), a wide signal of OH groups (4.10 ppm), and a signal of ArH groups (8.00 ppm, s) (*SI File*, **Figure S3**). The ^{31}P NMR spectra of the calixarenes contain signals 43.16 ppm (**CMPO**) and 45.7 ppm (**TCMPO**) (*SI File*, **Figures S2**, **S4**, respectively).

Tetrahydroxycalix[4]arene-methyldimethylphosphine oxide (CMPO)

A solution of 2.46 g (16.4 mmol) of dimethyltrimethylsilylphosphinite in 20 mL of a dry CH_2Cl_2 was added dropwise to a stirred solution of 1.24 g (2 mmol) tetrachloromethyltetrahydroxycalix[4]-arene **1** in 40 mL of a dry CH_2Cl_2 at room temperature. The reaction mixture was stirred for 24 hours. The solvent was evaporated under

ISSN 2308-8303 (Print) / 2518-1548 (Online)

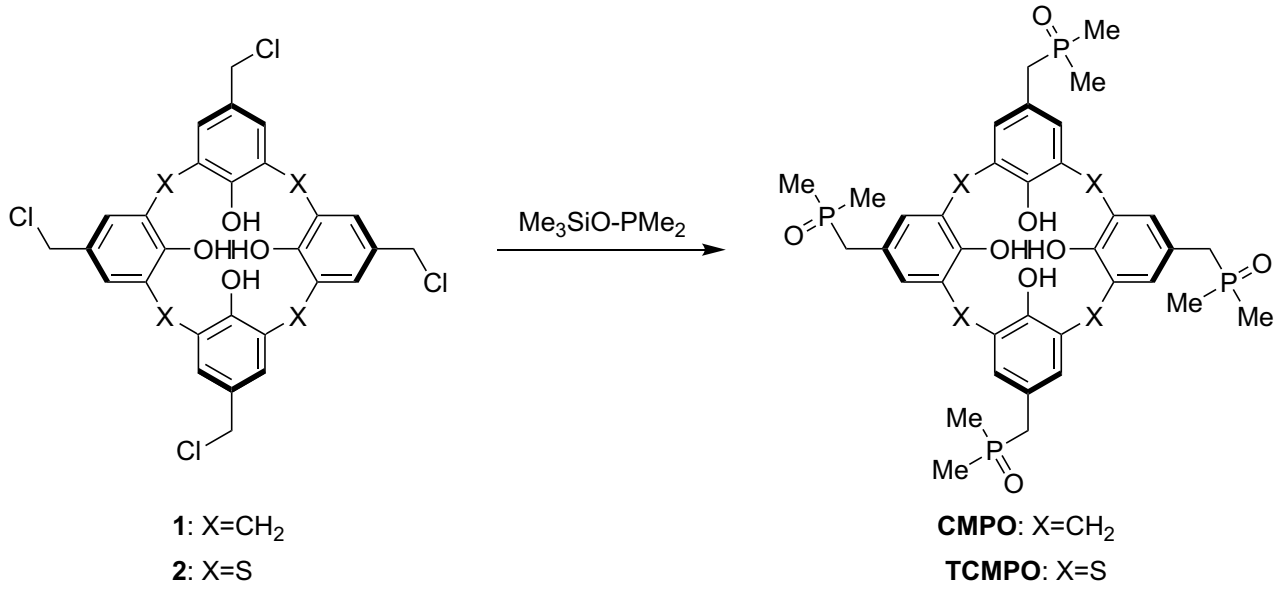

Scheme 1. The synthesis of **CMPO** and **TCMPO**

reduced pressure, and the viscous oil was dried under vacuum (8–10 Torr). The residue was dissolved in 25 mL of methanol and stirred for 6 hours, then the solution was evaporated to dryness under vacuum (8–10 Torr). The residue was triturated with hexane, filtered, and air-dried. The resulting product was obtained by crystallization from absolute isopropanol.

A white hygroscopic crystalline powder. Yield – 1.07 g (68%). M. p. 188–190 °C. Anal. Calcd. for $C_{40}H_{52}O_8P_4$, %: C 61.22, H 6.68, P 15.79. Found, %: C 61.00, H 6.50, P 15.43. ^{1}H NMR (300 MHz, DMSO-d_6), δ, ppm: 1.32 (24H, d, $^2J_{HP}$ = 15 Hz, P-CH_3), 2.88 (8H, d, $^2J_{HP}$ = 15 Hz, Ar-CH_2-P), 3.77 (4H, bs, Ar-$CH_{2(ax.)}$-Ar), 5.01 (4H, bs, Ar-$CH_{2(eq.)}$-Ar), 6.94 (8H, s, ArH), 9.61 (4H, bs, OH). ^{31}P NMR (80.95 MHz, DMSO-d_6), δ, ppm: 43.16.

Tetrahydroxythiacalix[4]arene-methyldimethylphosphine oxide (TCMPO)

A solution of 2.46 g (16.4 mmol) of dimethyltrimethylsilylphosphinite in 20 mL of a dry CH_2Cl_2 was added dropwise to a stirred solution of 1.38 g (2 mmol) tetrachloromethyltetrahydroxythiacalix[4]arene **2** in 40 mL of a dry CH_2Cl_2 at room temperature. The reaction mixture was stirred for 24 hours. The solvent was evaporated under reduced pressure, and the viscous oil was dried under the vacuum (8–10 Torr). The residue was dissolved in 25 mL of methanol and stirred for 6 hours, then the solution was filtered, evaporated to dryness under vacuum (8–10 Torr). The residue was triturated with hexane, collected by filtration, and air-dried. The resulting product was obtained by crystallization from absolute isopropanol.

A white hygroscopic powder. Yield – 1.06 g (62%). M. p. 220–222 °C. Anal. Calcd. for $C_{36}H_{44}O_8P_4S_4$, %: C 50.46, H 5.18, P 14.46, S 14.07. Found, %: C 50.81, H 5.03, P 14.20, S 13.75. ^{1}H NMR (300 MHz, DMSO-d_6), δ, ppm: 1.25 (24H, d, $^2J_{HP}$ = 15 Hz, P-CH_3), 2.98 (8H, d, $^2J_{HP}$ = 15 Hz, Ar-CH_2-P), 7.43 (8H, s, Ar*H*). ^{31}P NMR (80.95 MHz, DMSO-d_6), δ, ppm: 45.70.

HPLC analysis

The RP HPLC analysis of **CMPO**, **TCPO**, **CEPO**, and antiviral drugs was performed on a Hitachi high-pressure liquid chromatography equipment (Hitachi, Ltd., Tokyo, Japan) under isocratic conditions using a Zorbax CN chromatographic column (250×4.6 mm) (supplier Agilent) and a mobile phase of H_2O/MeCN (80/20, *v*/*v*). The choice of such a two-component mobile phase was due to the need for simultaneous solubility of calixarenes and antiviral drugs of different natures during chromatographic analyses. The concentration of **CMPO**, **TCPO**, and **CEPO** in the mobile phase varied within the range of 0.1×10^{-4}–1.4×10^{-4} M. Samples of the antiviral drugs for analysis were prepared in a solvent identical to the mobile phase (C = 1×10^{-5} M) and injected in amounts of 20 μL. All chromatograms were obtained at 28 °C. The wavelength of the UV detector was 254 nm. Each sample was analyzed in triplicate.

Molecular modeling

CMPO, **TCPO**, **CEPO**, and their complexes were simulated in vacuum (PM3, HyperChem software, evaluation version 8.0.10 [48]). The RMS gradient was 0.01 kcal mol^{-1}.

■ Results and discussion

The main criterion for assessing the complexing properties of host molecules is the value of the stability constant of the supramolecular complex with guest molecules. To determine the stability constants of the calixarene complexes, various physical methods are used: microcalorimetry [49], nuclear magnetic resonance [50], UV and fluorescence spectroscopy [51, 52], selective transport through liquid membranes [53], mass spectrometry [54], surface plasmon resonance [55], etc. However, the application of these methods may be limited by the unsatisfactory solubility of calixarene receptors and substrate molecules, or by the high cost of the methods.

A convenient and rapid method for determining the stability constants of complexes is reversed-phase high-performance liquid chromatography [56, 57]. This method has been used to determine the stability constants of calixarene complexes with organic substrates of various natures in aqueous or aqueous-organic solutions [58, 59]. According to this method, stability constants are determined from the dependence of the retention time or capacity factor of the substrate on the concentration of calixarene in the mobile phase. The addition of calixarenes to the mobile phase reduces the retention time of analytes due to the formation of supramolecular host-guest complexes and the increasing polarity of the chromatographic column surface upon the calixarene sorption. The inverse sorption of calixarenes by the column surface and the linear dependence of the capacity value $1/k'$ of the analyte on the calixarene concentration indicate 1:1 stoichiometry complexes in the mobile phase flow. This allows us to use equation (1) [56, 57] to calculate the stability constants of the host-guest complexes:

$$1/k' = 1/k'_0 + K_A \times [CA]/k'_0 \qquad (1)$$

where: k_0' and k' are the capacity factors of the analyte determined before and after the addition of calixarene to the mobile phase, $[CA]$ is the concentration of calixarene in the mobile phase.

Under the analysis conditions, the antiviral drugs and the calixarenes have retention times t_R: 6.735 min (Remdesivir), 6.915 min (Nevirapine), 7.327 min (Vesatolimod), 5.873 min (Bictegravir), 12.825 min (Emtricitabine), 3.573 min (Tenofovir), 6.040 min (**CMPO**), 3.943 min **(TCMPO)**, 3.543 min (**CEPO**) (*SI File*, **Figures S5**, **S6**).

Calixarenes **CMPO**, **TCPO**, and **CEPO** were characterized by linear adsorption isotherms (**Figures S7**, **S8**, **S9**), which indicated their reverse adsorption on the surface of the Zorbax CN column. The addition of the calixarenes to the mobile phase reduces the retention time t_R of the antiviral drugs. The linear dependence of the drug parameter $1/k'$ on the concentration of calixarenes in the mobile phase (**Figures 2**, **3**, **4**) indicates the formation of supramolecular host-guest complexes with the stoichiometry of 1:1.

The stability constants of the complexes K_A (1100–12000 M^{-1}) calculated by formula (1), and the values of the Gibbs free energies $-\Delta G$ (4.20–5.30 kcal×mol^{-1}) calculated by the equation $\Delta G = -RT \times \ln K_A$ are given in **Table 1**. The stability constants K_A are rather close to the stability constant of the 1:1 complex of the calix[4]arene-sulfonic acid with an antiretroviral drug Tenofovir disoproxil fumarate determined by the UV-Vis spectroscopy in the DMSO solution [29].

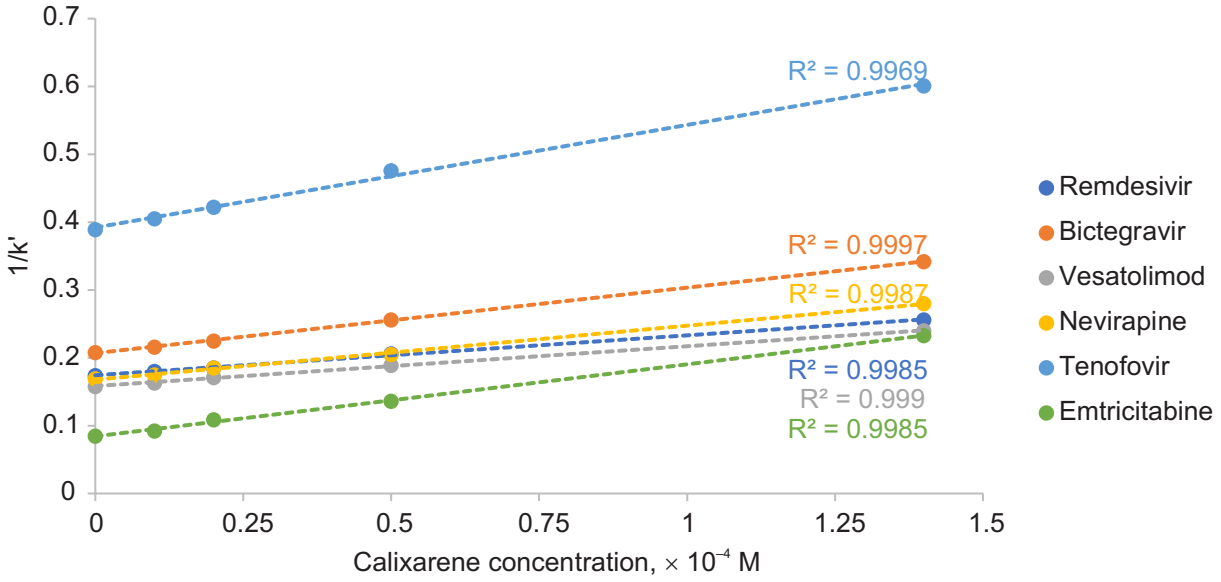

Figure 2. The dependence of $1/k'$ values of the antiviral drugs on the concentration of **CMPO** in the mobile phase

ISSN 2308-8303 (Print) / 2518-1548 (Online)

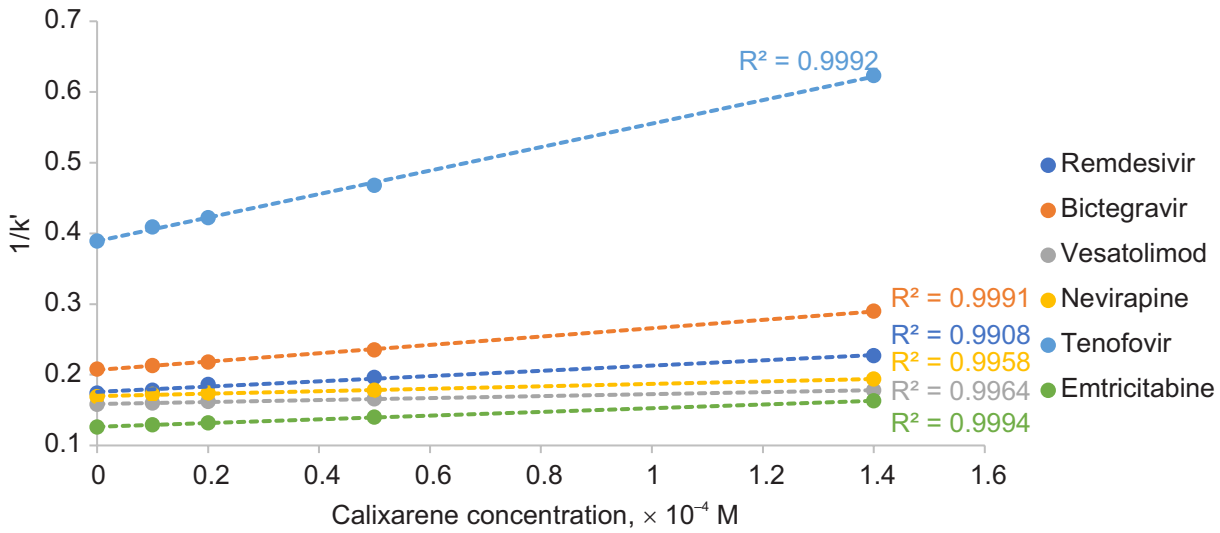

Figure 3. The dependence of 1/*k'* values of the antiviral drugs on the concentration of **TCMPO** in the mobile phase

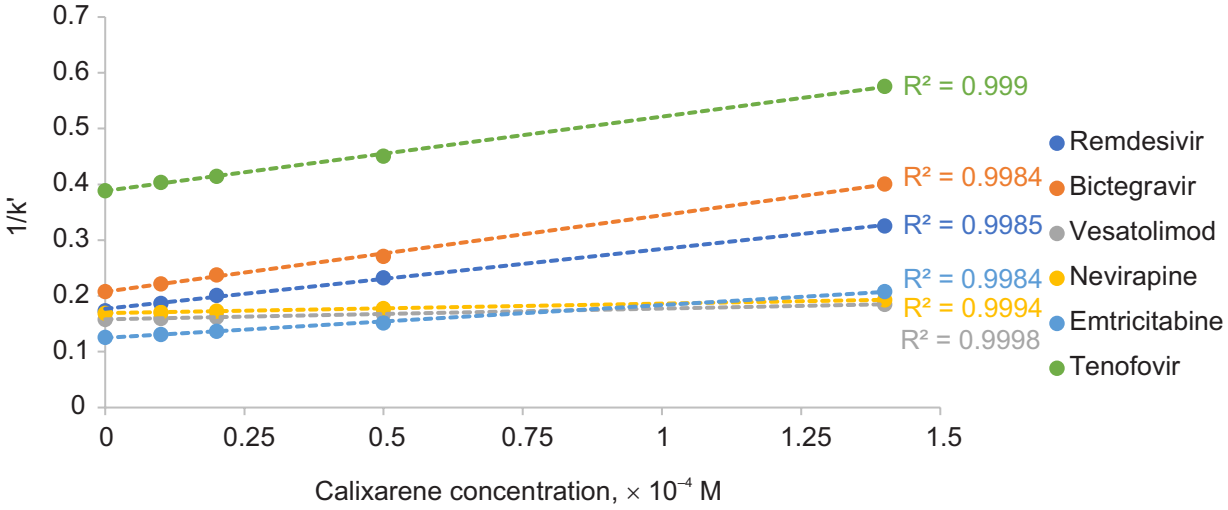

Figure 4. The dependence of 1/*k'* values of the antiviral drugs on the concentration of **CEPO** in the mobile phase

The values of the stability constants K_A and Gibbs free energies ΔG depend on the structure of the calixarene host and the antiviral drug guest and decrease in the order:

Emtricitabine > Nevirapine > Bictegravir > Tenofovir > Vesatolimod > Remdesivir

for complexes with **CMPO**;

Emtricitabine > Tenofovir > Remdesivir > Bictegravir > Nevirapine > Vesatolimod

for complexes with **TCPO**; and

Emtricitabine > Remdesivir > Tenofovir > Bictegravir > Vesatolimod > Nevirapine

for complexes with **CEPO**.

Table 1. Stability constants K_A M^{-1}, (RSD %), and Gibbs free energies ΔG kcal×mol^{-1} of the complexes of **CMPO, TCMPO** and **CEPO** with antiviral drugs

Antiviral drug	CMPO		TCMPO		CEPO	
	K_A	ΔG	K_A	ΔG	K_A	ΔG
Remdesivir	3400 (27)	4.81	2600 (28)	4.65	7050 (32)	5.24
Nevirapine	4300 (14)	4.95	1340 (11)	4.26	1100 (28)	4.15
Vesatolimod	3980 (17)	4.90	1200 (24)	4.20	1250 (23)	4.20
Bictegravir	4300 (18)	4.95	2230 (19)	4.56	2560 (17)	4.64
Emtricitabine	12000 (16)	5.55	7530 (22)	5.30	7800 (18)	5.30
Tenofovir	4200 (21)	4.93	4440 (18)	4.97	3450 (16)	4.82

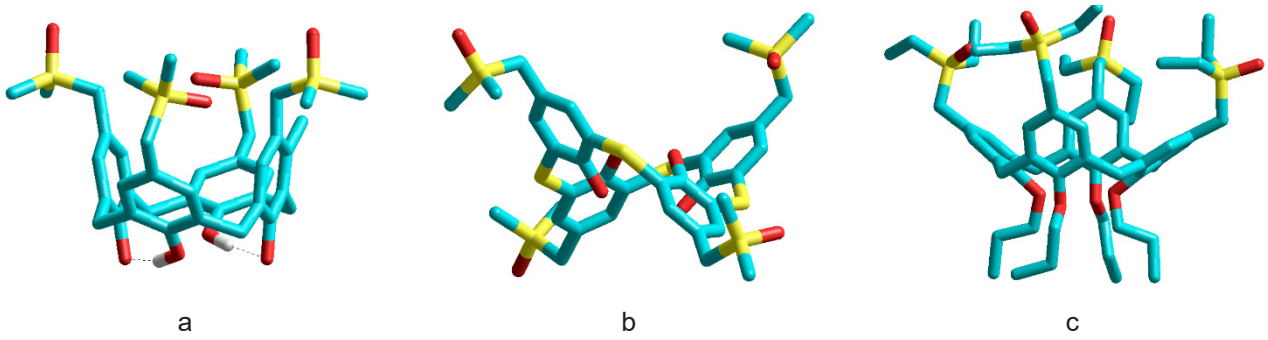

Figure 5. Energy-minimized molecular structures of **CMPA** (a), **TCMPO** (b), and **CEPO** (c)

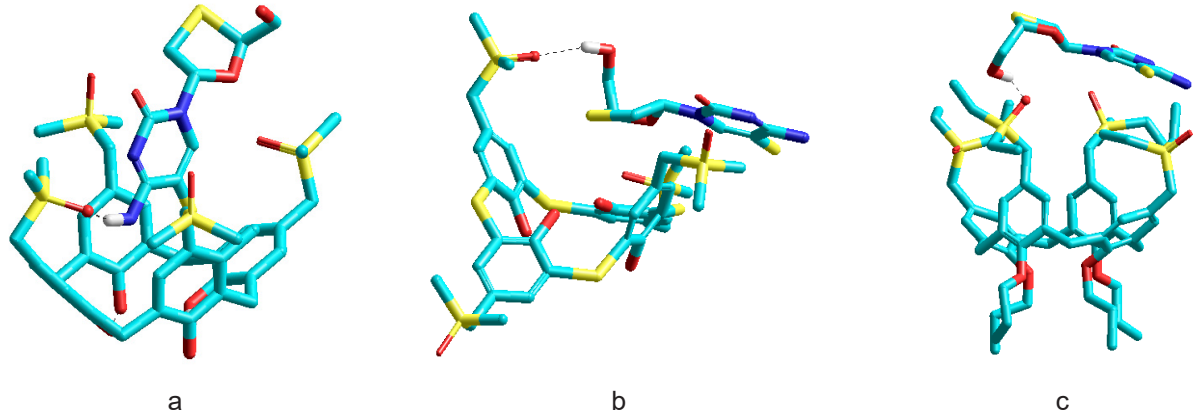

Figure 6. Energy-minimized molecular structures of supramolecular complexes **CMPA**×Emtricitabine (**a**), **TCMPO**×Emtricitabine (**b**) and **CEPO**×Emtricitabine (**c**)

The dependence of the stability constants on the structure of the calixarene and the antiviral agent is complex and can be determined by hydrogen bonds, van der Waals forces, solvatophobic, and other non-covalent interactions. To understand the nature of the complex formation, the structures of the calixarenes and their complexes with molecules of antiviral agents were energetically minimized. According to energy minimization data, **CMPO** and **CEPO** molecules exist in the *cone*-shaped conformations stabilized by strong intramolecular hydrogen bonds (δ_{OH} = 9.61 ppm) or voluminous propyl groups, respectively, which restrict rotation of the benzene ring through the macrocyclic annulus. The **TCMPO** molecule with rather weak intramolecular hydrogen bonds O-H···O-H (δ_{OH} = 4.10 ppm) is unable to stabilize the *cone* conformation and exists in the symmetrical conformation *1,3-alternate* (**Figure 5**).

Energy-minimized structures of the most stable complexes **CMPA** × Emtricitabine (a), **TCMPO** × Emtricitabine (b) and **CEPO** × Emtricitabine (c) (**Table 1**) are presented in **Figure 6**. According to the calculation, the calixarenes form the exo-complexes with the large and branched molecule Emtricitabine hanging over the upper rim of the macrocycle. The complexes are stabilized by intermolecular hydrogen bonds of the proton acceptor groups $Me_2P{=}O$ of the calixarenes with the amino group (**Figure 6a**) or the methylol group (**Figures 6b** and **6c**) of Emtricitabine.

Conclusions

The stability constants K_A (1100–12000 M^{-1}) of the supramolecular host-guest complexes between tetrahydroxycalix[4]arene-methyldimethylphosphine oxide (**CMPO**), tetrahydroxythiacalix[4]arene-methyldimethylphosphine oxide (**TCMPO**), and tetrapropoxycalix[4]arene-methyldiethylphosphine oxide (**CEPO**) with active pharmaceutical ingredients of antiviral drugs Remdesivir, Nevirapine, Vesatolimod, Bictegravir, Emtricitabine and Tenofovir in the water medium depend on the structures of the calixarene and the antiviral drug.

According to the energy minimization calculation, **CMPO** and **CEPO** molecules exist in the *cone* conformations stabilized by intramolecular hydrogen bonds or voluminous propyl groups, respectively, which restrict the rotation of the benzene ring through the macrocyclic annulus.

ISSN 2308-8303 (Print) / 2518-1548 (Online)

The **TCMPO** molecule, having rather weak intramolecular hydrogen bonds O-H···O-H, exists in the symmetrical conformation *1,3-alternate*.

Quantum-chemical calculations show that the calixarene-phosphine oxides form supramolecular complexes with molecules of the antiviral drugs. These complexes are stabilized by intermolecular hydrogen bonds between the proton acceptor P=O groups and the proton donor groups of the drugs.

Thus, the synthetically available water-soluble calixarene-phosphine oxides **CMPO**, **CEPO**, and **TCMPO** have the potential for application in formulations of antiviral drugs and in the creation of vectors for their delivery systems.

■ Acknowledgements

S.A.I. thanks for the scholarship for this work received in the framework of the Erasmus+ Program funded by the University of Seville within the Agreement on Academic, Scientific and Cultural Cooperation signed by the University of Seville (Spain) and the Institute of Organic Chemistry of the National Academy of Sciences of Ukraine (Ukraine).

■ References

1. Gupta, R. K.; Van De Vijver, D. A. M. C.; Manicklal, S.; Wainberg, M. A. Evolving Uses of Oral Reverse Transcriptase Inhibitors in the HIV-1 Epidemic: From Treatment to Prevention. *Retrovirology* **2013**, *10* (1), 82. https://doi.org/10.1186/1742-4690-10-82.
2. Arts, E. J.; Hazuda, D. J. HIV-1 Antiretroviral Drug Therapy. *Cold Spring Harbor Perspect. Med.* **2012**, *2* (4), a007161–a007161. https://doi.org/10.1101/cshperspect.a007161.
3. Margolis, A. M.; Heverling, H.; Pham, P. A.; Stolbach, A. A Review of the Toxicity of HIV Medications. *J. Med. Toxicol.* **2014**, *10* (1), 26–39. https://doi.org/10.1007/s13181-013-0325-8.
4. Paik, S. Fatal Nevirapine-Induced Toxic Epidermal Necrolysis in a HIV Infected Patient. *J. Clin. Diagn. Res.* **2016**. https://doi.org/10.7860/JCDR/2016/16360.7415.
5. *Calixarenes and Beyond*; Neri, P., Sessler, J. L., Wang, M.-X., Eds.; Springer International Publishing: Cham, 2016. https://doi.org/10.1007/978-3-319-31867-7.
6. Vicens, J.; Harrowfield, J. M., Eds. *Calixarenes in the Nanoworld*; Springer: Dordrecht, 2007.
7. Liu, Z.; Dai, X.; Sun, Y.; Liu, Y. Organic Supramolecular Aggregates Based on Water-soluble Cyclodextrins and Calixarenes. *Aggregate* **2020**, *1* (1), 31–44. https://doi.org/10.1002/agt2.3.
8. Español, E. S.; Villamil, M. M. Calixarenes: Generalities and Their Role in Improving the Solubility, Biocompatibility, Stability, Bioavailability, Detection, and Transport of Biomolecules. *Biomolecules* **2019**, *9* (3), 90. https://doi.org/10.3390/biom9030090.
9. Rodik, R. V.; Boyko, V. I.; Kalchenko, V. I. Calixarenes in Biotechnology and Bio-Medical Research. In *Frontiers in Medicinal Chemistry*; Atta-ur-Rahman, Choudhary, M. I., Reitz, A. B., Eds.; Bentham Science Publishers, 2016; pp 206–301. https://doi.org/10.2174/9781681081755116080008.
10. Pan, Y.; Hu, X.; Guo, D. Biomedical Applications of Calixarenes: State of the Art and Perspectives. *Angew. Chem. Int. Ed.* **2021**, *60* (6), 2768–2794. https://doi.org/10.1002/anie.201916380.
11. Fan, X.; Guo, X. Development of Calixarene-Based Drug Nanocarriers. *J. Mol. Liq.* **2021**, *325*, 115246. https://doi.org/10.1016/j.molliq.2020.115246.
12. Bai, H.; Wang, J.; Li, Z.; Tang, G. Macrocyclic Compounds for Drug and Gene Delivery in Immune-Modulating Therapy. *Int. J. Mater. Sci.* **2019**, *20* (9), 2097. https://doi.org/10.3390/ijms20092097.
13. Baldini, L.; Casnati, A.; Sansone, F. Multivalent and Multifunctional Calixarenes in Bionanotechnology. *Eur. J. Org. Chem.* **2020**, *2020* (32), 5056–5069. https://doi.org/10.1002/ejoc.202000255.
14. Ostos, F. J.; Lebrón, J. A.; López-Cornejo, P.; López-López, M.; García-Calderón, M.; García-Calderón, C. B.; Rosado, I. V.; Kalchenko, V. I.; Rodik, R. V.; Moyá, M. L. Self-Aggregation in Aqueous Solution of Amphiphilic Cationic Calix[4]Arenes. Potential Use as Vectors and Nanocarriers. *J. Mol. Liq.* **2020**, *304*, 112724. https://doi.org/10.1016/j.molliq.2020.112724.
15. Lebrón, J. A.; López-López, M.; García-Calderón, C. B.; V. Rosado, I.; Balestra, F. R.; Huertas, P.; Rodik, R. V.; Kalchenko, V. I.; Bernal, E.; Moyá, M. L.; López-Cornejo, P.; Ostos, F. J. Multivalent Calixarene-Based Liposomes as Platforms for Gene and Drug Delivery. *Pharmaceutics* **2021**, *13* (8), 1250. https://doi.org/10.3390/pharmaceutics13081250.
16. Perret, F.; Mazzorana, M.; Shahgaldian, P.; Coleman, A. W. First step in the study of the cellular toxicity of the calixarene. International Symposium on Supramolecular Chemistry XI, Fukuoka, 2000; PB-26, 387.
17. Da Silva, E.; Shahgaldian, P.; Coleman, A. W. Haemolytic Properties of Some Water-Soluble Para-Sulphonato-Calix-[n]-Arenes. *Int. J. Pharm.* **2004**, *273* (1–2), 57–62. https://doi.org/10.1016/j.ijpharm.2003.12.008.
18. Coleman, A. W.; Jebors, S.; Cecillon, S.; Perret, P.; Garin, D.; Marti-Battle, D.; Moulin, M. Toxicity and Biodistribution of Para-Sulfonato-Calix[4]Arene in Mice. *New J. Chem.* **2008**, *32* (5), 780. https://doi.org/10.1039/b718962a.
19. Chernyshenko, V. O.; Korolova, D. S.; Nikolaienko, T. V.; Dosenko, V. E.; Pashevin, D. O.; Kalchenko, V. I.; Cherenok, S. O.; Khranovska, N. N.; Garmanchuk, L. V.; Lugovskoy, E. V.; Komisarenko, S. V. Calix[4]Arene C-145 Effects on Cellular Haemostasis. Biotechnol. Acta 2016, 9 (3), 37–43. https://doi.org/10.15407/biotech9.03.037.
20. Shahgaldian, P.; Da Silva, E.; Coleman, A. W. A First Approach to the Study of Calixarene Solid Lipid Nanoparticle (SLN) Toxicity. *J. Inclusion Phenom.* **2003**, *46* (3–4), 175–177. https://doi.org/10.1023/A:1026301906487.
21. Dings, R. P. M.; Chen, X.; Hellebrekers, D. M. E. I.; Van Eijk, L. I.; Zhang, Y.; Hoye, T. R.; Griffioen, A. W.; Mayo, K. H. Design of Nonpeptidic Topomimetics of Antiangiogenic Proteins With Antitumor Activities. *JNCI, J. Natl. Cancer Inst.* **2006**, *98* (13), 932–936. https://doi.org/10.1093/jnci/djj247.
22. Perret, F.; Lazar, A. N.; Coleman, A. W. Biochemistry of the Para-Sulfonato-Calix[n]Arenes. *Chem. Commun.* **2006**, No. 23, 2425. https://doi.org/10.1039/b600720c.
23. Galindo-Murillo, R.; Olmedo-Romero, A.; Cruz-Flores, E.; Petrar, P. M.; Kunsagi-Mate, S.; Barroso-Flores, J. Calix[n]Arene-Based Drug Carriers: A DFT Study of Their Electronic Interactions with a Chemotherapeutic Agent Used against Leukemia. *Comput. Theor. Chem.* **2014**, *1035*, 84–91. https://doi.org/10.1016/j.comptc.2014.03.001.

24. Menon, S. K.; Mistry, B. R.; Joshi, K. V.; Modi, N. R.; Shashtri, D. Evaluation and Solubility Improvement of Carvedilol: PSC[n]Arene Inclusion Complexes with Acute Oral Toxicity Studies. *J. Incl. Phenom. Macrocycl. Chem.* **2012**, *73* (1–4), 295–303. https://doi.org/10.1007/s10847-011-0056-x.
25. Chen, M.-X.; Li, T.; Peng, S.; Tao, D. Supramolecular Nanocapsules from the Self-Assembly of Amphiphilic Calixarene as a Carrier for Paclitaxel. *New J. Chem.* **2016**, *40* (12), 9923–9929. https://doi.org/10.1039/C6NJ01986B.
26. Zhao, Q.-H.; Chen, C.-P.; Pang, T.-T.; Du, L.-M.; Li, Y.; Xie, J.-H.; Fu, Y.-L. Investigated the Supramolecular Interaction of Tramadol Hydrochloride with P-Sulfonated Calix[4,6,8]Arene. *J. Chil. Chem. Soc.* **2015**, *60* (4), 2659–2663. https://doi.org/10.4067/S0717-97072015000400007.
27. Wang, Y.-X.; Guo, D.-S.; Duan, Y.-C.; Wang, Y.-J.; Liu, Y. Amphiphilic P-Sulfonatocalix[4]Arene as "Drug Chaperone" for Escorting Anticancer Drugs. *Sci. Rep.* **2015**, *5* (1), 9019. https://doi.org/10.1038/srep09019.
28. Yang, W.; De Villiers, M. M. The Solubilization of the Poorly Water Soluble Drug Nifedipine by Water Soluble 4-Sulphonic Calix[n]Arenes. *Eur. J. Pharm. Biopharm.* **2004**, *58* (3), 629–636. https://doi.org/10.1016/j.ejpb.2004.04.010.
29. Jarange, A. B.; Patil, S. V.; Malkhede, D. D.; Deodhar, S. M.; Nandre, V. S.; Athare, S. V.; Kodam, K. M.; Gejji, S. P. P-Sulfonatocalixarene versus p-Thiasulfonatocalixarene: Encapsulation of Tenofovir Disoproxil Fumarate and Implications to ESI-MS, HPLC, NMR, DFT and Anti-MRSA Activities. *J. Incl. Phenom. Macrocycl. Chem.* **2021**, *99* (1–2), 43–59. https://doi.org/10.1007/s10847-020-01022-w.
30. Tauran, Y.; Coleman, A. W.; Perret, F.; Kim, B. Cellular and in Vivo Biological Activities of the Calix[n]Arenes. *Curr. Org. Chem.* **2015**, *19* (23), 2250–2270. https://doi.org/10.2174/1385272819666150608222114.
31. Kosterin, S. O.; Kalchenko, V. I.; Veklich, T. O.; Babich, L. G.; Shlikov, S. G. *Calix[4]arenes as modulators of ATP-hydrolase systems of smooth muscle cells*. Naukova Dumka: Kyiv, 2019.
32. Trush, V. V.; Kharchenko, S. G.; Tanchuk, V. Yu.; Kalchenko, V. I.; Vovk, A. I. Phosphonate Monoesters on a Thiacalix[4]Arene Framework as Potential Inhibitors of Protein Tyrosine Phosphatase 1B. *Org. Biomol. Chem.* **2015**, *13* (33), 8803–8806. https://doi.org/10.1039/C5OB01247C.
33. Bayrakcı, M.; Ertul, Ş.; Yilmaz, M. Phase Solubility Studies of Poorly Soluble Drug Molecules by Using *O*-Phosphorylated Calixarenes as Drug-Solubilizing Agents. *J. Chem. Eng. Data* **2012**, *57* (1), 233–239. https://doi.org/10.1021/je200992c.
34. Perret, F.; Nishihara, M.; Takeuchi, T.; Futaki, S.; Lazar, A. N.; Coleman, A. W.; Sakai, N.; Matile, S. Anionic Fullerenes, Calixarenes, Coronenes, and Pyrenes as Activators of Oligo/Polyarginines in Model Membranes and Live Cells. *J. Am. Chem. Soc.* **2005**, *127* (4), 1114–1115. https://doi.org/10.1021/ja043633c.
35. Kalchenko, O. I.; Rozhenko, A. B.; Cherenok, S. O.; Selikhova, A. I.; Drapailo, A. B.; López-Cornejo, P.; Kalchenko, V. I. Stability Constants and DFT Calculations of Anionic Calixarene Complexes with Antiretroviral Drugs Tenofovir and Emtricitabine. *J. Incl. Phenom. Macrocycl. Chem.* **2025**, *105* (5–6), 297–310. https://doi.org/10.1007/s10847-024-01273-x.
36. Rodik, R. V.; Cherenok, S. O.; Postupalenko, V. Y.; Oncul, S.; Brusianska, V.; Borysko, P.; Kalchenko, V. I.; Mely, Y.; Klymchenko, A. S. Anionic Amphiphilic Calixarenes for Peptide Assembly and Delivery. *J. Colloid Interface Sci.* **2022**, *624*, 270–278. https://doi.org/10.1016/j.jcis.2022.05.124.
37. *Organophosphorus Chemistry: Novel Developments*; Keglevich, G., Ed.; De Gruyter, 2018. https://doi.org/10.1515/9783110535839.
38. Finkbeiner, P.; Hehn, J. P.; Gnamm, C. Phosphine Oxides from a Medicinal Chemist's Perspective: Physicochemical and *in Vitro* Parameters Relevant for Drug Discovery. *J. Med. Chem.* **2020**, *63* (13), 7081–7107. https://doi.org/10.1021/acs.jmedchem.0c00407.
39. Fedyk, A.; Slobodyanyuk, E. Y.; Stotska, O.; Vashchenko, B. V.; Volochnyuk, D. M.; Sibgatulin, D. A.; Tolmachev, A. A.; Grygorenko, O. O. Heteroaliphatic Dimethylphosphine Oxide Building Blocks: Synthesis and Physico-Chemical Properties. *Eur. J. Org. Chem.* **2021**, *2021* (47), 6591–6603. https://doi.org/10.1002/ejoc.202100581.
40. Fedyk, A. V.; Chalyk, B. A. Synthesis of Functionalized 4,5-Dihydroisoxazoles Decorated with the Dimethylphosphinoyl Group. *J. Org. Pharm. Chem.* **2023**, *21* (2), 41–52. https://doi.org/10.24959/ophcj.23.283988.
41. National Cancer Institute. FDA grants Brigatinib accelerated approval for metastatic non-small cell lung cancer. https://www.cancer.gov/news-events/cancer-currents-blog/2017/brigatinib-fda-lung-cancer (accessed Jun 23, 2025).
42. Uchibori, K.; Inase, N.; Araki, M.; Kamada, M.; Sato, S.; Okuno, Y.; Fujita, N.; Katayama, R. Brigatinib Combined with Anti-EGFR Antibody Overcomes Osimertinib Resistance in EGFR-Mutated Non-Small-Cell Lung Cancer. *Nat. Commun.* **2017**, *8* (1), 14768. https://doi.org/10.1038/ncomms14768.
43. Yu, H.; Yang, H.; Shi, E.; Tang, W. Development and Clinical Application of Phosphorus-Containing Drugs. *Med. Drug Discovery* **2020**, *8*, 100063. https://doi.org/10.1016/j.medidd.2020.100063.
44. Laurence, C.; Brameld, K. A.; Graton, J.; Le Questel, J.-Y.; Renault, E. The p K_{BHX} Database: Toward a Better Understanding of Hydrogen-Bond Basicity for Medicinal Chemists. *J. Med. Chem.* **2009**, *52* (14), 4073–4086. https://doi.org/10.1021/jm801331y.
45. Kalchenko, O. I.; Rozhenko, A. B.; Cherenok, S. O.; Selikhova, A. I.; Suikov, S. Yu.; Kyrylchuk, A. A.; Kalchenko, V. I. Complexation of Water-Soluble Phosphorylated Calixarenes with Uracils. Stability Constants and DFT Study of the Supramolecular Complexes. *J. Incl. Phenom. Macrocycl. Chem.* **2023**, *103* (9–10), 369–383. https://doi.org/10.1007/s10847-023-01198-x.
46. Armarego, W. L. F. *Purification of Laboratory Chemicals*, 8th Edition; Butterworth-Heinemann: Amsterdam, 2017.
47. Iwamoto, K.; Araki, K.; Shinkai, S. Conformations and Structures of Tetra-O-Alkyl-p-Tert-Butylcalix[4]Arenes. How Is the Conformation of Calix[4]Arenes Immobilized? *J. Org. Chem.* **1991**, *56* (16), 4955–4962. https://doi.org/10.1021/jo00016a027.
48. Hypercube Downloads http://www.hypercubeusa.com/Download/tabid/357/Default.aspx (accessed May 11, 2025).
49. Zielenkiewicz, W.; Marcinowicz, A.; Poznański, J.; Cherenok, S.; Kalchenko, V. Complexation of Isoleucine by Phosphorylated Calix[4]Arene in Methanol Followed by Calorimetry, NMR and UV–VIS Spectroscopies, and Molecular Modeling Methods. *J. Mol. Liq.* **2005**, *121* (1), 8–14. https://doi.org/10.1016/j.molliq.2004.08.031.
50. Yakovenko, A. V.; Boyko, V. I.; Kalchenko, V. I.; Baldini, L.; Casnati, A.; Sansone, F.; Ungaro, R. *N*- Linked Peptidocalix[4]Arene Bisureas as Enantioselective Receptors for Amino Acid Derivatives. *J. Org. Chem.* **2007**, *72* (9), 3223–3231. https://doi.org/10.1021/jo062410x.
51. Acharya, A.; Ramanujam, B.; Chinta, J. P.; Rao, C. P. 1,3-Diamido-Calix[4]Arene Conjugates of Amino Acids: Recognition of −COOH Side Chain Present in Amino Acids, Peptides, and Proteins by Experimental and Computational Studies. *J. Org. Chem.* **2011**, *76* (1), 127–137. https://doi.org/10.1021/jo101759f.
52. Li, W. Y.; Li, H.; Zhang, G. M.; Chao, J. B.; Ling, L. X.; Shuang, S. M.; Dong, C. Interaction of Water-Soluble Calix[4]Arene with l-Tryptophan Studied by Fluorescence Spectroscopy. *J. Photochem. Photobiol., A* **2008**, *197* (2–3), 389–393. https://doi.org/10.1016/j.jphotochem.2008.02.002.
53. Kim, L.; Hamdi, A.; Stancu, A. D.; Souane, R.; Mutihac, L.; Vicens, J. Selective Membrane Transport of Amino Acids by Functionalised Calix[4]Arenes. *J. Incl. Phenom. Macrocycl. Chem.* **2010**, *66* (1–2), 55–59. https://doi.org/10.1007/s10847-009-9622-x.
54. Stone, M. M.; Franz, A. H.; Lebrilla, C. B. Non-Covalent Calixarene-Amino Acid Complexes Formed by MALDI-MS. *J. Am. Soc. Mass Spectrom.* **2002**, *13* (8), 964–974. https://doi.org/10.1016/S1044-0305(02)00417-8.

ISSN 2308-8303 (Print) / 2518-1548 (Online)

55. Chen, H.; Gu, L.; Yin, Y.; Koh, K.; Lee, J. Molecular Recognition of Arginine by Supramolecular Complexation with Calixarene Crown Ether Based on Surface Plasmon Resonance. *Int. J. Mater. Sci.* **2011**, *12* (4), 2315–2324. https://doi.org/10.3390/ijms12042315.
56. Lipkowski, J.; Kalchenko, O. I.; Slowikowska, J.; Kalchenko, V. I.; Lukin, O. V.; Markovsky, L. N.; Nowakowski, R. Host-Guest Interactions of Calix[4]Resorcinarenes with Benzene Derivatives in Conditions of Reversed-Phase High-Performance Liquid Chromatography. Determination of Stability Constants. *J. Phys. Org. Chem.* **1998**, *11* (6), 426–437. https://doi.org/10.1002/(SICI)1099-1395(199806)11:6%253C426::AID-POC963%253E3.0.CO;2-R.
57. Kalchenko, O. I.; Lipkowsk, J.; Kalchenko, V. I.; Vysotsky, M. A.; Markovsky, L. N. Effect of Octakis(Diethoxyphosphoryloxy)-Tert-Butyl-Calix[8]Arene in Mobile Phase on the Reversed-Phase Retention Behavior of Aromatic Compounds: Host-Guest Complex Formation and Stability Constants Determination. *J. Chromatogr. Sci.* **1998**, *36* (5), 269–273. https://doi.org/10.1093/chromsci/36.5.269.
58. Kalchenko, O. I.; Da Silva, E.; Coleman, A. W. Determination of the Stability Constants of Inclusion Complexes of P-H-37-(2-Carboxy-Methyloxy)-Calix-[6]-Arene and p-Sulphonato-37-(2-Carboxy-Methyloxy)-Calix-[6]-Arene with 15 Amino Acids by RP-HPLC. *J. Inclusion Phenom.* **2002**, *43* (3–4), 305–310. https://doi.org/10.1023/A:1021203505307.
59. Solovyov, A. V.; Cherenok, S. O.; Kalchenko, O. I.; Atamas, L. I.; Kazantseva, Z. I.; Koshets, I. A.; Tsymbal, I. F.; Kalchenko, V. I. Synthesis and Complexation of Amphiphilic Calix[4]Arene Phosphonates with Organic Molecules in Solutions and Langmuir-Blodgett Films. *J. Mol. Liq.* **2011**, *159* (2), 117–123. https://doi.org/10.1016/j.molliq.2010.12.007.

Information about the authors:
Olga I. Kalchenko, Ph.D. in Chemistry, Engineer of the Department of Physicochemical Research, Institute of Organic Chemistry of the National Academy of Sciences of Ukraine, https://orcid.org/0000-0002-3364-4625.
Andrii B. Drapailo, Ph.D. in Chemistry, Senior research fellow of the Department of Macrocyclic Compounds, Institute of Organic Chemistry of the National Academy of Sciences of Ukraine, https://orcid.org/0000-0002-8701-1380.
Serhii O. Cherenok (*corresponding author*), Dr.Sci. in Chemistry, Head of the Department of Macrocyclic Compounds, Institute of Organic Chemistry of the National Academy of Sciences of Ukraine, https://orcid.org/0000-0003-1736-3062; e-mail for correspondence cherenokserhii@gmail.com.
Anna I. Selikhova, Ph.D. student of the Department of Macrocyclic Compounds, Institute of Organic Chemistry of the National Academy of Sciences of Ukraine, https://orcid.org/0000-0001-6773-8796.
Pilar López-Cornejo, Dr.Sci. in Chemistry, Professor of the Department of Physical Chemistry, Faculty of Chemistry, University of Seville, https://orcid.org/0000-0002-5825-9483.
Vitaly I. Kalchenko, Dr.Sci. in Chemistry, Professor, Principal Research Fellow of the Department of Macrocyclic Compounds, Institute of Organic Chemistry of the National Academy of Sciences of Ukraine, https://orcid.org/0000-0002-0325-7544.

Journal of Organic and Pharmaceutical Chemistry

Original Research

OPEN ACCESS
Freely available online on
http://ophcj.nuph.edu.ua

UDC 547.678.3; 547.812; 547.752; 535.34; 544.174.2

I. V. Kurdiukova, V. V. Kurdyukov, A. V. Kulinich
Institute of Organic Chemistry of the National Academy of Sciences of Ukraine,
5 Akademika Kukharya St., 02094 Kyiv, Ukraine

The Synthesis and Spectral Properties of Merocyanine Dyes Based on 9*H*-Fluorene-2,7-Dicarbonitrile

Dedicated to the cherished memory of Academician Alexander A. Ishchenko, a brilliant mentor and lifelong friend

Abstract
Di-, tetra-, and hexamethine merocyanine dyes bearing donor heterocyclic end groups of different electron-donating abilities and the 9*H*-fluorene-2,7-dicarbonitrile moiety as the acceptor end group have been synthesized. Their UV/Vis absorption spectra have been studied in solvents of varying polarity, and their electronic nature and vertical transitions have been investigated via (TD)-DFT calculations. The results indicate that the electronic structure of these merocyanines approaches the neutral polyene limit, becoming increasingly polyene-like in low-polarity solvents and upon increasing the polymethine chain length, which indicates the weak electron-acceptor ability of the 9*H*-fluorene-2,7-dicarbonitrile moiety. Nevertheless, longer vinylogs, especially those containing the 4*H*-pyran donor end group, exhibit the inverse solvatochromic behavior, which is highly unusual for such weakly dipolar merocyanines. A possible explanation for this effect has been proposed although its rigorous verification would require higher-level quantum-chemical calculations with solvent effects taken into account.
Keywords: merocyanines; fluorene; electronic absorption spectra; solvatochromism; TD-DFT calculations

І. В. Курдюкова, В. В. Курдюков, А. В. Кулініч
Інститут органічної хімії Національної академії наук України,
вул. Академіка Кухаря, 5, м. Київ, 02094, Україна

Синтез і спектральні властивості мероціанінів на основі 9*H*-флуорен-2,7-дикарбонітрилу

Анотація
Синтезовано ди-, тетра- та гексаметинові мероціанінові барвники, що містять донорні гетероциклічні кінцеві групи з різною електронодонорністю та фрагмент 9*H*-флуорен-2,7-дикарбонітрилу як акцепторну кінцеву групу. Їхні електронні спектри поглинання досліджено в розчинниках різної полярності, а електронну природу та електронні переходи проаналізовано за допомогою (TD)-DFT розрахунків. Отримані результати демонструють, що електронна структура цих мероціанінів близька до структури неполярного полієну, стаючи ще більш полієноподібною в малополярних розчинниках та зі збільшенням довжини поліметинового ланцюга, що свідчить про слабку електроноакцепторність фрагмента 9*H*-флуорен-2,7-дикарбонітрилу. Водночас довші вінілоги, особливо ті, що містять 4*H*-піран як донорну кінцеву групу, виявляють обернену сольватохромію, що є вкрай нетиповим для таких малополярних мероціанінів. Запропоновано можливе пояснення цього ефекту, однак його пильна перевірка потребуватиме квантово-хімічних обчислень методами вищого рівня та з урахуванням впливу розчинника.
***Ключові слова*:** мероціаніни; флуорен; електронні спектри поглинання; сольватохромія; TD-DFT розрахунки

Citation: Kurdiukova, I. V.; Kurdyukov, V. V.; Kulinich, A. V. The Synthesis and Spectral Properties of Merocyanine Dyes Based on 9*H*-Fluorene-2,7-Dicarbonitrile. *Journal of Organic and Pharmaceutical Chemistry* **2025**, *23* (4), 22–32.
https://doi.org/10.24959/ophcj.25.350444
Received: *2 October 2025*; **Revised:** *15 November 2025*; **Accepted:** *23 November 2025*

Funding: The authors received no specific funding for this work.
Conflict of interests: The authors have no conflict of interests to declare.

ISSN 2308-8303 (Print) / 2518-1548 (Online)

■ Introduction

Merocyanine dyes, owing to their broad range of practically important properties, such as pronounced solvatochromism, the ability to undergo substantial changes in the dipole moment upon electronic excitation, and the capacity to sensitize various physicochemical and chemical transformations, are increasingly being used in optoelectronics, nonlinear optics, data recording and processing technologies, as well as in medicine and biology [1, 2].

Among these, a special class features merocyanine dyes bearing a fluorene unit with electron-withdrawing substituents (EWGs) as the acceptor end group [3]. It has previously been shown that dyes containing nitro-substituted fluorene moieties exhibit the multi-band absorption in the Vis-NIR range, featuring additional charge-transfer bands at longer wavelengths, which may hamper their potential applications [4]. Therefore, it was of interest to develop analogs incorporating other EWGs capable of the effective conjugation with the TT-electron system of the fluorene core, in particular cyano groups.

A preliminary (TD)-DFT evaluation of the electronic structure and electronic transitions in 9*H*-fluorene-2,7-dicarbonitrile derivatives suggested that, for such merocyanines, the polymethine $S_1^{FC} \leftarrow S_0$ transition is more clearly separated from higher-lying electronic transitions compared with nitro-substituted fluorene dyes. Accordingly, to verify this theoretical prediction, we synthesized and studied a series of merocyanine dyes for the first time incorporating the 9*H*-fluorene-2,7-dicarbonitrile moiety as the acceptor end group.

■ Results and Discussion

Synthesis and Structural Characterization

New merocyanines were synthesized via the Knoevenagel condensation between 9*H*-fluorene-2,7-dicarbonitrile (**1**) and the corresponding heterocyclic aldehydes or hemicyanines, giving two vinylogous series of dyes bearing 1,3,3-trimethyl-2*H*-indole and 2,6-di-*tert*-butyl-4*H*-pyran moieties as the donor end groups. For derivatives containing the more electron-donating indole core, the reaction was carried out under conventional conditions using triethylamine in acetic anhydride. In contrast, for the 2,6-di-*tert*-butyl-4*H*-pyran systems, a stronger base (DBU) and the higher-boiling solvent *N*,*N*-dimethylacetamide (DMAA) were required to increase the reaction rate and improve the yields (**Scheme 1**).

In the ^{1}H NMR spectra of the fluorene-based merocyanines **2**–**4** and **8**–**10** (see the ESI), as is

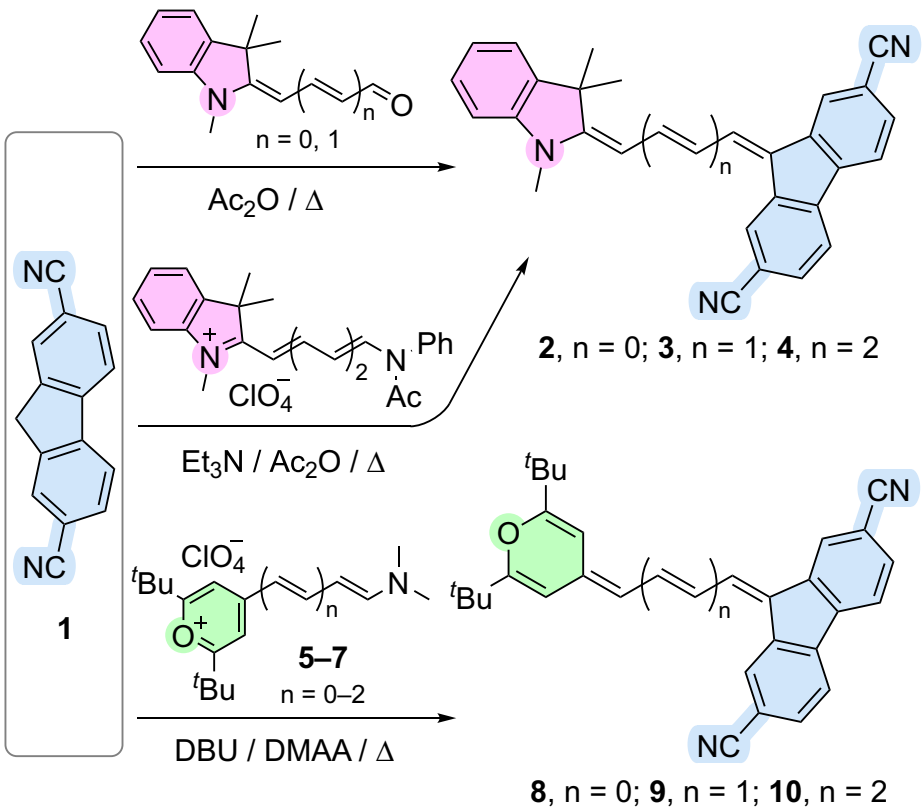

Scheme 1. The synthesis of novel fluorene-based merocyanines

generally the case for polymethines [2], an alternating pattern of chemical shifts is observed for the chain –CH= groups. This alternation reflects the corresponding alternation of the electron density along the polymethine chain. However, for these dyes, its value is lower than for more typical merocyanines. Thus, in compound **4**, the average chemical shift alternation for the polymethine chain protons H2, H3, and H4 is 0.71 ppm. (Counting starts from the donor heterocycle; these specific protons were selected as they were remote from the end groups, and thus not significantly affected by anisotropic end-group effects.) For similar indole-based hexamethines bearing malononitrile or thiobarbiturate acceptor groups, this alternation is equal to 1.00 and 1.11 ppm, respectively [5, 6] (all data recorded in $CDCl_3$).

For the pyran-based merocyanine **10**, the alternation is even smaller (0.55 ppm) and remains nearly unchanged (0.56 ppm) upon switching to highly polar $(CD_3)_2SO$. These data can be interpreted as evidence for a substantial contribution of the nonpolar polyene limiting structure to the electronic structure of the dyes synthesized [7].

This conclusion is further supported by the alternation of $^3J_{HH}$ spin–spin coupling constants in the polymethine chain, which amounts to 1.2 Hz for tetramethines **3** and **9** and increases to 2.2 Hz for hexamethine **10** [for compound **4**, the coupling constant between protons H4 and H5 could not be determined due to signal overlap and higher-order effects within the multiplet].

A decrease in the dipolar character of the merocyanines synthesized with chromophore lengthening is also evident in the series **2**–**4** from the decreasing chemical shift of the NMe group, which for vinylog **4** is 3.24 ppm (for comparison, the corresponding thiobarbituric-acid-acceptor analog exhibits a shift of 3.37 ppm [6]).

A decrease in the dipolar character of the merocyanines synthesized with chromophore lengthening is also evident in the series **2** – **3** – **4** from the decreasing chemical shift of the NMe group, which are 3.48, 3.35, and 3.24 ppm, respectively.

Solvatochromic Behavior

The solvents selected for the study of solvatochromism of the dyes synthesized included low-polarity cyclohexane (cHex; ε_D 2.02, n_D 1.427) and toluene (ε_D 2.37, n_D 1.496), medium-polarity dichloromethane (DCM; ε_D 8.9, n_D 1.424), and two polar non-protogenic solvents, acetonitrile (ε_D 36.2, n_D 1.344; electrophilic) and DMF (ε_D 36.7, n_D 1.430; nucleophilic) [8]. The corresponding spectral characteristics are summarized in **Table 1** (while the UV–Vis spectra of all dyes are provided in the ESI). The Bouguer–Lambert–Beer law is obeyed for merocyanines **2**–**4** and **8**–**10** over the concentration range of 1×10^{-6} to 3×10^{-5} M in all solvents studied, indicating that the recorded spectra arise from molecular (non-aggregated) species. Protogenic solvents (e.g., ethanol and methanol) were excluded from this study owing to the very low solubility of the dyes in these media.

Upon lengthening of the polymethine chain in the series **2**–**4**, broadening of the long-wavelength absorption band and a decrease in its intensity are observed (**Figure 1A**), along with a reduction in the vinylene shifts (**Table 1**). Even in the medium-polarity solvent DCM, the vinylene shifts for pairs **2** – **3** and **3** – **4** are only 42 and 39 nm, respectively. Taken together, these observations indicate, in accordance with the ^{1}H NMR data, that the ground-state electronic structure of merocyanines **2**–**4** is very close to that of a nonpolar polyene.

Table 1. Characteristics of the long-wavelength absorption bands of dyes **2**–**4** and **8**–**10** at 20 °C

Dye	Solvent	λ_{max} [nm]	$\varepsilon\times10^{-4}$ [$M^{-1}\times cm^{-1}$]
2	cHex	**498**; 470	**6.51**; 4.40
	PhMe	509	5.81
	DCM	512	5.77
	MeCN	510	5.53
	DMF	518	5.46
3	cHex	561; **530**	6.12; **7.40**
	PhMe	543	6.45
	DCM	554	6.65
	MeCN	552	6.55
	DMF	562	6.12
4	cHex	611; **580**; 549	3.06; **5.93**; 5.04
	PhMe	585	5.09
	DCM	593	4.98
	MeCN	580	4.89
	DMF	592	4.64
8	cHex	529; **498**; 472	2.69; **4.55**; 3.60
	PhMe	504	4.53
	DCM	512	4.60
	MeCN	508	4.52
	DMF	514	4.44
9	cHex	592; 554; **522**	2.27; 5.77; **6.02**
	PhMe	**556**; 534	**5.51**; 5.31
	DCM	551	5.37
	MeCN	538	5.55
	DMF	546	5.06
10	cHex	648; 598; **567**	1.23; 4.62; **6.17**
	PhMe	569	6.51
	DCM	579	6.27
	MeCN	559	6.34
	DMF	570	5.64

ISSN 2308-8303 (Print) / 2518-1548 (Online)

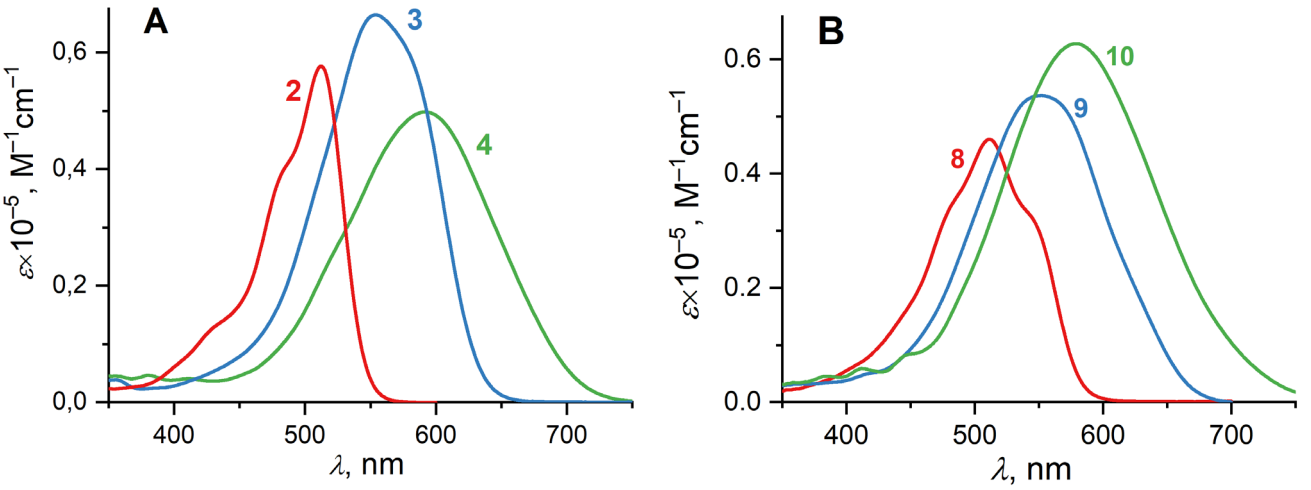

Figure 1. Electronic absorption spectra of dyes **2–4** (A) and **8–10** (B) in dichloromethane

For merocyanines **8–10**, increasing the chromophore length likewise leads to broadening and smoothing of the long-wavelength absorption band (**Figure 1B**). The vinylene shifts in DCM for pairs **8** – **9** and **9** – **10** are even smaller than those observed for the indole-based analogs **2–4**, amounting to 39 and 28 nm, respectively. These values are significantly lower than the typical ~100 nm vinylene shifts characteristic of symmetric cationic and anionic polymethines [9]. Once again, the spectral data for dyes **8–10** indicate that their electronic structure more closely resembles that of typical polyenes.

This conclusion is confirmed by comparison of the absorption ranges of the series **2–4** and **8–10**. Although the 4*H*-pyran moiety as the end group of polymethine dyes has a much greater "effective length" than the indole moiety [10, 11], the absorption maxima of merocyanines **8–10** are matching or even blue-shifted relative to those of their analogs **2–4** (**Table 1**).

Solvatochromic studies of dyes **2–4** and **8–10** revealed low sensitivity to the solvent nature. The position and shape of their long-wavelength absorption bands vary only slightly and not always consistently with increasing polarity. This is evident when comparing their absorption in the medium-polarity DCM and highly polar DMF (**Figure 2**). The only notable exceptions are the spectra in the least polar solvent, cHex, which exhibit a significant hypsochromic shift and a more pronounced fine structure (**Figure 2**, ESI). This striking divergence from just slightly more polar toluene can be attributed to the toluene higher refractive index, inducing a bathochromic shift [12], and the stronger solvation of polymethine chromophores by aromatic solvents via the solute–solvent π–π interactions [13].

Although small and only weakly dependent on the polymethine chain length, the solvatochromism of merocyanines **2–4** is positive (**Table 1**, **Figure 2**A). This effect is most evident for the

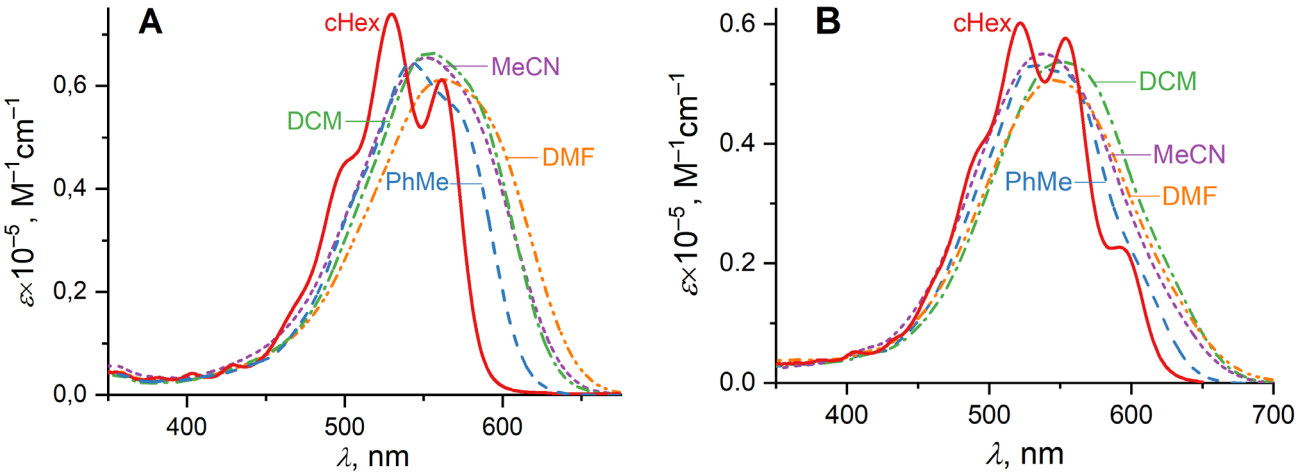

Figure 2. Electronic absorption spectra of dyes **3** (A) and **9** (B) in solvents of varying polarity

toluene–DCM and DCM–DMF solvent pairs, for which the refractive index changes only slightly or even decreases upon going to the more polar solvent [*this point is essential since the hypsochromic shifts observed upon going from DCM to MeCN can indeed be attributed to the decrease in the solvent refractive index* [12]]. In both cases, bathochromic shifts occur with increasing the solvent polarity, except for the longest vinylog **4**, for which the absorption maximum shifts 1 nm hypsochromically upon changing the solvent from DCM to DMF. Notably, the value of the solvatochromic effect, even when expressed on an energy scale (cm^{-1}), is maximal for tetramethine **3** and then decreases for hexamethine **4**. Such behavior may be considered indicative of an increasingly polyene-like nature of these chromophores with increasing the polymethine chain length, as is typical for merocyanines [2] since nonpolar polyenes are known to be insensitive to the solvent polarity, with their solvatochromism being governed entirely by the solvent polarizability [14].

A more intricate solvatochromic behavior is observed for the pyran-based dyes **8–10** (**Table 1**, **Figure 2**B). These compounds exhibit positive a solvatochromism in the toluene–DCM solvent pair, whereas in the DCM–DMF pair the changes in λ_{max} vary from +2 to –6 and then to –9 nm with increasing the polymethine chain length (**Table 1**). Even larger hypsochromic shifts are observed upon changing the solvent from DCM to MeCN; considering their value, these shifts cannot, as in the case of dyes **2–4**, be attributed solely to the lower refractive index of acetonitrile. Taken together, these observations point to the inverse solvatochromism for merocyanines **8–10**, at least for the longer vinylogs.

This result is highly unusual, given that (i) the pyran moiety is a weaker electron-donating end group than indole, and the indole-based analogs **2–4** exhibit a positive solvatochromism; (ii) trends in band shapes, and vinylene shifts indicate a polyene-like electronic structure for both merocyanine series; and (iii) higher vinylogs, due to their decreased dipolarity, typically tend toward a positive solvatochromism even when shorter vinylogs display the inverse behavior [2] rather than the opposite trend observed here.

DFT and TD-DFT Calculations

For all merocyanines **2–4** and **8–10**, the values of the $^3J_{HH}$ spin–spin coupling constants in the polymethine chain indicate the all-*trans* geometry, which is typical for polymethines. Accordingly, this geometry was chosen as the initial guess for the geometry optimization, performed in the vacuum approximation at the DFT-B3LYP/6-31G(d,p) level of theory and followed by frequency calculations to confirm that the located stationary points corresponded to true minima. The same functional and basis set were employed in the TD-DFT calculations of electronic transitions.

Although no symmetry constraints were imposed, the optimized ground-state geometries of the longer vinylogs **3**, **4**, **9**, and **10** were found to be essentially planar, with only negligible deviation from C_S-symmetry (the optimized atomic coordinates are provided in the ESI). Molecules **2** and **7** are more distorted, but even in these cases the interplanar angle between the end groups does not exceed 4.5°.

The proximity of the electronic structure of a merocyanine dye to one of the ideal limiting structures – nonpolar polyene, ideal polymethine or dipolar polyene – can be estimated from the degree of the bond-length (bond-order) alternation in its chromophore [15]. Usually, the bond-length alternation (BLA) and bond-order alternation (BOA) parameters are calculated as the difference between the averaged lengths or orders of formally single and formally double bonds in the "open" part of the polymethine chain (for merocyanines, the formal bond orders correspond to those in the nonpolar polyene limiting structure [7]). The BLA parameter takes positive values for structures in the nonpolar polyene–ideal polymethine range and negative values for those in the ideal polymethine–zwitterionic polyene range [15]; BOA has the opposite sign to BLA.

In the ground state S_0, the bond-length alternation in merocyanines **2–4** and **8–10** lies well within the positive range (**Table 2**), indicating a significant contribution from the nonpolar polyene limiting structure. This observation is in good agreement with the conclusions drawn from experimental ^{1}H NMR and UV–Vis spectral data. The BLA values increase with increasing the polymethine chain length, again correlating with the experimental results and well-established trends for such systems. However, a decrease in BLA is observed when going from indole- to 4*H*-pyran-based derivatives (**Table 2**), which is not consistent with the other results. At present, we do not have a satisfactory explanation for this behavior although it may indicate a case where long-range-corrected functionals, such as CAM-B3LYP or ωB97X, would be more appropriate.

According to the TD-DFT calculations, for all six molecules studied, the longest-wavelength

ISSN 2308-8303 (Print) / 2518-1548 (Online)

Table 2. Some results of the (TD-)DFT-B3LYP/6-31G(d,p) calculations for molecules **2**–**4** and **8**–**10**

Dye	BLA [Å]	$\mu(S_0)$ [Debye]	$\mu(S_1^{FC})$ [Debye]	$\mu(S_2^{FC})$ [Debye]	$S_1^{FC}\leftarrow S_0$		$S_2^{FC}\leftarrow S_0$	
					ΔE [eV]	f	ΔE [eV]	f
2	0.047	5.3	12.3	11.2	2.77	0.599	3.14	0.487
3	0.049	7.3	14.4	17.4	2.56	1.239	2.94	0.372
4	0.050	9.0	16.8	23.1	2.36	1.794	2.81	0.285
8	0.035	6.9	11.6	11.5	2.75	0.809	3.08	0.507
9	0.040	8.9	13.7	17.7	2.52	1.467	2.89	0.400
10	0.043	10.6	16.0	23.4	2.32	2.030	2.76	0.320

electronic transition is an allowed polymethine-type $^1\pi\pi^*$ transition, dominated by the HOMO→LUMO excitation, whose contribution ranges from 80 to 96% and increases for higher vinylogs. The calculated energies of the $S_1^{FC}\leftarrow S_0$ transition (**Table 2**) are in all cases somewhat higher than those estimated from the long-wavelength absorption maxima, which is in good agreement with literature data on the performance of TD-DFT for polymethine systems [16, 17]. This excitation is separated from the $S_2^{FC}\leftarrow S_0$ transition by an energy gap of 0.33–0.45 eV. The gap increases with the polymethine chain length (**Table 2**), yet remains comparatively narrow relative to that typically observed for polymethine dyes. Such a small separation can lead to a strong vibronic coupling and mixing of the two excited states. Indeed, the analysis of the contributing orbital transitions shows that the second-largest contribution to the $S_1^{FC}\leftarrow S_0$ transition arises from the HOMO→LUMO+1 excitation. Conversely, the HOMO→LUMO and HOMO→LUMO+1 contributions are interchanged in the $S_2^{FC}\leftarrow S_0$ transition. This state mixing is reflected as well in the relatively high oscillator strengths of the latter (0.28–0.51).

Comparative TD-DFT calculations for molecules **4** and **10** performed with the long-range-corrected CAM-B3LYP functional (using B3LYP-optimized molecular geometries) yielded results differing markedly from those obtained with B3LYP. Within this approximation, the energy gap between the S_1^{FC} and S_2^{FC} states is about 1 eV, significantly larger than in the B3LYP calculations, and the HOMO→LUMO excitation provides the dominant contribution (>95%) to the long-wavelength transition. A reduction in vibronic coupling between these states is reflected in the oscillator strengths for the $S_1^{FC}\leftarrow S_0$ transition that are 5–7 times smaller than those obtained with B3LYP. Overall, these calculations show substantially poorer agreement with the experimental observations than the B3LYP results.

Hence, despite preliminary TD-DFT evaluations suggesting that in 9*H*-fluorene-2,7-dicarbonitrile-based merocyanines the polymethine $S_1^{FC}\leftarrow S_0$ transition is more strongly separated from higher-lying electronic transitions than in (polynitro)fluorene-based analogs, this gap remains sufficiently small to allow their interaction, thereby influencing the photophysical properties of the new dyes. We therefore reckon that the absence of detectable fluorescence for dyes **2**–**4** and **8**–**10** can be attributed to this effect, which leads to a stronger vibronic coupling and, consequently, an enhanced excited-state deactivation via the internal conversion. Notably, the presence of a higher-lying electronic transition can be discerned at first glance only from the band shapes of dye **2** (**Figure 1A**). In the other cases, the absorption bands are too broad and diffuse to allow its direct identification. Nevertheless, based on the above data, it must be assumed that for all dyes studied the long-wavelength absorption band corresponds not to a single but to two electronic transitions. Such a situation, which is unusual for polymethine dyes, may be responsible for the atypical solvatochromism observed for these compounds.

The analysis of the topography of the molecular orbitals involved (**Figure 3**), as well as of the electron-density redistribution associated with the discussed transitions (**Figure 4**), reveals that the $S_1^{FC}\leftarrow S_0$ transition is predominantly of the polymethine type. However, the HOMO and LUMO exhibit an increased localization on the donor and acceptor end groups, respectively, which imparts a partial charge-transfer character to this excitation. Accordingly, it is accompanied by the donor-to-acceptor electron-density redistribution, manifested as an increase in the molecular dipole moment (**Table 2**).

In contrast, the LUMO+1 exhibits a substantially stronger localization than the LUMO on the 9*H*-fluorene-2,7-dicarbonitrile moiety (**Figure 3**), implying that the $S_2^{FC}\leftarrow S_0$ transition should possess a more pronounced charge-transfer

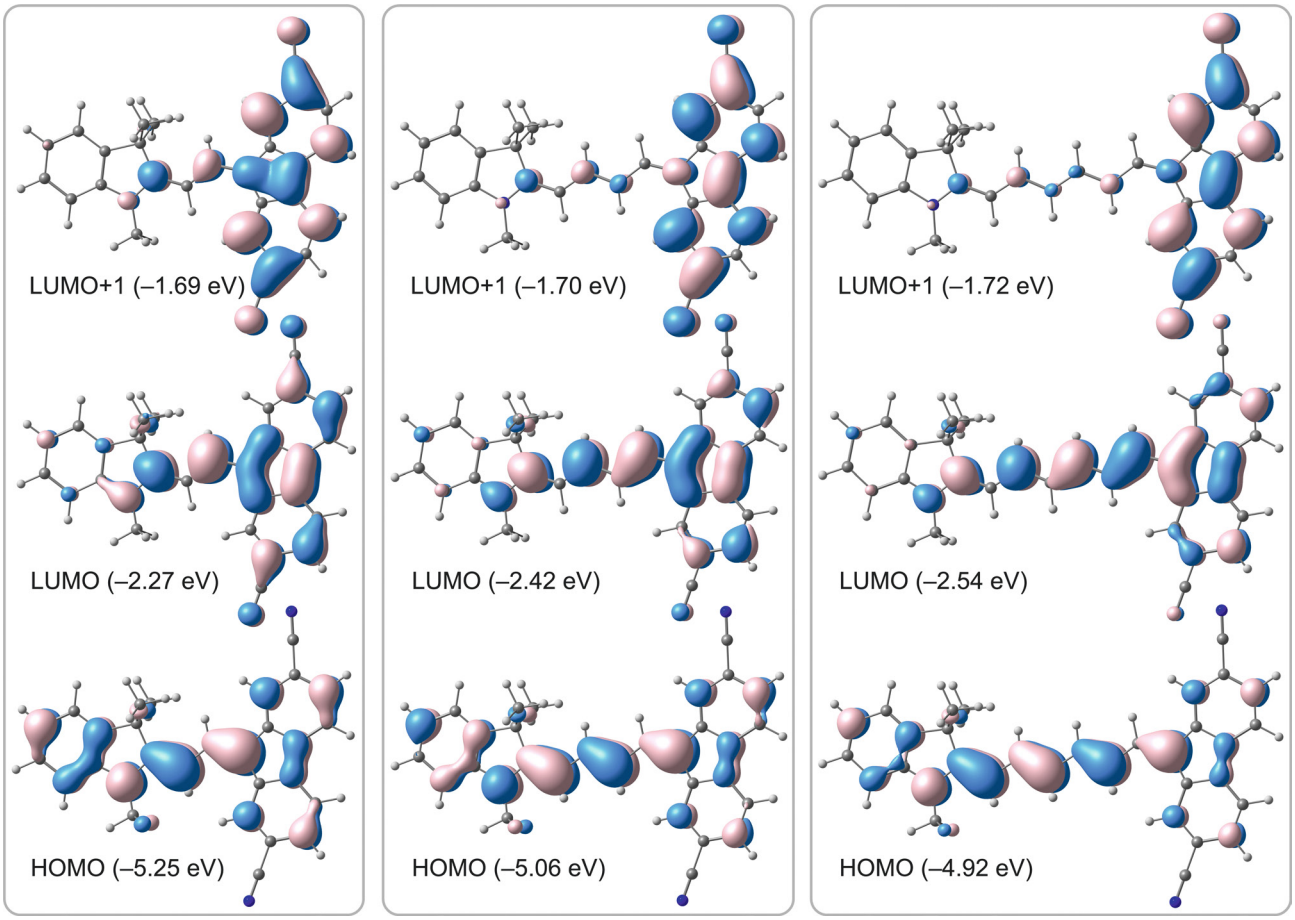

Figure 3. Molecular orbitals of dyes **2**–**4** (DFT-B3LYP/6-31G(d,p); the contour value is 0.03 bohr$^{-3/2}$)

nature (**Figure 4**) and give rise to a more dipolar excited state. Nevertheless, for dimethines **2** and **9**, for which the short polymethine chain length results in very similar spatial localizations of the LUMO and LUMO+1 (**Figure 3**), the increase in the dipole moment upon the $S_2^{FC}\leftarrow S_0$ excitation is smaller than that associated with the $S_1^{FC}\leftarrow S_0$ transition (**Table 2**).

We assume that the more dipolar nature of the S_2^{FC} state, at least in the higher vinylogs of the dyes studied, may be responsible for their atypical solvatochromism. Its preferential stabilization relative to the S_1^{FC} state in high-polarity solvents can lead to further enhancement of the vibronic coupling between these two states and to an increase in the oscillator strength of the $S_2^{FC}\leftarrow S_0$ transition. In the case of broad and diffuse long-wavelength absorption bands, this would shift the band maximum hypsochromically in agreement with the experimental observations.

However, verification of this assumption would require both the solvent modelling and the application of higher-level electronic-structure methods, such as ADC(2), to reliably describe the strongly coupled excited states. An argument against relying on TD-DFT for this purpose is the appearance of pronounced de-excitation contributions in the TD-DFT description of the lowest electronic transition for merocyanines **4**, **9**, and **10** (precisely those exhibiting inverse solvatochromism), which

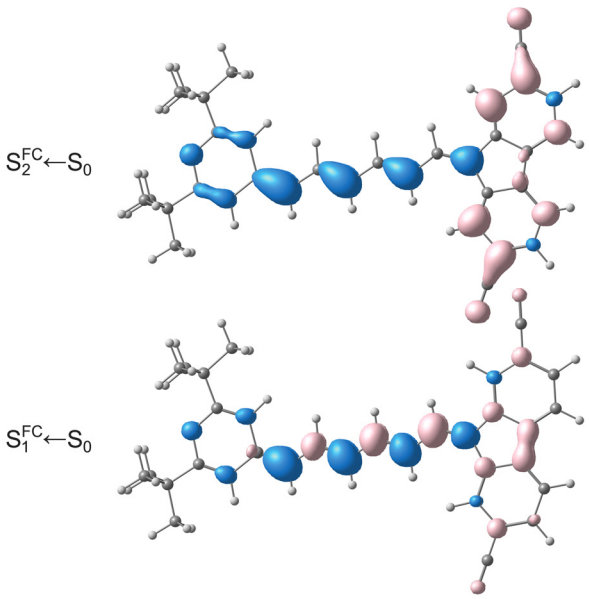

Figure 4. Electron density changes upon excitations in molecule **10** (increase in light-red, decrease in blue; the contour value is 0.002 e×bohr^{-3})

ISSN 2308-8303 (Print) / 2518-1548 (Online)

suggests a substantial ground–excited-state mixing [18]. In such cases, even small solvent-induced perturbations may alter the balance between excitation and de-excitation contributions, potentially giving rise to the anomalous solvatochromic behavior.

■ Conclusions

A series of di-, tetra-, and hexamethine merocyanine dyes incorporating heterocyclic donor end groups and the 9*H*-fluorene-2,7-dicarbonitrile acceptor moiety has been synthesized and comprehensively characterized by the UV–Vis spectroscopy and (TD)-DFT calculations. The combined experimental and computational analysis demonstrates that the electronic structure of these dyes lies close to the neutral polyene limit (the polyene-like character becomes more pronounced with increasing polymethine chain length) suggesting the relatively weak electron-acceptor character of the 9*H*-fluorene-2,7-dicarbonitrile fragment.

Surprisingly, despite their overall weak dipolar character, the longer vinylogs, particularly those bearing the 4*H*-pyran donor end group, exhibit a pronounced inverse solvatochromism. TD-DFT calculations suggest that this unusual behavior may be associated with a small energy separation between the two lowest $^1\pi\pi^*$ excited states, resulting in a strong vibronic coupling and state mixing. The higher-lying excited state possesses a more pronounced charge-transfer character and, for the higher vinylogs, a larger dipole moment, making it especially sensitive to the solvent polarity. Preferential stabilization of this state in polar media may enhance its contribution to the long-wavelength absorption band, leading to its hypsochromic shift despite the weak ground-state dipolarity of the dyes.

The absence of detectable fluorescence for all these merocyanines is likewise attributed, in addition to their polyene-like electronic structure, to efficient nonradiative deactivation pathways promoted by a strong vibronic coupling between closely spaced excited states. The presence of significant de-excitation contributions in the TD-DFT description of the lowest electronic transition for dyes exhibiting the inverse solvatochromism further suggests a substantial ground–excited-state mixing, underscoring the limitations of TD-DFT for the quantitative description of such systems.

Overall, this study has revealed an unconventional mechanism that can influence the solvatochromic behavior even of weakly dipolar donor–acceptor systems when their excited-state manifold is strongly coupled and sensitive to solvent-induced perturbations. For the final verification of the mechanism proposed, higher-level excited-state methods combined with solvent modelling will be required.

■ Experimental Part

Solvents for spectral measurements were purified according to standard procedures [19]. ^{1}H NMR spectra were recorded on Varian VXR (300 MHz) and Varian Unity (400 MHz) spectrometers. The residual solvent peaks were used as internal standards: $CDCl_3$, δ_H = 7.27 ppm; $(CD_3)_2SO$, δ_H = 2.50 ppm. Electronic absorption spectra were recorded at 20 °C using a Shimadzu UV-3100 spectrophotometer and 1-cm quartz cuvettes. Analytical TLC was performed on Silufol UV-254 silica gel plates. Purification of dyes was carried out by column chromatography using Silica gel (70–230 μm, Merck) or Aluminum oxide 90 (63–200 μm, Merck). Melting (decomposition) points were determined in open capillaries and are reported without correction. DFT and TD-DFT calculations were performed with the Gaussian-09 program suite [20] using the B3LYP hybrid functional [21] and the double-ζ basis set 6-31G(d,p).

9-[2-(1,3,3-Trimethylindol-2-ylidene)ethylidene]-9*H*-fluorene-2,7-dicarbonitrile (2)

A mixture of 9*H*-fluorene-2,7-dicarbonitrile **1** [22] (108 mg, 0.5 mmol) and 2-(1,3,3-trimethylindol-2-ylidene)acetaldehyde (101 mg, 0.5 mmol) in acetic anhydride (1.5 mL) was heated until complete dissolution of the reagents was achieved. The resulting solution was then refluxed for an additional 3 min, during which time it turned deep red. After cooling to room temperature, the precipitate was filtered off and washed successively with acetic acid and water. The crude product was purified by column chromatography on silica gel using chloroform as an eluent.

A red solid. Yield 60 mg (30%). M. p. 243–245 °C. Anal. Calcd for $C_{28}H_{21}N_3$, %: C 84.18; H 5.30; N 10.52. Found, %: C 83.97; H 5.24; N 10.39. ^{1}H NMR (300 MHz, $CDCl_3$), *δ,* ppm: 1.82 (6H, s, $C(CH_3)_2$), 3.48 (3H, s, NCH_3), 6.31 (1H, d, *J* = 13.5 Hz, –CH=), 6.91 (1H, d, *J* = 8.0 Hz), 7.08 (1H, t, *J* = 7.5 Hz), 7.29–7.36 (2H, m), 7.57 (1H, dd, *J* = 8.0, 1.3 Hz), 7.64 (1H, dd, *J* = 8.0, 1.3 Hz), 7.94 (1H, d, *J* = 8.0 Hz), 8.01 (1H, d, *J* = 8.1 Hz), 8.03 (1H, s), 8.09 (1H, d, *J* = 13.5 Hz, –CH=), 8.27 (1H, s).

9-[4-(1,3,3-Trimethylindol-2-ylidene)-2-buten-1-ylidene]-9*H*-fluorene-2,7-dicarbonitrile (3)

The compound was synthesized similarly to **2**, starting from 4-(1,3,3-trimethylindol-2-ylidene)-2-butenal. The crude product was purified by column chromatography on silica gel using DCM as an eluent and then crystallized from acetonitrile.

A khaki with a metal shine solid. Yield 120 mg (56%). M. p. > 280 °C. Anal. Calcd for $C_{30}H_{23}N_3$, %: C 84.68; H 5.45; N 9.87. Found, %: C 84.45; H 5.40; N 9.78. ^{1}H NMR (300 MHz, $CDCl_3$), δ, ppm: 1.71 (6H, s, $C(CH_3)_2$), 3.35 (3H, s, NCH_3), 5.81 (1H, d, J = 12.4 Hz, –CH=), 6.79 (1H, d, J = 7.9 Hz), 6.99 (1H, t, J = 7.5 Hz), 7.06 (1H, t, J = 13.0 Hz, –CH=), 7.22–7.30 (2H, m), 7.50 (1H, t, J = 13.0 Hz, –CH=), 7.54 (1H, d, J = 12.5 Hz, –CH=), 7.57 (1H, dd, J = 8.0, 1.3 Hz), 7.63 (1H, dd, J = 7.9, 1.3 Hz), 7.89 (1H, d, J = 7.9 Hz), 7.94 (1H, d, J = 8.0 Hz), 8.08 (1H, s), 8.38 (1H, s).

9-[6-(1,3,3-Trimethylindol-2-ylidene)-2,4-hexadien-1-ylidene]-9*H*-fluorene-2,7-dicarbonitrile (4)

A mixture of **1** (108 mg, 0.5 mmol) and 2-[6-(acetylphenylamino)-1,3,5-hexatrien-1-yl]-1,3,3-trimethyl-3*H*-indolium perchlorate (236 mg, 0.5 mmol) in acetic anhydride (2 mL) was heated until complete dissolution of the reagents. Then triethylamine (150 mg, 1.5 mmol) was added, and the reaction mixture was refluxed for additional 15 min. After cooling, it was poured into a saturated $NaHCO_3$ solution (100 mL) and left for 12 h. The solid precipitate was filtered off, washed with water, dried, and then purified by column chromatography on Al_2O_3 using DCM as an eluent.

A brown-bronze solid. Yield 50 mg (11%). M. p. 235–236 °C. Anal. Calcd for $C_{32}H_{25}N_3$, %: C 85.11; H 5.58; N 9.31. Found, %: C 84.93; H 5.55; N 9.19. ^{1}H NMR (300 MHz, $CDCl_3$), δ, ppm: 1.66 (6H, s, $C(CH_3)_2$), 3.24 (3H, s, NCH_3), 5.56 (1H, d, J = 12.3 Hz, –CH=), 6.42 (1H, dd, J = 13.8, 10.4 Hz, –CH=), 6.72 (1H, d, J = 7.9 Hz), 6.94 (1H, t, J = 7.5 Hz), 7.04 (1H, t, J = 12.7 Hz, –CH=), 6.98–7.17 (2H, m, 2 –CH=), 7.17–7.29(3H, m, 2ArH + –CH=), 7.43 (1H, d, J = 11.3 Hz, –CH=), 7.59 (1H, dd, J = 8.0, 1.3 Hz), 7.64 (1H, dd, J = 8.1, 1.3 Hz), 7.87 (1H, d, J = 8.0 Hz), 7.92 (1H, d, J = 8.1 Hz), 8.00 (1H, s), 8.30 (1H, s).

Hemicyanines 5 and 6 were prepared according to the ref [23].

2,6-Di-*tert*-butyl-4-[6-(dimethylamino)-1,3,5-hexatrien-1-yl]pyrylium perchlorate (7)

(i) A mixture of 2,6-di-*tert*-butyl-4-methylpyrylium perchlorate (1.53 g, 5.0 mmol) and *N*-[5-(phenylimino)-1,3-pentadienyl]aniline hydrochloride (1.43 g, 5.0 mmol) in a mixture of acetic anhydride and acetic acid (2:1, *v*/*v*; 10 mL) was refluxed for 10 min, then cooled to room temperature. The resulting intermediate hemicyanine was precipitated by the addition of an aqueous sodium perchlorate solution, filtered off, and dried. The crude product was used in the subsequent step without further purification.

(ii) The material thus obtained was dissolved in acetonitrile (5 mL), after which a 25% ethanol solution of dimethylamine (2 mL) was added. The reaction mixture was stirred for 30 min at 20 °C. Hemicyanine **7** was precipitated by the addition of an aqueous sodium perchlorate solution, filtered off, washed with water, and dried. The final purification was achieved by column chromatography on silica gel using chloroform–ethanol (98:2, *v*/*v*) as an eluent, followed by crystallization from an acetonitrile–diethyl ether mixture.

Blue-violet bladed crystals. Yield 0.58 g (28%). M. p. 174–175 °C. Anal. Calcd for $C_{21}H_{32}ClNO_5$, %: C 60.93; H 7.79; Cl 8.56; N 3.38. Found, %: C 60.77; H 7.75; Cl 8.59; N 3.40. ^{1}H NMR (400 MHz, $CDCl_3$), δ, ppm: 1.27 (9H, s, $C(CH_3)_3$), 1.32 (9H, s, $C(CH_3)_3$), 3.24 (3H, s, NCH_3), 3.51 (3H, s, NCH_3), 5.78 (1H, d, J = 12.9 Hz, –CH=), 5.98 (1H, t, J = 12.3 Hz, –CH=), 6.06 (1H, d, J = 1.8 Hz), 6.34 (1H, t, J = 12.8 Hz, –CH=), 6.63 (1H, d, J = 1.8 Hz), 7.66 (1H, t, J = 13.1 Hz, –CH=), 7.76 (1H, t, J = 12.8 Hz, –CH=), 8.12 (1H, d, J = 11.4 Hz, –CH=).

9-[2-(2,6-Di-*tert*-butyl-4*H*-pyran-4-ylidene)-ethylidene]-9*H*-fluorene-2,7-dicarbonitrile (8)

To the solution of hemicyanine **5** (180 mg, 0.5 mmol) in DMAA (2 mL), compound **1** (110 mg, 0.5 mmol) and DBU (80 mg, 0.53 mmol) were added. The mixture was heated at 160 °C for 2.5 h. After cooling to room temperature, the dye was precipitated with brine, filtered off, and washed with water. The crude product was purified by column chromatography using chloroform–ethyl acetate (98:2, *v*/*v*) as an eluent, followed by crystallization from acetonitrile.

A beetroot-red solid. Yield 76 mg (28%). M. p. > 280 °C. Anal. Calcd for $C_{30}H_{28}N_2O$, %: C 83.30; H 6.52; N 6.48. Found, %: C 83.11; H 6.50; N 6.40. ^{1}H NMR (400 MHz, $CDCl_3$), δ, ppm: 1.32 (9H, s, $C(CH_3)_3$), 1.37 (9H, s, $C(CH_3)_3$), 6.17 (1H, s), 6.47 (1H, d, J = 13.2 Hz, –CH=), 6.53 (1H, s), 7.57 (1H, d, J = 8.0 Hz), 7.63 (1H, d, J = 8.1 Hz), 7.79 (1H, d, J = 13.2 Hz, –CH=), 7.91 (1H, d, J = 8.0 Hz), 7.96 (1H, d, J = 8.1 Hz), 8.09 (1H, s), 8.37 (1H, s).

ISSN 2308-8303 (Print) / 2518-1548 (Online)

9-[4-(2,6-Di-*tert*-butyl-4*H*-pyran-4-ylidene)-2-buten-1-ylidene]-9*H*-fluorene-2,7-dicarbonitrile (9)

The compound was synthesized similarly to **8**, starting from hemicyanine **6**, purified by column chromatography using chloroform as an eluent, and then crystallized from acetonitrile.

Dark-green needles. Yield 62 mg (28%). M. p. > 280 °C. Anal. Calcd for $C_{32}H_{30}N_2O$, %: C 83.81; H 6.59; N 6.11. Found, %: C 83.59; H 6.50; N 6.00. ^{1}H NMR (400 MHz, $CDCl_3$), δ, ppm: 1.25 (9H, s, $C(CH_3)_3$), 1.30 (9H, s, $C(CH_3)_3$), 5.85 (1H, d, J = 12.3 Hz, −CH=), 5.86 (1H, s), 6.28 (1H, s), 7.07 (1H, t, J = 13.0 Hz, −CH=), 7.26 (1H, t, J = 12.9 Hz, −CH=), 7.51 (1H, d, J = 12.5 Hz, −CH=), 7.57 (1H, dd, J = 7.9, 1.3 Hz), 7.63 (1H, dd, J = 8.0, 1.3 Hz), 7.87 (1H, d, J = 7.9 Hz), 7.92 (1H, d, J = 8.0 Hz), 8.04 (1H, s), 8.30 (1H, s).

9-[6-(2,6-Di-*tert*-butyl-4*H*-pyran-4-ylidene)-2,4-hexadien-1-ylidene]-9*H*-fluorene-2,7-dicarbonitrile (10)

The compound was synthesized similarly to **8**, starting from hemicyanine **7**, at 120 °C for 1 h, and purified similarly to **9**.

Dark green with metal shine needles. Yield 77 mg (32%). M. p. 273–275 °C. Anal. Calcd for $C_{34}H_{32}N_2O$, %: C 84.26; H 6.67; N 5.78. Found, %: C 83.59; H 6.62; N 5.70. ^{1}H NMR (300 MHz, $CDCl_3$), δ, ppm: 1.22 (9H, s, $C(CH_3)_3$), 1.26 (9H, s, $C(CH_3)_3$), 5.63 (1H, d, J = 12.2 Hz, −CH=), 5.76 (1H, s), 6.15 (1H, s), 6.44 (1H, dd, J = 14.0, 11.2 Hz, −CH=), 6.92–7.05(2H, m, 2 −CH=), 7.13 (1H, t, J = 13.0 Hz, −CH=), 7.38 (1H, d, J = 12.2 Hz, −CH=), 7.59 (1H, d, J = 7.9 Hz), 7.64 (1H, d, J = 7.9 Hz), 7.86 (1H, d, J = 7.9 Hz), 7.91 (1H, d, J = 7.9 Hz), 7.98 (1H, s), 8.29 (1H, s). *The ^{1}H NMR chemical shifts of this dye in $CDCl_3$ were found to be concentration-dependent, likely due to aggregation. The values reported herein correspond to the solution of 4 mg of the dye in 0.67 mL of $CDCl_3$.* ^{1}H NMR (300 MHz, $(CD_3)_2SO$), δ, ppm: 1.18 (9H, s, $C(CH_3)_3$), 1.22 (9H, s, $C(CH_3)_3$), 5.66 (1H, d, J = 12.2 Hz, −CH=), 6.32 (1H, s), 5.89 (1H, s), 6.59 (1H, dd, J = 14.1, 11.5 Hz, −CH=), 7.09 (1H, dd, J = 13.9, 11.5 Hz, −CH=), 7.20 (1H, dd, J = 14.1, 12.2 Hz, −CH=), 7.52 (1H, dd, J = 13.9, 12.5 Hz, −CH=), 7.78 (1H, d, J = 8.0 Hz), 7.79 (1H, d, J = 12.5 Hz, −CH=), 7.85 (1H, d, J = 7.9 Hz), 8.21 (1H, d, J = 8.0 Hz), 8.27 (1H, d, J = 7.9 Hz), 8.48 (1H, s), 8.70 (1H, s).

Acknowledgement

The quantum-chemical calculations were performed using the computational facilities of the joint computational cluster of the State Scientific Institution “Institute for Single Crystals”, and the Institute for Scintillation Materials of NAS of Ukraine incorporated into the Ukrainian National Grid.

References

1. Mishra, A.; Behera, R. K.; Behera, P. K.; Mishra, B. K.; Behera, G. B. Cyanines during the 1990s: A Review. *Chem. Rev.* **2000,** *100* (6), 1973–2012. https://doi.org/10.1021/cr990402t.
2. Kulinich, A. V.; Ishchenko, A. A. Merocyanines: Electronic Structure and Spectroscopy in Solutions, Solid State, and Gas Phase. *Chem. Rev.* **2024,** *124* (21), 12086–12144. https://doi.org/10.1021/acs.chemrev.4c00317.
3. Kurdyukova, I. V.; Ishchenko, A. A. Organic dyes based on fluorene and its derivatives. *Russ. Chem. Rev.* **2012,** *81* (3), 258. https://doi.org/10.1070/RC2012v081n03ABEH004211.
4. Kurdyukova, I. V.; Ishchenko, A. A.; Derevyanko, N. A.; Mysyk, D. D. Synthesis and Spectral Properties of Merocyanine Dyes Derived from Tetranitrofluorene and Heterocycles of Various Electron-donating Ability. *Chem. Heterocycl. Comp.* **2013,** *49* (2), 281–293. https://doi.org/10.1007/s10593-013-1245-x.
5. Kulinich, A. V.; Ishchenko, A. A.; Groth, U. M. Electronic structure and solvatochromism of merocyanines: NMR spectroscopic point of view. *Spectrochim. Acta, Part A* **2007,** *68* (1), 6–14. https://doi.org/10.1016/j.saa.2006.10.043.
6. Kulinich, A. V.; Derevyanko, N. A.; Ishchenko, A. A. Electronic structure and solvatochromism of merocyanines based on N,N-diethylthiobarbituric acid. *J. Photoch. Photobio. A* **2007,** *188* (2), 207–217. https://doi.org/10.1016/j.jphotochem.2006.12.014.
7. Dähne, S. Der Ideale Polymethinzustand. *Chimia* **1991**, *45* (10), 288. https://doi.org/10.2533/chimia.1991.288.
8. Reichardt, C.; Welton, T. Solvents and solvent effects in organic chemistry: Fourth edition, Wiley-VCH, Weinheim, 2010. https://doi.org/10.1002/9783527632220.
9. König, W. Über den Begriff der „Polymethinfarbstoffe” und eine davon ableitbare allgemeine Farbstoff-Formel als Grundlage einer neuen Systematik der Farbenchemie. *Journal für Praktische Chemie* **1926,** *112* (1), 1–36. https://doi.org/10.1002/prac.19261120101.
10. Reynolds, G. A.; Drexhage, K. H. Stable heptamethine pyrylium dyes that absorb in the infrared. *J. Org. Chem.* **1977,** *42* (5), 885–888. https://doi.org/10.1021/jo00425a027.
11. Pascal, S.; Getmanenko, Y. A.; Zhang, Y.; Davydenko, I.; Ngo, M. H.; Pilet, G.; Redon, S.; Bretonnière, Y.; Maury, O.; Ledoux-Rak, I.; Barlow, S.; Marder, S. R.; Andraud, C. Design of Near-Infrared-Absorbing Unsymmetrical Polymethine Dyes with Large Quadratic Hyperpolarizabilities. *Chem. Mater.* **2018,** *30* (10), 3410–3418. https://doi.org/10.1021/acs.chemmater.8b00960.
12. Renge, I. Refractive index dependence of solvatochromism. *J. Photoch. Photobio. A* **2018,** *353*, 433–444. https://doi.org/10.1016/j.jphotochem.2017.11.048.
13. Ishchenko, A. A.; Svidro, V. A.; Derevyanko, N. A. Solvatofluorochromy of cationic cyanine dyes. *Dyes Pigments* **1989,** *10* (2), 85–96. https://doi.org/10.1016/0143-7208(89)85001-6.

14. Catalán, J. Toward a Generalized Treatment of the Solvent Effect Based on Four Empirical Scales: Dipolarity (SdP, a New Scale), Polarizability (SP), Acidity (SA), and Basicity (SB) of the Medium. *J. Phys. Chem. B* **2009,** *113* (17), 5951–5960. https://doi.org/10.1021/jp8095727.
15. Meyers, F.; Marder, S. R.; Pierce, B. M.; Bredas, J. L. Electric Field Modulated Nonlinear Optical Properties of Donor-Acceptor Polyenes: Sum-Over-States Investigation of the Relationship between Molecular Polarizabilities (.alpha., .beta., and .gamma.) and Bond Length Alternation. *J. Am. Chem. Soc.* **1994,** *116* (23), 10703–10714. https://doi.org/10.1021/ja00102a040.
16. Fabian, J. TDDFT-calculations of Vis/NIR absorbing compounds. *Dyes Pigments* **2010,** *84* (1), 36–53. https://doi.org/10.1016/j.dyepig.2009.06.008.
17. Tomar, R.; Bernasconi, L.; Fazzi, D.; Bredow, T. Theoretical Study on the Optoelectronic Properties of Merocyanine-Dyes. *J. Phys. Chem. A* **2023,** *127* (46), 9661–9671. https://doi.org/10.1021/acs.jpca.3c04226.
18. Plasser, F. On the Meaning of De-Excitations in Time-Dependent Density Functional Theory Computations. *J. Comput. Chem.* **2025,** *46* (8), e70072. https://doi.org/10.1002/jcc.70072.
19. Armarego, W. L. F.; Chai, C. Purification of Laboratory Chemicals, 6th ed., Butterworth-Heinemann, Oxford, 2009. https://doi.org/10.1016/C2009-0-26589-5.
20. Frisch, M. J.; Trucks, G. W.; Schlegel, H. B.; Scuseria, G. E.; Robb, M. A.; Cheeseman, J. R.; Scalmani, G.; Barone, V.; Petersson, G. A.; Nakatsuji, H.; Li, X.; Caricato, M.; Marenich, A.; Bloino, J.; Janesko, B. G.; Gomperts, R.; Mennucci, B.; Hratchian, H. P.; Ortiz, J. V.; Izmaylov, A. F.; Sonnenberg, J. L.; Williams-Young, D.; Ding, F.; Lipparini, F.; Egidi, F.; Goings, J.; Peng, B.; Petrone, A.; Henderson, T.; Ranasinghe, D.; Zakrzewski, V. G.; Gao, J.; Rega, N.; Zheng, G.; Liang, W.; Hada, M.; Ehara, M.; Toyota, K.; Fukuda, R.; Hasegawa, J.; Ishida, M.; Nakajima, T.; Honda, Y.; Kitao, O.; Nakai, H.; Vreven, T.; Throssell, K.; Montgomery Jr., J. A.; Peralta, J. E.; Ogliaro, F.; Bearpark, M.; Heyd, J. J.; Brothers, E.; Kudin, K. N.; Staroverov, V. N.; Keith, T.; Kobayashi, R.; Normand, J.; Raghavachari, K.; Rendell, A.; Burant, J. C.; Iyengar, S. S.; Tomasi, J.; Cossi, M.; Millam, J. M.; Klene, M.; Adamo, C.; Cammi, R.; Ochterski, J. W.; Martin, R. L.; Morokuma, K.; Farkas, O.; Foresman, J. B.; Fox, D. J. Gaussian 09, Rev. D.01, Gaussian Inc., Wallingford, CT. (2009).
21. Becke, A. D. Density-functional thermochemistry. III. The role of exact exchange. *The Journal of Chemical Physics* **1993,** *98* (7), 5648–5652. https://doi.org/10.1063/1.464913.
22. Spychala, J. A Convenient Way to Methylated 2-Imidazolines. Syntheses of Fluorene and Triazine Cyclic Diamidines. *Monatsh Chem* **2006,** *137* (9), 1203–1210. https://doi.org/10.1007/s00706-006-0516-y.
23. Andreu, R.; Carrasquer, L.; Franco, S.; Garín, J.; Orduna, J.; Martínez de Baroja, N.; Alicante, R.; Villacampa, B.; Allain, M. 4H-Pyran-4-ylidenes: Strong Proaromatic Donors for Organic Nonlinear Optical Chromophores. *J. Org. Chem.* **2009,** *74* (17), 6647–6657. https://doi.org/10.1021/jo901142f.

Information about the authors:
Iryna V. Kurdiukova (*corresponding author*), Ph.D. in Chemistry, Senior Researcher of the Colour and Structure of Organic Compounds Department, Institute of Organic Chemistry of the National Academy of Sciences of Ukraine; https://orcid.org/0000-0001-6695-8535; e-mail for correspondence: *irina.kurdiukova@gmail.com.*
Volodymyr V. Kurdyukov, Ph.D. in Chemistry, Senior Researcher of the Colour and Structure of Organic Compounds Department, Institute of Organic Chemistry of the National Academy of Sciences of Ukraine; https://orcid.org/0000-0002-7668-5435.
Andrii V. Kulinich, Dr.Sci in Chemistry, Leading Researcher of the Colour and Structure of Organic Compounds Department, Institute of Organic Chemistry of the National Academy of Sciences of Ukraine; https://orcid.org/0000-0002-0857-6632.

ISSN 2308-8303 (Print) / 2518-1548 (Online)

Journal of Organic and Pharmaceutical Chemistry

Original Research

OPEN ACCESS
Freely available online on
http://ophcj.nuph.edu.ua

UDC 54.057:547.772.2:547.786.5

O. V. Kaliberda[1,2], E. V. Zarudnitskii[1,3]

[1] Institute of Organic Chemistry of the National Academy of Sciences of Ukraine, 5 Akademik Kuhar str., 02094 Kyiv, Ukraine
[2] Enamine Ltd, 78 Winston Churchill str., 02094 Kyiv, Ukraine
[3] National Technical University of Ukraine "Igor Sikorsky Kyiv Polytechnic Institute", 37 Beresteiskyi ave., 03056 Kyiv, Ukraine

A Scalable Synthesis of 4-Functionalized Isoxazolidines and Pyrazolidines

Abstract

A practical and scalable cyclization method for the preparation of C4-functionalized isoxazolidine and pyrazolidine building blocks is described. The methodology is based on the use of commercially available 1,3-dihalide and protected hydroxylamine or hydrazine derivatives under unified NaH/DMF conditions, enabling direct assembly of both *N*,*O*- and *N*,*N*-heterocycles. The process is operationally robust and successfully implemented on an over 100 g scale. The oxidative conversion of exocyclic alkene intermediates made it possible to obtain isoxazolidin-4-one and pyrazolidin-4-one scaffolds. The resulting pyrazolidine derivatives demonstrate a broad tolerance to reductive and oxidative conditions, whereas isoxazolidines exhibit certain stability limitations. The combination of the modular C4 diversification, orthogonal nitrogen protection, and preparative scalability transforms these saturated heterocycles into practically accessible building blocks for medicinal chemistry applications.

Keywords: synthesis; isoxazolidine; pyrazolidine; scale-up; functionalization

О. В. Каліберда[1,2], Є. В. Зарудницький[1,3]

[1] Інститут органічної хімії Національної академії наук України, вул. Академіка Кухаря, 5, м. Київ, 02094, Україна
[2] ТОВ НВП «Єнамін», вул. Вінстона Черчилля, 78, м. Київ, 02094, Україна
[3] Національний технічний університет України «Київський політехнічний інститут імені Ігоря Сікорського», Берестейський просп., 37, 03056, м. Київ, Україна

Масштабований синтез 4-функціоналізованих ізоксазолідинів та піразолідинів

Анотація

У статті описано практичний та масштабований метод одержання С4-функціоналізованих білдинг-блоків ізоксазолідину та піразолідину. Методологія базується на використанні комерційно доступних 1,3-дигалогеніду й захищених похідних гідроксиламіну або гідразину в уніфікованих умовах NaH/DMF, що забезпечує пряме утворення як *N*,*O*-, так і *N*,*N*-гетероциклів. Процес характеризується надійністю та масштабуванням понад 100 г. Окиснення проміжних продуктів з екзоциклічним алкеновим фрагментом дозволило одержати похідні ізоксазолідин-4-ону та піразолідин-4-ону. Отримані піразолідини демонструють стійкість до відновних та окиснювальних умов, тоді як ізоксазолідини характеризуються певними обмеженнями стабільності. Поєднання модульної С4-функціоналізації, ортогонального захисту атомів нітрогену та можливості масштабування перетворює ці насичені гетероцикли на доступні білдинг-блоки для застосування в медичній хімії.

Ключові слова: синтез; ізоксазолідин; піразолідин; масштабування; функціоналізація

Citation: Kaliberda, O. V.; Zarudnitskii, E. V. A Scalable Synthesis of Functionalized Isoxazolidines and Pyrazolidines. *Journal of Organic and Pharmaceutical Chemistry* **2025**, *23* (4), 33–43.
https://doi.org/10.24959/ophcj.25.353295
Received: *15 July 2025;* **Revised:** *28 September 2025;* **Accepted:** *3 October 2025*

Funding: The authors received no specific funding for this work.
Conflict of interests: The authors have no conflict of interests to declare.

Introduction

In contemporary medicinal chemistry, it is virtually impossible to envision drug-like molecules devoid of cyclic frameworks. More than 90% of approved small-molecule drugs contain at least one ring system, and 67% of compounds currently in the clinical development rely on ring motifs already present in marketed drugs [1]. Among these, heterocycles play a particularly prominent role as the introduction of heteroatoms enables fine-tuning of the electronic distribution, hydrogen-bonding capacity, conformational preferences, and key physicochemical parameters, such as lipophilicity, solubility, and metabolic stability [2].

Nitrogen-containing heterocycles are especially dominant [3]. The analysis of 321 small-molecule drugs approved between 2013 and 2023 revealed that 82% of them incorporate at least one *N*-heterocyclic unit [4]. While aromatic systems are extensively represented in pharmaceutical chemistry, their saturated counterparts remain comparatively underexplored. Among them, there are isoxazolidines and pyrazolidines, fully hydrogenated analogs of isoxazoles and pyrazoles, which represent structurally intriguing yet underutilized five-membered heterocycles. Despite the prevalence of their aromatic congeners in approved drugs [1, 5], saturated isoxazolidine and pyrazolidine motifs are rarely encountered in medicinal chemistry programs (**Figure 1**A). This discrepancy likely stems not from intrinsic limitations of the scaffolds, but from the lack of general, practical, and scalable synthetic routes that enable structural diversification. Nevertheless, emerging examples suggest their untapped potential (**Figure 1**B). Cevidoplenib (SKI-O-703), an experimental SYK kinase inhibitor that received Orphan Drug designation from the FDA in 2024 for the treatment of immune thrombocytopenia, incorporates an isoxazolidine ring [6, 7]. Similarly, the pyrazolidine framework has appeared in drug discovery efforts, including the antiemetic candidate dazopride [8] and, more recently, in dual orexin receptor antagonist IDOR-1117-1680 [9]. Notably, these examples share the substitution in position C4 of the heterocycle, underscoring the synthetic and medicinal relevance of this diversification site.

Despite these precedents, synthetic access to C4-functionalized isoxazolidines (**Figure 1**C) and pyrazolidines (**Figure 1**D) remains limited. Most reported methodologies rely on the cyclization of protected hydroxylamines [10–14] or hydrazines [15–20] with 1,3-dielectrophiles. While efficient in selected cases, these approaches often focus on the *N*-functionalization, provide a limited carbon-centered diversification (particularly in C4), require the multi-step precursor preparation, or are demonstrated only on small scales. In the case of isoxazolidines, the 4-hydroxy derivative remains the most commonly accessible functionalized variant. Similar limitations apply to the pyrazolidine synthesis where examples of C4-functionalized derivatives are sporadic and frequently lack scalable or operationally simple protocols [21–25]. Thus, a practical, scalable synthetic platform that enables reliable access to structurally diverse C4-substituted isoxazolidine and pyrazolidine building blocks remains highly desirable.

Herein, we report a straightforward, robust, and multigram-scale method for the synthesis of C4-functionalized isoxazolidines and pyrazolidines bearing orthogonal *N*-protecting groups from inexpensive, commercially available starting materials (**Figure 1**E). In addition to developing an operationally simple synthetic route, we addressed the reactivity and stability profiles of the resulting heterocycles, thereby establishing their suitability as building blocks for medicinal chemistry and diversity-oriented synthesis. Collectively, this work expands the accessible chemical space of saturated *N*,*O*- and *N*,*N*-heterocycles and provides practical entry points to previously underrepresented scaffolds.

Results and discussion

For the synthesis of the targeted five-membered heterocycles, we adopted a strategy historically recognized for its reliability, involving the reaction of protected hydroxylamine or hydrazine derivatives with 1,3-dielectrophilic reagents. This approach enables a predictable ring closure and, importantly, the modular introduction of substituents in the future C4 position by varying the dihalide component.

Our design was inspired by our previous work on the reaction of 3-chloro-2-(chloromethyl)prop-1-ene with *N*-Boc-2-aminoethanol, which provided access to functionalized 1,4-oxazepanes *via* a robust multigram protocol [26]. In that study, careful control of the reagent order, concentration, and temperature proved essential for ensuring reproducibility and scalability, while also enabling safe handling of NaH/DMF systems. The successful diversification of 6-methylene and

ISSN 2308-8303 (Print) / 2518-1548 (Online)

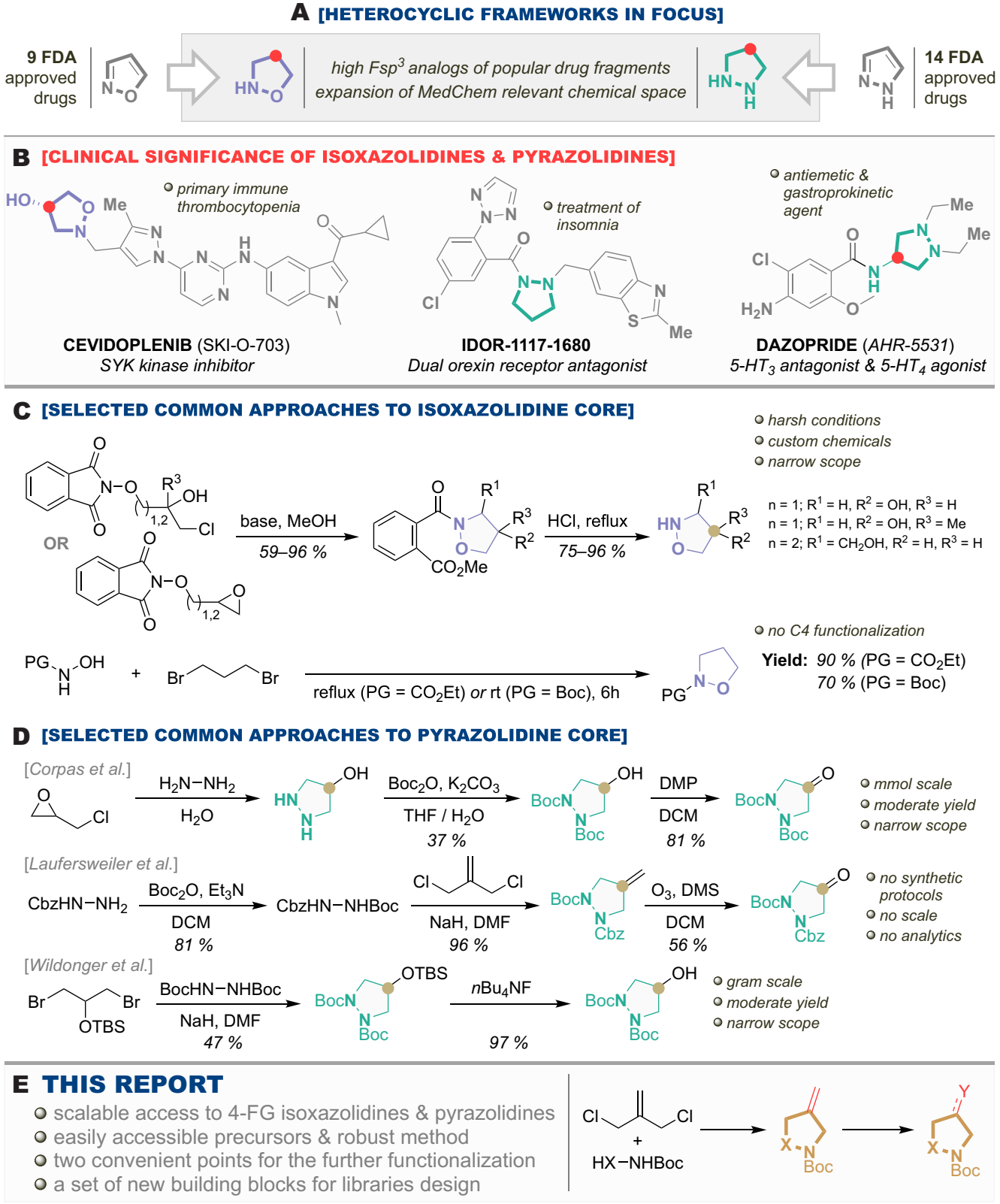

Figure 1. The hallmarks of the work

6-oxo oxazepane cores demonstrated the synthetic flexibility of this platform and encouraged us to extend the methodology to insufficiently explored five-membered heterocycles. We therefore sought to adapt this operationally simple strategy to the preparation of 4-functionalized isoxazolidines and pyrazolidines.

Isoxazolidin-4-one **4** was envisioned as a versatile intermediate for further structural diversification. However, no practical protocol for its scalable preparation has been described. Alkene **3** was obtained *via* the nucleophilic substitution of *N*-Boc-protected hydroxylamine (**1**) with 3-chloro-2-(chloromethyl)prop-1-ene (**2**) in the presence of

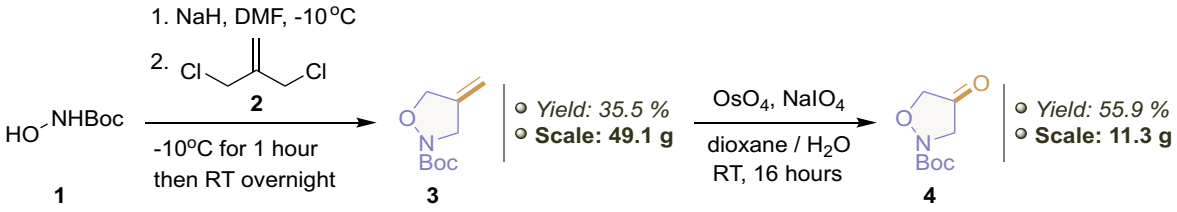

Scheme 1. The synthesis and functionalization of the oxazolidine core

NaH in DMF (**Scheme 1**), following the optimized protocol developed in our previous work to suppress undesired excessive foaming. In particular, deviations from the procedure described in the *Experimental Section*, especially with respect to the reaction time and temperature, may result in uncontrolled foaming, which ultimately leads to the reaction mixture solidification and subsequent complications during the alkylation step. Surprisingly, despite the favorable formation of five-membered rings, alkene **3** was obtained with an isolated yield of only about 35%, even after extensive optimization efforts. Nevertheless, the operational simplicity of the transformation and the use of inexpensive, commercially available reagents allowed the process to be implemented reproducibly on a scale of about 50 g without significant complications. The purification of product **3** was achieved without chromatographic techniques by the vacuum distillation, which proved convenient for the multigram-scale synthesis. However, the spontaneous ignition of the hot residue in the distillation flask upon exposure to air may occur, likely due to residual *N*-Boc-hydroxylamine (see the *Experimental Section*).

The oxidation of the exocyclic double bond proved more challenging than anticipated. In contrast to our earlier oxazepane study, the $RuCl_3$-mediated oxidation resulted in unidentifiable resinous by-products. Improved results were achieved using OsO_4 with periodate as the stoichiometric oxidant, giving ketone **4** in the yield of 56% on a gram scale. Further functional diversification of alkene **3** and ketone **4** was explored, but did not yield satisfactory results. In particular, the hydroboration/oxidation of alkene **3** proved impractical due to low yields and poor purity of the corresponding hydroxymethyl derivative. Attempts to obtain the corresponding carboxylic acid *via* the crude hydroxymethyl intermediate oxidation using the $RuCl_3/NaIO_4$ system were likewise unsuccessful.

The next step was to extend the strategy to the pyrazolidine synthesis. *N*,*N*′-*di*-Boc-protected hydrazine **5** was reacted with 3-chloro-2-(chloromethyl)prop-1-ene (**2**) under similar conditions to obtain alkene **6**, which was subsequently oxidized using $OsO_4/NaIO_4$ to give pyrazolidin-4-one **7** (**Scheme 2**A). One worth noting that compounds **6** and **7** were previously described [27]. Although the reported protocols demonstrate the feasibility of accessing these structures, they do not address key experimental aspects of such transformations as discussed in our previous work [26] likely because they were implemented on a small scale.

In contrast to the isoxazolidine system, the pyrazolidin-4-one core demonstrated greater tolerance toward the downstream functionalization. Exocyclic alkene **6** underwent the hydroboration/oxidation to give alcohol **8**, which was further oxidized to acid **9** using the $RuCl_3/NaIO_4$ system (**Scheme 2**B). Additionally, the carbonyl group reduction with sodium borohydride furnished alcohol **10**, which was smoothly converted to bromide **11** *via* the Appel reaction. The carbonyl functionality was also transformed into an amino group *via* oxime intermediate **12**, followed by the Raney Ni-mediated hydrogenation. Collectively, these transformations demonstrate the versatility of the C4-functionalized pyrazolidine scaffold as a synthetic intermediate.

A defining feature of the pyrazolidine core is the presence of two endocyclic nitrogen atoms, offering multiple points for the selective modification. To enable the controlled functionalization, an orthogonally Boc- and Cbz-protected alkene **15** was prepared in a similar way (**Scheme 3**A). Subsequent transformations confirmed the practical value of this design. The downstream hydroboration/oxidation of the double bond, followed by the oxidation to the corresponding acid and the methylation with methyl iodide, provided a series of crude pyrazolidine derivatives that could further be transformed into mono-*N*-deprotected building blocks. Thus, the Cbz group was removed selectively by the hydrogenolysis, cleanly providing access to alcohol **19** and ester **20** (**Scheme 3**B). If needed, the Boc deprotection could be achieved independently under standard acidic conditions. In this way, the orthogonal protection strategy enables the stepwise and predictable functionalization of the pyrazolidine framework, significantly enhancing its synthetic utility.

ISSN 2308-8303 (Print) / 2518-1548 (Online)

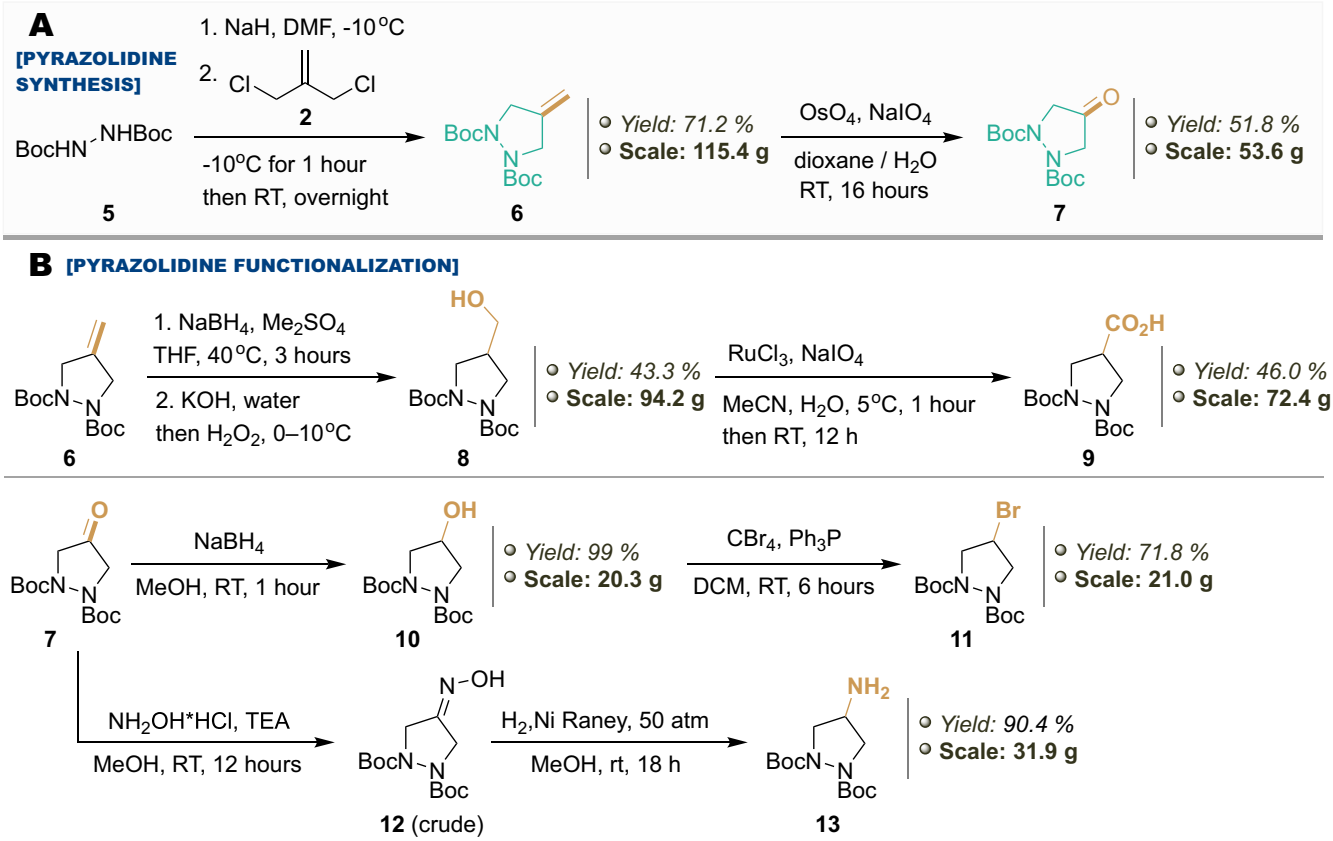

Scheme 2. The synthesis (A) and functionalization (B) of the pyrazolidine core

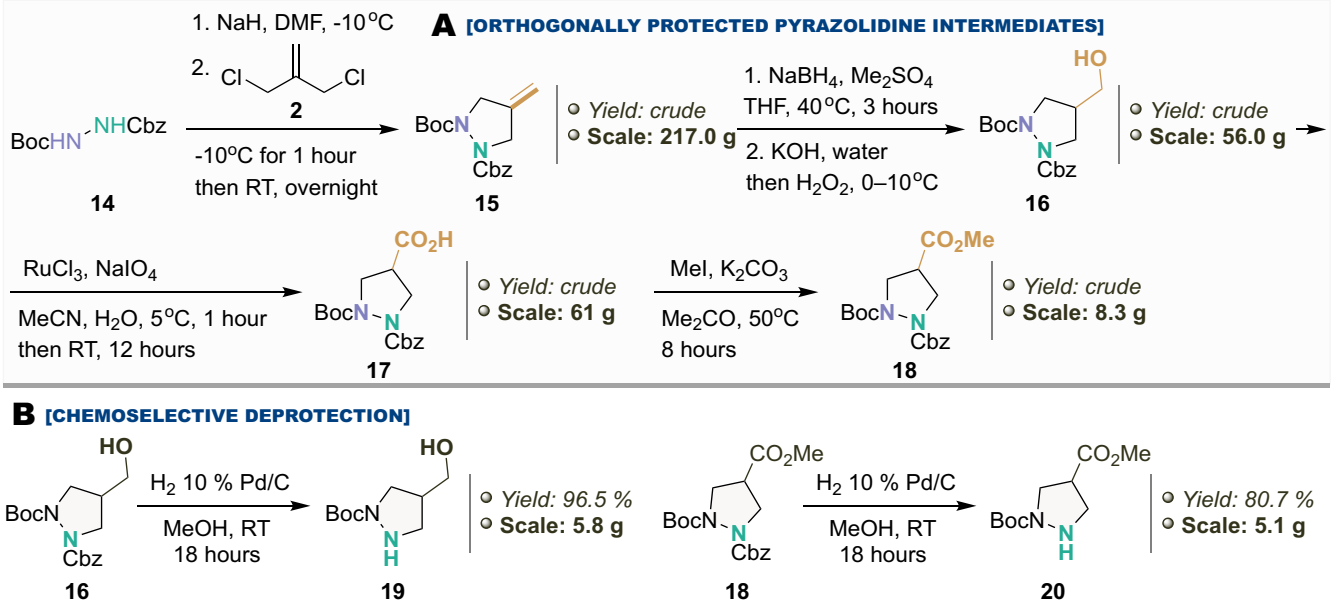

Scheme 3. The synthesis of orthogonally protected pyrazolidines

Conclusion

Thus, we have developed a practical and scalable cyclization method that allows us to obtain C4-functionalized isoxazolidine and pyrazolidine building blocks from commercially available materials. It has been found that a single set of reaction conditions is applicable to both *N*,*O*- and *N*,*N*-heterocycles, simplifying the experimental workflow. The protocol has been demonstrated to be operationally robust, including its implementation at an over 100 g scale. Systematic downstream transformations have confirmed the synthetic versatility of the pyrazolidine scaffold and defined stability limitations of the isoxazolidine core under reductive conditions. The combination of the modular C4 functionalization, orthogonal nitrogen protection, and preparative

scalability transforms these previously underutilized heterocycles into practically accessible building blocks for medicinal chemistry applications.

■ Experimental part

All starting compounds were obtained from commercial sources and used without additional purification. All solvents were purified according to standard procedures. ^{1}H NMR spectra were recorded on a Varian Unity Plus 400 (400 MHz), or a Bruker 170 AVANCE 500 (500 MHz) instrument; ^{13}C NMR spectra were recorded on a Varian Unity Plus 400 (101 MHz) or an Agilent ProPulse 600 (151 MHz) spectrometer. The NMR chemical shifts are referenced using the solvent signals at 7.26 and 77.1 ppm for ^{1}H and ^{13}C nuclei, respectively, in $CDCl_3$, and 2.48 and 39.5 ppm for ^{1}H and ^{13}C nuclei, respectively, in DMSO-d_6. LCMS and GCMS analyses were performed using an Agilent LC/MSD SL 1100 instrument (atmospheric pressure electrospray ionization (ES-API)) or an Agilent 5890 Series II 5972 GCMS instrument (electron impact (EI) ionization (70 eV)), respectively. The elemental analysis results were obtained at the Analytical Laboratory of the Institute of Organic Chemistry of the National Academy of Sciences of Ukraine. Melting points were determined on an MPA100 OptiMelt automated melting point system.

***Tert*-butyl 4-methyleneisoxazolidine-2-carboxylate (3)**

tert-Butyl hydroxycarbamate (**1**) (100 g, 0.75 mol) was dissolved in DMF (1 L), and the resulting solution was cooled to -10 °C. Sodium hydride (60% dispersion in mineral oil, 63.1 g, 1.58 mol) was added in one portion, and the suspension was stirred at -10 °C for 40 min. The solution of 3-chloro-2-(chloromethyl)prop-1-ene (**2**) (104.3 mL, 0.90 mol) was then added dropwise, maintaining the internal temperature between -5 and -10 °C. After the completion of the addition, the reaction mixture was stirred at -10 °C for 1 h, then warmed to room temperature and stirred overnight. The reaction was carefully quenched by the dropwise addition of water (1 L). The resulting mixture was extracted with MTBE (2 × 1 L). The combined organic layers were washed with water (3 × 500 mL) and a brine (500 mL), dried over the anhydrous sodium sulfate, filtered, and concentrated under reduced pressure. The crude product was purified by distillation under reduced pressure to give *tert*-butyl 4-methyleneisoxazolidine-2-carboxylate (**3**).

Caution: To avoid a potential ignition, the distillation flask must be cooled completely before the residue is exposed to air.

A colorless liquid. Yield – 49.1 g (35.5%). Anal. Calcd. for $C_9H_{15}NO_3$, %: C 58.36, H 8.16, N 7.56. Found, %: C 58.43, H 8.20, N 7.43. ^{1}H NMR (400 MHz, $CDCl_3$), δ, ppm: 1.46 (9H, s), 4.14 (2H, s), 4.36 (2H, s), 5.04 (1H, t, J = 2.5 Hz), 5.07 (1H, t, J = 2.3 Hz). ^{13}C NMR (101 MHz, $CDCl_3$), δ, ppm: 27.6, 51.8, 71.2, 81.8, 104.1, 145.0, 157.3. LC-MS, m/z (ES-API): 86.2 $[M\text{-}C_4H_8\text{-}CO_2+H]^+$.

***Tert*-butyl 4-oxoisoxazolidine-2-carboxylate (4)**

Osmium tetroxide (0.27 g, 10.8 mmol) was added to a stirred solution of *tert*-butyl 4-methyleneisoxazolidine-2-carboxylate (**3**, 20 g, 0.108 mol) and sodium periodate (57.7 g, 0.27 mol) in the mixture of dioxane (400 mL) and water (100 mL) precooled to 10 °C. The resulting reaction mixture was allowed to warm to room temperature and stirred for 16 h. The precipitated solids were removed by filtration and washed with MTBE (2 × 200 mL). The combined filtrates were diluted with water (500 mL) and extracted with MTBE (3 × 500 mL). The combined organic layers were washed successively with a brine (500 mL), 2 M aqueous Na_2SO_3 solution (2 × 500 mL), and water (500 mL), then dried over the anhydrous sodium sulfate, filtered, and concentrated under reduced pressure. The crude product was purified by distillation under reduced pressure to give *tert*-butyl 4-oxoisoxazolidine-2-carboxylate **4**.

A colorless oil. Yield – 11.3 g (55.9%). Anal. Calcd. for $C_8H_{13}NO_4$, %: C 51.33, H 7.00, N 7.48. Found, %: C 51.45, H 6.91, N 7.59. ^{1}H NMR (500 MHz, $CDCl_3$), δ, ppm: 1.52 (9H, s), 3.97 (2H, s), 4.08 (2H, s). ^{13}C NMR (126 MHz, $CDCl_3$), δ, ppm: 28.1, 53.8, 70.9, 83.6, 156.8, 209.0. GC-MS, m/z (EI): 87.0 $[M\text{-}C_4H_8\text{-}CO_2]^+$.

Di-*tert*-butyl 4-methylenepyrazolidine-1,2-dicarboxylate (6) [27]

Di-*tert*-butyl hydrazine-1,2-dicarboxylate (**5**, 132.3 g, 0.57 mol) was dissolved in DMF (1.3 L), and the resulting solution was cooled to -10 °C. Sodium hydride (60% dispersion in mineral oil, 83.5 g, 2.1 mol) was added in one portion, and the suspension was stirred at -10 °C for 40 min. The solution of 3-chloro-2-(chloromethyl)prop-1-ene (**2**) (138.0 mL, 1.2 mol) was then added dropwise, maintaining the internal temperature between -5 and -10 °C. After the completion of the addition, the reaction mixture was stirred at -10 °C for 1 h, then warmed to room temperature and stirred overnight. The reaction mixture was carefully

ISSN 2308-8303 (Print) / 2518-1548 (Online)

quenched by the dropwise addition of water (1.3 L). The resulting mixture was extracted with MTBE (2 × 1 L). The combined organic layers were washed with water (3 × 500 mL) and a brine (500 mL), dried over the anhydrous sodium sulfate, filtered, and concentrated under reduced pressure. The crude product was purified by the flash column chromatography (EtOAc/hexane, gradient 0–40%) to give di-*tert*-butyl 4-methylenepyrazolidine-1,2-dicarboxylate (**6**).

A light-yellow solid. Yield – 115.4 g (71.2%). M. p. 88–90 °C. Anal. Calcd. for $C_{14}H_{24}N_2O_4$, %: C 59.14, H 8.51, N 9.85. Found, %: C 59.26, H 8.39, N 9.60. ^{1}H NMR (500 MHz, $CDCl_3$), δ, ppm: 1.47 (18H, s), 3.83 (2H, d, J = 16.0 Hz), 4.43 (2H, d, J = 15.0 Hz), 5.04–5.09 (2H, m). ^{13}C NMR (101 MHz, $CDCl_3$), δ, ppm: 28.2, 51.1, 81.3, 105.8, 143.5, 155.6. LC-MS, *m*/*z* (ES-API): 129.0 $[M\text{-}2C_4H_8\text{-}CO_2+H]^+$.

Di-*tert*-butyl 4-oxopyrazolidine-1,2-dicarboxylate (7) [27]

Osmium tetroxide (0.92 g, 36.1 mmol) was added to a stirred solution of di-*tert*-butyl 4-methylenepyrazolidine-1,2-dicarboxylate **6** (102.7 g, 0.36 mol) and sodium periodate (193.0 g, 0.90 mol) in the mixture of dioxane (1.2 L) and water (300 mL) pre-cooled to 10 °C. The resulting reaction mixture was allowed to warm to room temperature and stirred for 16 h. The precipitated solids were removed by filtration and washed with MTBE (2 × 400 mL). The combined filtrates were diluted with water (1.0 L) and extracted with MTBE (3 × 700 mL). The combined organic layers were washed successively with a brine (800 mL), 2 M aqueous Na_2SO_3 solution (2 × 800 mL), and water (900 mL), then dried over the anhydrous sodium sulfate, filtered, and concentrated under reduced pressure. The crude product was purified by flash column chromatography to give di-*tert*-butyl 4-oxopyrazolidine-1,2-dicarboxylate (**7**).

A white solid. Yield – 53.6 g (51.8%). M. p. 109–111 °C. Anal. Calcd. for $C_{13}H_{22}N_2O_5$, %: C 54.53, H 7.74, N 9.78. Found, %: C 54.40, H 7.70, N 9.67. ^{1}H NMR (500 MHz, $CDCl_3$), δ, ppm: 1.49 (18H, s), 3.65 (2H, d, J = 18.1 Hz), 4.25 (2H, d, J = 18.1 Hz). ^{13}C NMR (151 MHz, $CDCl_3$), δ, ppm: 28.1, 53.2, 82.5, 155.0, 207.9. GC-MS, *m*/z (EI): 186.1 $[M\text{-}C_4H_8\text{-}CO_2]^+$.

Di-*tert*-butyl 4-(hydroxymethyl)pyrazolidine-1,2-dicarboxylate (8)

To the suspension of sodium borohydride (28.7 g, 0.76 mol) and di-*tert*-butyl 4-methylenepyrazolidine-1,2-dicarboxylate **6** (204.8 g, 0.72 mol) in THF (1.5 L), dimethyl sulfate (75.8 mL, 0.79 mol) was added dropwise under the argon atmosphere, while maintaining the internal temperature below 40 °C. After the completion of the addition, the reaction mixture was stirred for 3 h. The mixture was then cooled to 0 °C, and water (210 mL) was added slowly dropwise, followed by the addition of KOH (46.5 g, 0.83 mol) dissolved in water (210 mL). After stirring for 15 min, hydrogen peroxide (210 mL, 33 wt%) was added dropwise at 0-10 °C, and the reaction mixture was stirred for the additional 30 min after the addition was complete. MTBE (1.0 L) was added, and the organic phase was decanted from the inorganic precipitate. The organic layer was washed successively with water (700 mL), 2 M aqueous Na_2SO_3 solution (2 × 700 mL), and a brine (700 mL), then dried over the anhydrous sodium sulfate, filtered, and concentrated under reduced pressure. The crude product was purified by the flash column chromatography (MeCN/$CHCl_3$, gradient 0–50%) to give di-*tert*-butyl 4-(hydroxymethyl)pyrazolidine-1,2-dicarboxylate (**8**).

A yellow oil. Yield – 94.2 g (43.3%). Anal. Calcd. for $C_{14}H_{26}N_2O_5$, %: C 55.61, H 8.67, N 9.26. Found, %: C 55.42, H 8.55, N 9.07. ^{1}H NMR (400 MHz, DMSO-d_6), δ, ppm: 1.39 (18H, s), 2.90 (1H, dd, J = 10.2, 5.4 Hz), 3.16 (1H, t, J = 9.5 Hz), 3.27 (2H, t, J = 5.9 Hz), 3.62 (1H, dd, J = 11.0, 3.7 Hz), 3.76 (1H, t, J = 9.5 Hz), 4.82 (1H, t, J = 5.0 Hz). GC-MS, *m*/z (EI): 302.1 $[M]^+$. LC-MS, *m*/*z* (ES-API): 147.0 $[M\text{-}2C_4H_8\text{-}CO_2+H]^+$.

1,2-*bis*(*tert*-Butoxycarbonyl)pyrazolidine-4-carboxylic acid (9)

Sodium periodate (467.2 g, 2.17 mol) was dissolved in the mixture of water (1.0 L) and MeCN (1.0 L), and the resulting solution was cooled to 5 °C. Ruthenium(III) chloride hydrate (5.9 g, 27.3 mmol) was then added, followed by the dropwise addition of the solution of di-*tert*-butyl 4-(hydroxymethyl)pyrazolidine-1,2-dicarboxylate (**8**) (180 g, 0.53 mol) in MeCN (300 mL), while maintaining the internal temperature between 0 and 10 °C. After the completion of the addition, the reaction mixture was stirred at 5 °C for 1 h, then warmed to room temperature and stirred for the additional 12 h. The precipitated solids were removed by filtration and washed with MTBE (2 × 700 mL). The combined filtrates were diluted with water (700 mL) and extracted with MTBE (3 × 50 mL). The combined organic layers were washed successively with a brine (700 mL) and water (700 mL), then dried over the anhydrous sodium sulfate, filtered, and concentrated under reduced pressure to give 1,2-*bis*(*tert*-butoxycarbonyl)pyrazolidine-4-carboxylic acid (**9**).

A white solid. Yield – 72.4 g (46%). M. p. 130–132 °C. Anal. Calcd. for $C_{14}H_{24}N_2O_6$, %: C 53.15, H 7.65, N 8.86. Found, %: C 53.29, H 7.81, N 8.75. ^{1}H NMR (400 MHz, $CDCl_3$), δ, ppm: 1.48 (18H, s), 3.25–3.32 (1H, m), 3.43 (1H, t, *J* = 10.1 Hz), 3.53 (1H, dd, *J* = 11.5, 5.9 Hz), 3.89–3.98 (1H, m), 4.12 (1H, t, *J* = 10.0 Hz), 4.25 (1H, dd, *J* = 11.7, 3.7 Hz), 9.16 (1H, s). ^{13}C NMR (101 MHz, $CDCl_3$), *δ*, ppm: 28.0, 28.1, 41.1, 43.9, 48.7, 49.4, 76.7, 77.0, 77.3, 81.8, 155.4, 155.8, 176.7. LC-MS, *m*/*z* (ES-API): 117.2 $[M\text{-}2C_4H_8\text{-}2CO_2+H]^+$.

Di-*tert*-butyl 4-hydroxypyrazolidine-1,2-dicarboxylate (10) [22, 24]

Sodium borohydride (1.6 g, 42 mmol) was added portionwise to the stirred solution of di-*tert*-butyl 4-oxopyrazolidine-1,2-dicarboxylate (**7**, 20.0 g, 0.070 mol) in MeOH (250 mL) at room temperature. The resulting reaction mixture was stirred at room temperature for 1 h. The solvent was then removed under reduced pressure, and the residue was diluted with water (200 mL) and MTBE (200 mL). The organic layer was separated, washed with a brine (100 mL), dried over the anhydrous sodium sulfate, filtered, and concentrated under reduced pressure to give di-*tert*-butyl 4-hydroxypyrazolidine-1,2-dicarboxylate (**10**).

A white solid. Yield – 20.3 g (99%). Anal. Calcd. for $C_{13}H_{24}N_2O_5$, %: C 54.15, H 8.39, N 9.72. Found, %: C 54.36, H 8.57, N 9.81. ^{1}H NMR (400 MHz, DMSO-d_6), δ, ppm: 1.39 (18H, s), 3.04 (2H, t, *J* = 12.9 Hz), 3.63–3.76 (2H, m), 4.38 (1H, s), 5.11 (1H, d, *J* = 2.4 Hz). ^{13}C NMR (101 MHz, DMSO-d_6), δ, ppm: 28.2 and 28.3 (rotamers), 55.2, 70.1, 80.2 and 80.5 (rotamers), 154.9 and 157.0 (rotamers). LC-MS, *m*/*z* (ES-API): 133.2 $[M\text{-}2C_4H_8\text{-}CO_2+H]^+$.

Di-*tert*-butyl 4-bromopyrazolidine-1,2-dicarboxylate (11)

To the stirred solution of di-*tert*-butyl 4-hydroxypyrazolidine-1,2-dicarboxylate (**10**, 24.0 g, 83.2 mmol) in DCM (400 mL), triphenylphosphine (32.8 g, 0.125 mol) was added in one portion, followed by the portionwise addition of tetrabromomethane (41.4 g, 0.125 mol). The resulting reaction mixture was stirred at room temperature for 6 h. The solvent was removed under reduced pressure, and the resulting residue was purified by flash column chromatography (EtOAc/hexane, gradient 0–30%) to give di-*tert*-butyl 4-bromopyrazolidine-1,2-dicarboxylate (**11**).

A white solid. Yield – 21.0 g (71.8%). M. p. 98–100 °C. Anal. Calcd. for $C_{13}H_{23}BrN_2O_4$, %: C 44.45, H 6.60, N 7.98. Found, %: C 44.29, H 6.79, N 7.81. ^{1}H NMR (500 MHz, DMSO-d_6), δ, ppm: 1.39 and 1.41 (18H, s, rotamers), 3.54 (1H, d, *J* = 13.4 Hz), 3.59 (1H, d, *J* = 12.6 Hz), 4.07 (1H, d, *J* = 13.4 Hz), 4.13 (1H, dd, *J* = 12.7, 5.8 Hz), 4.87 (1H, t, *J* = 5.0 Hz). ^{13}C NMR (101 MHz, DMSO-d_6), δ, ppm: 28.1 and 28.3 (rotamers), 48.3, 57.1, 80.9 and 81.2 (rotamers), 154.9 and 156.5 (rotamers). LC-MS, *m*/*z* (ES-API): 195.0 $[M\text{-}2C_4H_8\text{-}CO_2+H]^+$.

Di-*tert*-butyl 4-(hydroxyimino)pyrazolidine-1,2-dicarboxylate (12)

Triethylamine (7.3 mL, 52.4 mmol) was added to the stirred solution of di-*tert*-butyl 4-oxopyrazolidine-1,2-dicarboxylate (**7**, 10.0 g, 0.035 mol) in the appropriate solvent, followed by the addition of hydroxylamine hydrochloride (3.6 g, 52.4 mmol). The resulting reaction mixture was stirred at room temperature for 12 h. The solvent was removed under reduced pressure, and the residue was diluted with DCM (100 mL) and washed with water (2 × 50 mL). The organic layer was dried over the anhydrous sodium sulfate, filtered, and concentrated under reduced pressure to give di-*tert*-butyl 4-(hydroxyimino)pyrazolidine-1,2-dicarboxylate (**12**, 10.1 g, crude), which was used directly in the next step without further purification.

Di-*tert*-butyl 4-aminopyrazolidine-1,2-dicarboxylate (13)

The mixture of di-*tert*-butyl 4-(hydroxyimino)pyrazolidine-1,2-dicarboxylate (**12**, 37.1 g, 122.4 mmol) and freshly prepared Raney Ni (17 g) in methanol (500 mL) was hydrogenated at 50 atm and 20 °C for 18 h. After the completion, the catalyst was filtered off and washed with methanol (100 mL). The combined filtrates were concentrated under reduced pressure. Water (200 mL) was added to the residue, and the aqueous phase was acidified to pH 3 using sodium hydrogen sulfate. The mixture was washed with DCM (2 × 100 mL), then basified to pH 12 with aqueous KOH and extracted with DCM (2 × 200 mL). The combined organic layers were dried over anhydrous sodium sulfate, filtered, and concentrated under reduced pressure to give di-*tert*-butyl 4-aminopyrazolidine-1,2-dicarboxylate (**13**).

A white solid. Yield – 31.9 g (90.4%). M. p. 98–100 °C. Anal. Calcd. for $C_{13}H_{25}N_3O_4$, %: C 54.34, H 8.77, N 14.62. Found, %: C 54.49, H 8.56, N 14.83. ^{1}H NMR (500 MHz, DMSO-d_6), δ, ppm: 1.38 (18H, s), 2.84 (1H, d, *J* = 10.5 Hz), 3.08 (1H, dd, *J* = 11.1, 5.2 Hz), 3.44 (1H, d, *J* = 11.1 Hz), 3.58 (1H, tq, *J* = 5.7, 2.6 Hz), 3.64 (1H, dd, *J* = 10.6, 6.0 Hz). ^{13}C NMR (101 MHz, DMSO-d_6), δ, ppm: 28.27 and 28.31 (rotamers), 51.8, 54.9 and 55.9 (rotamers), 80.2, 155.1 and 156.7 (rotamers). LC-MS, *m*/*z* (ES-API): 88.4 $[M\text{-}2C_4H_8\text{-}2CO_2+H]^+$.

ISSN 2308-8303 (Print) / 2518-1548 (Online)

1-Benzyl 2-(*tert*-butyl) 4-methylenepyrazolidine-1,2-dicarboxylate (15)

1-Benzyl 2-(*tert*-butyl) hydrazine-1,2-dicarboxylate (**14**, 200 g, 1.65 mol) was dissolved in DMF (2 L), and the resulting solution was cooled to -10 °C. Sodium hydride (60% dispersion in mineral oil, 66.1 g, 1.65 mol) was added in one portion, and the suspension was stirred at -10 °C for 40 min. The solution of 3-chloro-2-(chloromethyl)-prop-1-ene (**2**, 104.3 mL, 0.90 mol) was then added dropwise, maintaining the internal temperature between -5 and -10 °C. After the completion of the addition, the reaction mixture was stirred at -10 °C for 1 h, then warmed to room temperature and stirred overnight. The reaction was carefully quenched by the dropwise addition of water (1 L). The resulting mixture was extracted with MTBE (2 × 1 L). The combined organic layers were washed with water (3 × 500 mL) and a brine (500 mL), dried over the anhydrous sodium sulfate, filtered, and concentrated under reduced pressure. The crude product was purified by the flash column chromatography (EtOAc/hexane, gradient 0–40%) to give 1-benzyl 2-(*tert*-butyl) 4-methylenepyrazolidine-1,2-dicarboxylate (**15**, 217 g, crude) as a light-yellow oil, which was used directly in the next step without further purification.

1-Benzyl 2-(*tert*-butyl) 4-(hydroxymethyl)-pyrazolidine-1,2-dicarboxylate (16)

To the suspension of sodium borohydride (6.23 g, 165 mmol) and 1-benzyl 2-(*tert*-butyl) 4-methylenepyrazolidine-1,2-dicarboxylate (**15**, 50.0 g, 157 mmol) in THF (100 mL), dimethyl sulfate (16.38 mL, 173 mmol) was added dropwise under the argon atmosphere, while maintaining the internal temperature below 40 °C. After the completion of the addition, the reaction mixture was stirred for 3 h. The mixture was then cooled to 0 °C, and water (50 mL) was added slowly dropwise, followed by the addition of KOH (10.1 g, 180 mmol) dissolved in water (50 mL). After stirring for 15 min, hydrogen peroxide (50 mL, 33 wt%) was added dropwise at 0–10 °C, and the reaction mixture was stirred for the additional 30 min after the addition was complete. MTBE (500 mL) was added, and the organic phase was decanted from the inorganic precipitate. The organic layer was washed successively with water (300 mL), 2 M aqueous Na_2SO_3 solution (2 × 200 mL), and a brine (200 mL), then dried over the anhydrous sodium sulfate, filtered, and concentrated under reduced pressure to give 1-benzyl 2-(*tert*-butyl) 4-(hydroxymethyl)-pyrazolidine-1,2-dicarboxylate **16** (56 g, crude), which was used directly in the next step without further purification.

A white oil. Yield – 56 g (crude). ^{1}H NMR (400 MHz, $CDCl_3$), δ, ppm: 1.43 (9H, s), 1.98 (1H, d, *J* = 33.0 Hz), 2.59–2.70 (1H, m), 3.02–3.45 (2H, m), 3.55 (2H, s), 3.83–3.94 (1H, m), 4.05 (1H, d, *J* = 12.4 Hz), 5.11 (1H, d, *J* = 12.5 Hz), 5.26 (1H, d, *J* = 11.8 Hz), 7.26 – 7.42 (5H, m). LC-MS, *m*/*z* (ES-API): 337.2 $[M+H]^+$.

1-((Benzyloxy)carbonyl)-2-(*tert*-butoxycarbonyl)pyrazolidine-4-carboxylic acid (17)

Sodium periodate (127.2 g, 0.59 mol) was dissolved in the mixture of water (500 mL) and MeCN (500 mL), and the resulting solution was cooled to 5 °C. Ruthenium(III) chloride hydrate (1.66 g, 7.4 mmol) was then added, followed by the dropwise addition of the solution of 1-benzyl 2-(*tert*-butyl) 4-(hydroxymethyl)pyrazolidine-1,2-dicarboxylate (**16**, 50.0 g, 149 mmol) in MeCN (100 mL), while maintaining the internal temperature between 0 and 10 °C. After the completion of the addition, the reaction mixture was stirred at 5 °C for 1 h, then allowed to warm to room temperature and stirred for the additional 12 h. The precipitated solids were removed by filtration and washed with MTBE (2 × 500 mL). The combined filtrates were diluted with water (500 mL) and extracted with MTBE (3 × 400 mL). The combined organic layers were washed successively with a brine (500 mL) and water (500 mL), then dried over the anhydrous sodium sulfate, filtered, and concentrated under reduced pressure to give 1-((benzyloxy)carbonyl)-2-(*tert*-butoxycarbonyl)pyrazolidine-4-carboxylic acid (**17**, 61 g, crude), which was used directly in the next step without further purification.

1-Benzyl 2-(*tert*-butyl) 4-methyl pyrazolidine-1,2,4-tricarboxylate (18)

The mixture of 1-((benzyloxy)carbonyl)-2-(*tert*-butoxycarbonyl)pyrazolidine-4-carboxylic acid **17** (25 g, 71.3 mmol), potassium carbonate (19.7 g, 143 mmol), and methyl iodide (8.88 mL, 143 mmol) in acetone (250 mL) was heated at 50 °C for 8 h. The reaction mixture was cooled to room temperature and concentrated under reduced pressure. The residue was diluted with EtOAc (200 mL) and washed with water (2 × 200 mL). The crude product was purified by the flash column chromatography (EtOAc/hexane, gradient 20–40%) to give 1-benzyl 2-(*tert*-butyl) 4-methyl pyrazolidine-1,2,4-tricarboxylate (**18**).

A yellow oil. Yield – 8.3 g (crude). Anal. Calcd. for $C_{18}H_{24}N_2O_6$, %: C 59.33, H 6.64, N 7.69.

Found, %: C 59.25, H 6.80, N 7.50. ^{1}H NMR (500 MHz, DMSO-d_6), δ, ppm: 1.43 (9H, s), 3.20–3.30 (1H, m), 3.36–3.63 (2H, m), 3.64–3.75 (3H, m), 4.09–4.28 (2H, m), 5.07–5.32 (2H, m), 7.28–7.40 (5H, m). LC-MS, *m/z* (ES-API): 265.1 [M-C_4H_8-CO_2+H]$^+$.

***tert*-Butyl 4-(hydroxymethyl)pyrazolidine-1-carboxylate (19)**

The mixture of 1-benzyl 2-(*tert*-butyl) 4-(hydroxymethyl)pyrazolidine-1,2-dicarboxylate **16** (10 g, 29.7 mmol) and 10% Pd/C (1 g) in methanol (100 mL) was hydrogenated at 50 atm and 20 °C for 18 h. After the completion, the catalyst was removed by filtration and washed with methanol (30 mL). The combined filtrates were concentrated under reduced pressure to give tert-butyl 4-(hydroxymethyl)pyrazolidine-1-carboxylate **19**.

A white solid. Yield – 5.8 g (96.5%). M. p. 60–63 °C. Anal. Calcd. for $C_9H_{18}N_2O_3$, %: C 53.45, H 8.97, N 13.85. Found, %: C 53.61, H 9.12, N 13.98. ^{1}H NMR (400 MHz, $CDCl_3$), δ, ppm: 1.43 (s, 9H), 2.51–2.64 (1H, m), 2.99 (1H, dd, *J* = 11.6, 4.9 Hz), 3.10 (1H, dd, *J* = 11.6, 6.8 Hz), 3.21 (1H, dd, *J* = 10.8, 5.0 Hz), 3.52 – 3.67 (3H, m), 4.02 (2H, s). ^{13}C NMR (101 MHz, $CDCl_3$) δ 28.4, 42.9, 48.7, 50.3, 63.0, 80.5, 154.9. LC-MS, *m/z* (ES-API): 147.2 [M-C_4H_8+H]$^+$.

1-(*tert*-Butyl) 4-methyl pyrazolidine-1,4-dicarboxylate (20)

The mixture of 1-benzyl 2-(*tert*-butyl) 4-methyl pyrazolidine-1,2,4-tricarboxylate (**18**, 10.0 g, 27.4 mmol) and 10% Pd/C (1 g) in methanol (100 mL) was hydrogenated at 50 atm and 20 °C for 18 h. After the completion, the catalyst was filtered off and washed with methanol (30 mL). The combined filtrates were concentrated under reduced pressure. Water (50 mL) was added to the residue, and the aqueous phase was acidified to pH 3 using sodium hydrogen sulfate. The mixture was washed with DCM (2 × 40 mL), then basified to pH 12 with the aqueous KOH and extracted with DCM (2 × 50 mL). The combined organic layers were dried over the anhydrous sodium sulfate, filtered, and concentrated under reduced pressure to give 1-(*tert*-butyl) 4-methyl pyrazolidine-1,4-dicarboxylate (**20**).

A yellow oil. Yield – 5.1 g (80.7%). Anal. Calcd. for $C_{10}H_{18}N_2O_4$, %: C 52.16, H 7.88, N 12.17. Found, %: C 52.29, H 7.69, N 12.01. ^{1}H NMR (500 MHz, $CDCl_3$), δ, ppm: 1.48 (9H, s), 3.14 (1H, dd, *J* = 11.5, 6.5 Hz), 3.21–3.31 (2H, m), 3.63 (1H, dd, *J* = 11.1, 4.3 Hz), 3.72 (3H, s), 3.76 (1H, dd, *J* = 11.1, 8.4 Hz), 4.14 (1H, s). LC-MS, *m/z* (ES-API): 231.2 [M+H]$^+$.

References

1. Shearer, J.; Castro, J. L.; Lawson, A. D. G.; MacCoss, M.; Taylor, R. D. Rings in Clinical Trials and Drugs: Present and Future. *J. Med. Chem.* **2022**, *65* (13), 8699–8712. https://doi.org/10.1021/acs.jmedchem.2c00473.
2. Pibiri, I. Recent Advances: Heterocycles in Drugs and Drug Discovery. *Int. J. Mol. Sci.* **2024**, *25* (17), 9503. https://doi.org/10.3390/ijms25179503.
3. Amin, A.; Qadir, T.; Sharma, P. K.; Jeelani, I.; Abe, H. A Review on The Medicinal And Industrial Applications of N-Containing Heterocycles. *Open Med. Chem. J.* **2022**, *16* (1), e187410452209010. https://doi.org/10.2174/18741045-v16-e2209010.
4. Marshall, C. M.; Federice, J. G.; Bell, C. N.; Cox, P. B.; Njardarson, J. T. An Update on the Nitrogen Heterocycle Compositions and Properties of U.S. FDA-Approved Pharmaceuticals (2013–2023). *J. Med. Chem.* **2024**, *67* (14), 11622–11655. https://doi.org/10.1021/acs.jmedchem.4c01122.
5. Vitaku, E.; Smith, D. T.; Njardarson, J. T. Analysis of the Structural Diversity, Substitution Patterns, and Frequency of Nitrogen Heterocycles among U.S. FDA Approved Pharmaceuticals: Miniperspective. *J. Med. Chem.* **2014**, *57* (24), 10257–10274. https://doi.org/10.1021/jm501100b.
6. Cevidoplenib (SYK inhibitor). https://oscotec.com/Rheumatoidarthritis (accessed 17 August 2025).
7. Search Orphan Drug Designations and Approvals https://www.accessdata.fda.gov/scripts/opdlisting/oopd/detailedIndex.cfm?cfgridkey=994823 (accessed 29 August 2025).
8. Costall, B.; Domeney, A. M.; Gunning, S. J.; Kelly, M. E.; Naylor, R. J.; Nohria, V.; Owera-Atepo, J. B.; Simpson, K. M.; Tan, C. C. W.; Tattersall, D. The action of dazopride to enhance gastric emptying and block emesis. *Neuropharmacology* **1987,** *26* (7, Part 1), 669–677. https://doi.org/10.1016/0028-3908(87)90227-9.
9. Surivet, J.-P.; Jacob, E. M.; Kessler, M.; Kohl, C.; Vaillant, C.; Bezençon, O.; Bouis, P.; Busch, L.; Gauvin, J.-C.; Kiry, M.; Litou, C.; Masse, F.; Mathieu, C.-A.; Mirre, A.; Peters, J.-U.; Rager, T.; Rey, M.; Ruetsch, R.; Steiner, M. A. Discovery of IDOR-1117-1680, a dual orexin receptor antagonist with fast onset and short duration of action for the treatment of insomnia. *Bioorg. Med. Chem.* **2025,** *122*, 118132. https://doi.org/10.1016/j.bmc.2025.118132.
10. Amlaiky, N.; Leclerc, G. Synthesis of the New Heterocyclic Hydroxy Compounds 4-Hydroxyisoxazolidine, 3-Hydroxymethylisoxazolidine, 3-Hydroxymethylhexahydro-1,2-Oxazine, and 4-Hydroxy Hexahydro-1,2-Oxazepine. *Synthesis* **1982**, *1982* (05), 426–428. https://doi.org/10.1055/s-1982-29825.
11. Martin, B. P.; Cooper, M. E.; Donald, D. K.; Guile, S. D. A Simple and Efficient Synthesis of Optically Pure 4-Alkylisoxazolidin-4-Ols. *Tetrahedron Lett.* **2006**, *47* (43), 7635–7639. https://doi.org/10.1016/j.tetlet.2006.08.054.
12. Bouzoubaa, M.; Leclerc, G. The Reaction of Amines with Phthalimide Derivatives a Convenient Synthesis of Isoxazolidine. *Tetrahedron Lett.* **1984**, *25* (29), 3067–3070. https://doi.org/10.1016/0040-4039(84)80009-X.
13. Rohrbacher, F.; Baldauf, S.; Wucherpfennig, T.; Bode, J. Product Selectivity in KAHA Ligations: Ester vs. Amide Formation with Cyclic Hydroxylamines. *Synlett* **2017**, *28* (15), 1929–1933. https://doi.org/10.1055/s-0036-1588480.
14. King, H. 81. isoOxazolidine and Tetrahydro-1 : 2-Isooxazine. *J. Chem. Soc. Resumed* **1942**, 432. https://doi.org/10.1039/jr9420000432.
15. Gerhard, F. Ueber Die Base C_9 H_{12} N_2 O Aus Epichlorhydrin Und Phenylhydrazin. *Berichte Dtsch. Chem. Ges.* **1891**, *24* (1), 352–357. https://doi.org/10.1002/cber.18910240168.

ISSN 2308-8303 (Print) / 2518-1548 (Online)

16. Sherrill, R. G. The First Synthesis of 1,5-Diazacyclooctan-2-One and Differentially Protected 1,5-Diazacyclooctanes. *Tetrahedron Lett.* **2007**, *48* (39), 7053–7056. https://doi.org/10.1016/j.tetlet.2007.07.083.
17. Ahn, J. H.; Kim, J. A.; Kim, H.-M.; Kwon, H.-M.; Huh, S.-C.; Rhee, S. D.; Kim, K. R.; Yang, S.-D.; Park, S.-D.; Lee, J. M.; Kim, S. S.; Cheon, H. G. Synthesis and Evaluation of Pyrazolidine Derivatives as Dipeptidyl Peptidase IV (DP-IV) Inhibitors. *Bioorg. Med. Chem. Lett.* **2005**, *15* (5), 1337–1340. https://doi.org/10.1016/j.bmcl.2005.01.020.
18. Boros, E. E.; Bouvier, F.; Randhawa, S.; Rabinowitz, M. H. A Convenient Synthesis of Pyrazolidine and 3-amino-6,7-dihydro-1H,5H-pyrazolo[1,2-a] Pyrazol-1-one. *J. Heterocycl. Chem.* **2001**, *38* (3), 613–616. https://doi.org/10.1002/jhet.5570380310.
19. Surivet, J.-P.; Jacob, E. M.; Kessler, M.; Kohl, C.; Vaillant, C.; Bezençon, O.; Bouis, P.; Busch, L.; Gauvin, J.-C.; Kiry, M.; Litou, C.; Masse, F.; Mathieu, C.-A.; Mirre, A.; Peters, J.-U.; Rager, T.; Rey, M.; Ruetsch, R.; Steiner, M. A. Discovery of IDOR-1117-1680, a Dual Orexin Receptor Antagonist with Fast Onset and Short Duration of Action for the Treatment of Insomnia. *Bioorg. Med. Chem.* **2025**, *122*, 118132. https://doi.org/10.1016/j.bmc.2025.118132.
20. Michaelis, A.; Lampe, O. III. Ueber Synthesen Vermittelst Natriumphenylhydrazins. 5. Ueber Das Phenylpyrazolidin. *Justus Liebigs Ann. Chem.* **1893**, *274* (3), 316–331. https://doi.org/10.1002/jlac.18932740306.
21. Laufersweiler, M. J.; Brugel, T. A.; Clark, M. P.; Golebiowski, A.; Bookland, R. G.; Laughlin, S. K.; Sabat, M. P.; Townes, J. A.; VanRens, J. C.; De, B.; Hsieh, L. C.; Heitmeyer, S. A.; Juergens, K.; Brown, K. K.; Mekel, M. J.; Walter, R. L.; Janusz, M. J. The Development of Novel Inhibitors of Tumor Necrosis Factor-α (TNF-α) Production Based on Substituted [5,5]-Bicyclic Pyrazolones. *Bioorg. Med. Chem. Lett.* **2004**, *14* (16), 4267–4272. https://doi.org/10.1016/j.bmcl.2004.06.001.
22. Corpas, J.; Caldora, H. P.; Di Tommaso, E. M.; Hernandez-Perez, A. C.; Turner, O.; Azofra, L. M.; Ruffoni, A.; Leonori, D. A General Strategy for the Amination of Electron-Rich and Electron-Poor Heteroaromatics by Desaturative Catalysis. *Nat. Catal.* **2024**, *7* (5), 593–603. https://doi.org/10.1038/s41929-024-01152-1.
23. Damavarapu, R.; Surapaneni, R.; Duddu, R.; Farhor, F.; Dave, P.; Parrish, D. Synthesis of Nitropyrazolidines. *J. Heterocycl. Chem.* **2007**, *44* (1), 241–244. https://doi.org/10.1002/jhet.5570440141.
24. Wildonger, K. J.; Ratcliffe, R. W. Heteroaryliumthio Substituted Carbapenem Derivatives: Synthesis and in Vitro Activity of 1.BETA.-Methyl-2-(Dihydropyrrolotriazoliumthio)Carbapenems. *J. Antibiot. (Tokyo)* **1993**, *46* (12), 1866–1882. https://doi.org/10.7164/antibiotics.46.1866.
25. Guggenheim, K. G.; Butler, J. D.; Painter, P. P.; Lorsbach, B. A.; Tantillo, D. J.; Kurth, M. J. Synthesis of Spiro-Fused Pyrazolidoylisoxazolines. *J. Org. Chem.* **2011**, *76* (14), 5803–5812. https://doi.org/10.1021/jo200924y.
26. Kaliberda, O. V.; Leha, D. O.; Peredrii, V. S.; Levchenko, K.; Zarudnitskii, E. V.; Ryabukhin, S. V.; Volochnyuk, D. M. Scalable Synthesis of 6-Functionalized 1,4-Oxazepanes. *Org. Process Res. Dev.* **2026**. https://doi.org/10.1021/acs.oprd.5c00494.
27. Wang, C.; Zhen, Z.; Zhao, J.; Dowd, P. The Synthesis of 3-Cyclopentadienylidenecyclobutanone. *Synthetic Communications* **1999,** *29* (4), 631–643. https://doi.org/10.1080/00397919908085812.

Information about the authors:
Oleksandr V. Kaliberda (*corresponding author*), Ph.D. Student, Institute of Organic Chemistry of the National Academy of Sciences of Ukraine; Laboratory Head, Enamine Ltd.; e-mail for correspondence: o.kaliberda@enamine.net.
Evgenij V. Zarudnitskii, Ph.D. in Chemistry, Senior Researcher of the Medicinal Chemistry Department, Institute of Organic Chemistry of the National Academy of Sciences of Ukraine; Associate Professor of the Department of Organic Chemistry and Technology of Organic Compounds, Faculty of Chemistry and Technology, National Technical University of Ukraine "Igor Sikorsky Kyiv Polytechnic Institute". https://orcid.org/0000-0003-2038-4243.

Journal of Organic and Pharmaceutical Chemistry

Original Research

OPEN ACCESS
Freely available online on
http://ophcj.nuph.edu.ua

UDC [547.792.9+547.789.69]:615.31

N. I. Korol[1], V. V. Pantyo[1], V. O. Bestritska[1], K. A. Avdeeva[1],
D. I. Molnar-Babilya[2,3], M. M. Fizer[4], M. V. Slivka[1]

[1] Uzhhorod National University, 53/1 Fedytca Str., 88000 Uzhhorod, Ukraine
[2] Ferenc Rákóczi II Transcarpathian Hungarian Institute, 6 Kossuth Sq., Beregovo 90200, Ukraine
[3] Mukachevo State University, 26 Uzhhorodska Str., 89608 Mukachevo, Ukraine
[4] University of Nevada Reno, 1664 N. Virginia Str., 89557 Reno, NV, United States

Antimicrobial and Antifungal Study of Thiazolotriazolium Salts: *in vivo* Investigation, and Molecular Docking

Abstract

Three thiazolo[3,2-*b*][1,2,4]triazol-7-ium hexabromotellurates **1**–**3** were synthesized *via* the electrophilic heterocyclization of methallyl thioether precursors using a classical tellurium(IV) electrophilic reagent generated *in situ* from TeO_2 and 1 M hydrobromic acid. The resulting salts were comprehensively screened for the antimicrobial activity against five clinically relevant pathogens: *Staphylococcus aureus*, *Candida albicans*, *Klebsiella pneumoniae*, *Escherichia coli*, and *Pseudomonas aeruginosa*. Biological assays revealed that compound **1** containing a 2-(4-pyridyl) substituent demonstrated the strongest activity profile, particularly against *C. albicans* (MIC = 15.625 μg mL^{-1}) and *E. coli* (MIC = 31.25 μg mL^{-1}). Compound **2**, substituted with the 3-hydroxyphenyl moiety, also showed a significant antifungal efficacy, while compound **3** (with the 2-phenyl substituent) exhibited a relatively low activity. To rationalize these differences, the molecular docking was performed targeting MurB (UDP-N-acetylenolpyruvoylglucosamine reductase, PDB 1MBT) and DNA gyrase B (GyrB, PDB 4URO), two bacterial enzymes known to be essential for the viability of Gram-negative pathogens. The docking results confirmed the experimental data, showing strong π–π stacking and hydrogen bonding between compound **1** and the FAD-containing binding pocket of MurB. This work highlights the utility of the tellurium-induced annulation in producing biologically potent heterocycles and emphasizes the structure–activity relationships driven by substituents in position 2 of the fused scaffold.

Keywords: [1,3]thiazolo[3,2-*b*][1,2,4]triazol-7-ium hexabromotellurates; anti-microbial activity; docking; electrophilic cyclization; MurB; GyrB; molecular docking

Н. І. Король[1], В. В. Пантьо[1], В. О. Бестріцька[1], К. А. Авдєєва[1], Д. І. Молнар[2,3], М. М. Фізер[4], М. В. Сливка[1]

[1] Ужгородський національний університет, вул. Фединця, 53/1, м. Ужгород, 88000, Україна
[2] Ференца Ракоці ІІ Закарпатський Угорський Інститут, пл. Кошута, 6, м. Берегово, 90200, Україна
[3] Мукачівський державний університет, вул. Ужгородська, 26, м. Мукачево, 89608, Україна
[4] Університет Невади (Рено),
вул. Н. Вірджінія, 1664, м. Рено, 89557, Штат Невада, Сполучені Штати Америки

Антимікробне й протигрибкове дослідження солей тіазолотриазолію: *in vivo* вивчення та молекулярний докінг

Анотація

Три тіазоло[3,2-*b*][1,2,4]триазол-7-ій гексабромтелурати **1**–**3** синтезовано електрофільною гетероциклізацією металіл-тіоетерів з використанням класичного електрофільного реагенту на основі телуру(IV), отриманого *in situ* з TeO_2 та 1 М бромоводневої кислоти. Отримані солі ретельно досліджено на антимікробну активність проти п'яти клінічних штамів: *Staphylococcus aureus, Candida albicans, Klebsiella pneumoniae, Escherichia coli* та *Pseudomonas aeruginosa*. Мікробіологічними дослідженнями виявлено, що сполука **1**, яка містить 2-(4-піридил)-замісник, продемонструвала найсильніший профіль активності, особливо проти *C. albicans* (МІК = 15.625 мкг $мл^{-1}$) та *E. coli* (МІК = 31.25 мкг $мл^{-1}$). Сполука **2**, заміщена 3-гідроксифенільним фрагментом, також продемонструвала значну протигрибкову ефективність, тоді як сполука **3** (з 2-фенільним замісником) продемонструвала порівняно низьку активність. Щоб раціоналізувати ці відмінності, було проведено молекулярний докінг на ферментах MurB (UDP-N-ацетиленолпірувоїлглюкозамін редуктаза, PDB 1MBT) та ДНК-гірази B (GyrB, PDB 4URO), які відіграють важливу роль у життєдіяльності грамнегативних бактерій. Результати докінгу підтвердили експериментальні дані, показавши сильний π–π-стекінг та водневі зв'язки між сполукою **1** та кишенею зв'язування MurB, що містить FAD. Ця робота підкреслює корисність індукованої телуром

ISSN 2308-8303 (Print) / 2518-1548 (Online)

ануляції для отримання біологічно активних гетероциклів та акцентує на взаємозв'язках структура-активність, зумовлених замісниками в положенні 2 конденсованого каркаса.

Ключові слова: [1,3]тіазоло[3,2-*b*][1,2,4]триазол-7-ій гексабромтелурати; антимікробна активність; докінг; електрофільна циклізація; MurB; GyrB; молекулярний докінг

Citation: Korol, N. I.; Pantyo, V. V.; Bestritska, V. O.; Avdeeva, K. A.; Molnar-Babilya, D. I.; Fizer, M. M.; Slivka, M. V. The Antimicrobial and Antifungal Study of Thiazolotriazolium Salts: *in vivo* Investigation, and Molecular Docking. *Journal of Organic and Pharmaceutical Chemistry* **2025**, *23* (4), 44–56.

https://doi.org/10.24959/ophcj.25.344433

Received: *3 October 2025*; **Revised:** *17 November 2025*; **Accepted:** *25 November 2025*

Funding: The research was carried out with the grant support of the National Research Foundation of Ukraine (project No 2023.03/0176).

Conflict of interests: The authors have no conflict of interests to declare.

■ Introduction

The escalating global health threat posed by the antimicrobial resistance (AMR) across bacterial and fungal pathogens necessitates continuous, intensive efforts to identify structurally novel antimicrobial agents [1–3]. The emergence of multidrug-resistant (MDR) organisms has rendered many conventional antibiotics ineffective, leading to the increased morbidity and mortality worldwide. Consequently, modern medicinal chemistry prioritizes the development of new compounds with unique scaffolds that can circumvent resistance mechanisms [4, 5].

Among the most promising classes of molecules are heterocyclic compounds containing fused nitrogen- and sulfur-containing rings. These scaffolds exhibit a notable conformational rigidity, redox properties, and binding specificity, positioning them as privileged frameworks for the drug design [6–16]. Specifically, thiazole-fused systems, such as thiazolotriazoles, have attracted attention due to their broad spectrum of biological activities, including antimicrobial, antiviral, antioxidant, and enzyme-inhibitory effects [13, 17–23]. Their aromatic rigidity and electron-rich structure enable fine-tuning of pharmacodynamic and pharmacokinetic parameters.

A powerful synthetic approach for assembling such heterocycles involves electrophilic heterocyclization [24]. In particular, reactions mediated by tellurium(IV) electrophiles (generated *in situ* from TeO_2 and aqueous hydrobromic acid) have enabled the efficient introduction of the tellurium moiety into condensed heterocyclic salts with the pharmaceutical potential [25–27]. Tellurium-containing organic compounds have the biological potency [28–32], but their behavior in biological systems has not been elucidated to date [33]. As previously reported in our works, the electrophilic heterocyclization method provides access to bioactive thiazolotriazole $TeHal_3$ frameworks

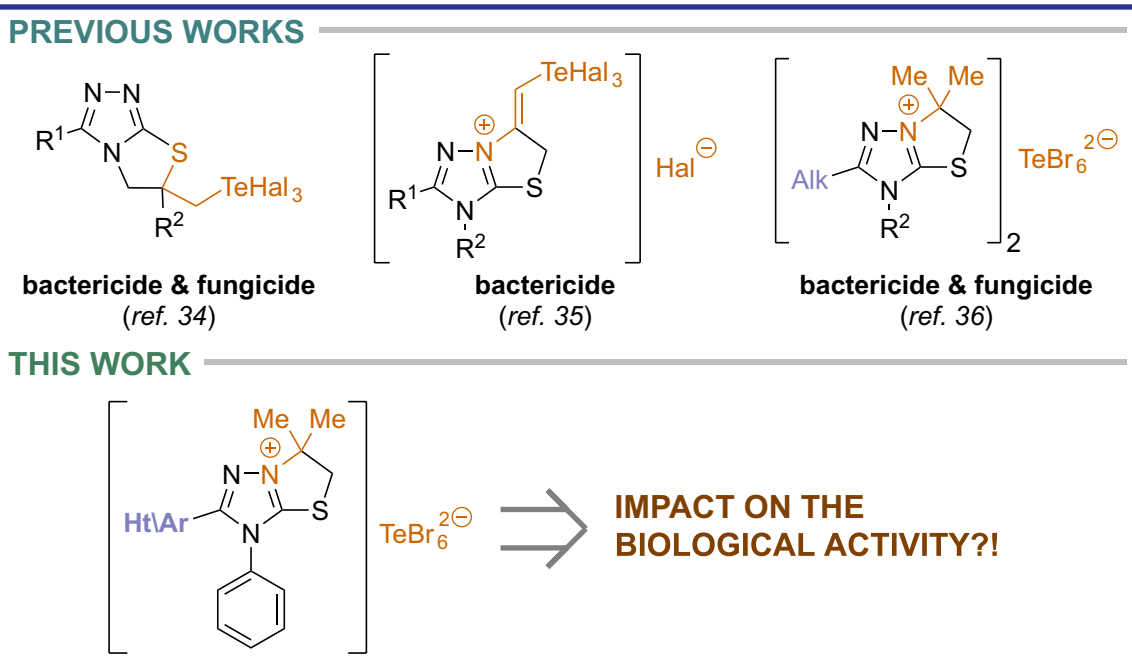

Figure 1. The synthesis of bioactive thiazolotriazole derivatives

in excellent yields under mild conditions [34, 35] (**Figure 1**). An additional design element involves incorporating the halotellurate anion, which can improve the bactericidal and fungicidal activity [36, 37]. This anion not only stabilizes the cationic framework, but also confers physicochemical properties that are beneficial for the biological activity, such as altered solubility, membrane permeability, and redox activity. Prior studies have shown that tellurium-based fragments can disrupt the microbial redox balance or form covalent bonds with intracellular thiols, thereby bypassing conventional resistance pathways [36].

Despite these promising features, the structure-activity relationship (SAR) studies for thiazolotriazolium salts remain underexplored. In particular, the effect of varying the substituent in position 2 of the heterocyclic core on the antimicrobial potency and selectivity is not well understood. To fill this gap, we synthesized and investigated three thiazolotriazolium hexabromotellurates with systematically varied position 2 substituents:

- Compound **1**: 2-(4-pyridyl), chosen for its capacity for the hydrogen bonding and the potential metal chelation.
- Compound **2**: 2-(3-hydroxyphenyl), to examine the role of the polar, hydrogen-bond-donating phenyl group.
- Compound **3**: 2-phenyl, serving as a neutral, lipophilic reference.

Following the synthesis, their antimicrobial activities were screened against representative Gram-positive (*Staphylococcus aureus*), Gram-negative (*Escherichia coli*, *Klebsiella pneumoniae*, *Pseudomonas aeruginosa*), and fungal (*Candida albicans*) strains. To rationalize the bioactivities observed, we conducted the predictive molecular docking against two bacterial enzymes: UDP-N-acetylenolpyruvoylglucosamine reductase (MurB, PDB ID: 1MBT), a key enzyme in the peptidoglycan biosynthesis, and DNA gyrase B (GyrB, PDB ID: 4URO), a crucial target for quinolone antibiotics [38]. These computational studies aimed to correlate the binding affinity and interaction profiles with experimental minimum inhibitory concentration (MIC) values and to identify structural determinants of activity.

Taken together, this study provides a comprehensive analysis of the antimicrobial potential of thiazolotriazolium hexabromotellurates and offers valuable insights into the SAR trends that govern their efficacy, supporting future optimization and development of this class of metallo-heterocyclic antibiotics.

■ Results and Discussion

Synthesis of compounds 1–3

The thiazolo[3,2-*b*]triazol-7-ium hexabromotellurate derivatives **1–3** were synthesized *via* a concise electrophilic heterocyclization of their respective methallyl thioether precursors (**Scheme 1**) similar to the procedure described [37]. This transformation was mediated by an *in situ*-generated tellurium(IV) electrophilic reagent, generated from tellurium dioxide (TeO_2) and hydrobromic acid in acetonitrile.

The above approach confers notable synthetic benefits as it simultaneously accomplishes the annulation of the fused heterocyclic core and the formation of the biologically active hexabromotellurate counterion $TeBr_6^{2-}$ in a single operational step. This dual-function transformation not only simplifies the workflow, but also enhances the atom economy and the isolation efficiency of the desired products **1–3**.

Antimicrobial and Antifungal Activity Evaluation

The antimicrobial and antifungal activities of compounds **1–3** were evaluated against *Staphylococcus aureus*, *Candida albicans*, *Klebsiella pneumoniae*, *Escherichia coli*, and *Pseudomonas aeruginosa* using MIC and MBC assays (**Table 1**). Specified strains were collected from the periodontal pockets of patients with chronic generalized

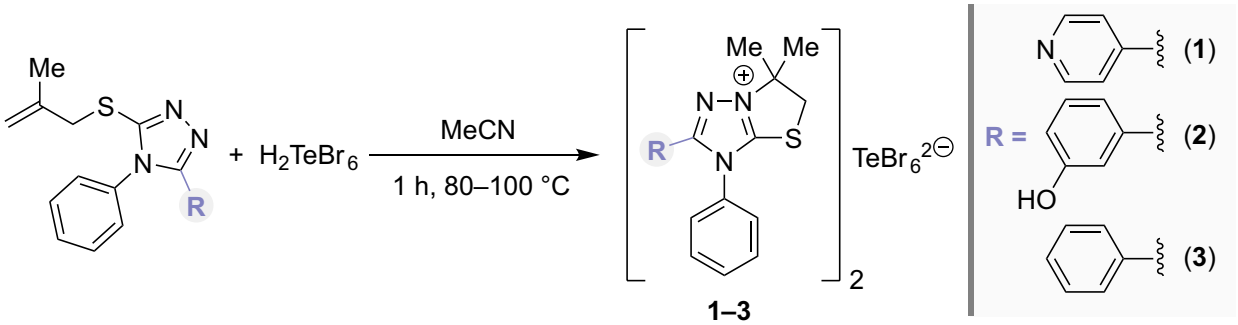

Scheme 1. The synthetic approach to [1,3]thiazolo[3,2-*b*][1,2,4]triazol-7-ium hexabromotellurates **1–3**

ISSN 2308-8303 (Print) / 2518-1548 (Online)

Table 1. The antimicrobial and antifungal activities of compounds **1–3** evaluated against *Staphylococcus aureus*, *Candida albicans*, *Klebsiella pneumoniae*, *Escherichia coli*, and *Pseudomonas aeruginosa* using MIC and MBC assays

Compound	Substituent	MIC / MBC, μg mL^{-1}				
		C. albicans	*S. aureus*	*K. pneumoniae*	*E. coli*	*P. aeruginosa*
1	4-pyridyl	15.625 / 62.5	125 / 250	125 / 125	31.25 / 62.5	125 / 125
2	3-hydroxyphenyl	15.625 / 31.25	62.5 / 250	125 / 125	125 / 125	125 / 250
3	phenyl	62.5 / 125	125 / 250	125 / 125	125 / 125	125 / 125
4[b]	methyl	31.25 / 125	31.25 / 62.5	7.81 / 15.63	1.95 / 3.9	– / –[a]
5[b]	heptyl	ND[a]	– / –[a]	1.95 / 15.63	62.5 / 125	250 / 500
6[b]	Pentadecyl	ND[a]	– / –[a]	31.25 / 62.5	15.63 / 31.25	62.5 / 125

Note: [a] "–" indicates that the compound was not active against the test organism at 500 μg mL^{-1}; ND – not determined; [b] compounds **4**, **5**, **6** were reported previously (**4** – compound **2a** [36]; **5** – compound **2b** [36]; **6** – compound 2d [36])

periodontitis who underwent treatment at the Uzhhorod University dental clinic. All three thiazolotriazolium salts demonstrated a measurable activity against this panel of clinically relevant pathogens, and were consistent with the well-established antimicrobial potential of thiazole- and triazole-based heterocycles [39–41].

To enrich the structure–activity relationship (SAR) analysis, the antimicrobial performance of compounds **1–3** was compared with that of previously reported 2-substituted thiazolotriazolium analogs from reference [36], specifically the aliphatic derivatives.

The MIC/MBC data reveal that the substituent in position 2 markedly influences the potency across both aromatic and aliphatic analogs. For the Gram-positive *S. aureus*, compound **2** (3-hydroxyphenyl) exhibited the lowest MIC (62.5 μg mL^{-1}) among compounds **1–3**. This potency is comparable to methyl derivative **4** (MIC ≈ 31.25 μg mL^{-1}), but superior to the bulky heptyl **5** and pentadecyl **6** (MIC > 500 μg mL^{-1}). All tested compounds **1–3** displayed primarily bacteriostatic effects, as evidenced by high MBC values (~250 μg mL^{-1}). Thus, while a polar aromatic substituent (compound **2**) or methyl group (**5**) improves MIC relative to the phenyl group or a bulky alkyl group, neither class substantially reduces the bactericidal concentration for this pathogen.

A different trend emerges with the fungal pathogen *C. albicans*. The aromatic derivatives **1** and **2** achieved a four-fold lower MIC (15.63 μg mL^{-1}) than the phenyl analog **3** and showed a stronger antifungal activity than the only aliphatic reference with available data (compound **4**, MIC ≈ 31.25 μg mL^{-1}). Antifungal data for the heptyl and pentadecyl derivatives (compounds **5** and **6**) were not determined (ND). These results indicate that polar and π-conjugated 2-substituents confer a superior antifungal potency, likely by facilitating stronger interactions with fungal targets or enhancing the membrane insertion, whereas very short or long alkyl groups are less favorable.

As MIC values are reported in μg mL^{-1}, equal mass concentrations do not always correspond to equal molar concentrations. When converted to micromoles per liter (μM), compounds **1** and **2** have nearly identical MIC values due to similar molecular weights, whereas among the aliphatic analogs, the heptyl derivative (compound **5**) has a higher molecular weight than the methyl derivative **4**, leading to the lower molar potency despite the identical MIC in μg mL^{-1}.

Against Gram-negative bacteria, distinct SAR profiles were observed. Compound **1** (4-pyridyl) was uniquely potent against *E. coli* (MIC 31.25 μg mL^{-1}), whereas compounds **2** and **3** required 125 μg mL^{-1} to inhibit the growth. None of the simple alkyl analogs from [36] matched this activity: even the heptyl derivative **5** inhibited *E. coli* only in 125 μg mL^{-1}. This underscores that the basic 4-pyridyl substituent that is capable of protonation and hydrogen bonding is far more effective in penetrating the Gram-negative outer membrane or engaging intracellular targets than hydrophobic groups. In contrast, all compounds displayed a modest activity against *K. pneumoniae* and *P. aeruginosa* (MIC ≥ 125 μg mL^{-1}). Even the long-chain **6** did not improve potency. It is consistent with the notion that excessive lipophilicity hinders penetration of Gram-negative envelopes. The heptyl analog **5** achieved sub-2 μg mL^{-1} MICs against certain *Klebsiella* isolates in [36], but lost its activity against Gram-positives, indicating a compromise, in which hydrophobicity favored Gram-negative uptake at the cost of Gram-positive efficacy. The small methyl substituent (**4**) maintained a broader, balanced profile.

Introducing polar functionality in position 2 markedly enhanced the activity against *C. albicans* and *S. aureus*. Compounds **1** (4-pyridyl) and **2** (3-hydroxyphenyl) both lowered the MIC four-fold relative to the unsubstituted phenyl

analog **3**, suggesting that hydrogen-bonding or dipolar groups were highly beneficial for the antifungal efficacy. The 4-pyridyl moiety introduces a basic nitrogen that can accept a proton and engage in the hydrogen bonding, while the 3-hydroxyphenyl group offers both donor and acceptor capability. These functionalities likely strengthen interactions with fungal biomolecules (e.g. enzymes or membrane components) and improve distribution in aqueous media. Compound **2** exhibited the lowest MBC against *C. albicans* (31.25 μg mL^{-1}), indicating a more rapid fungicidal effect when a hydroxyl group was present. On the contrary, the nonpolar phenyl group of compound **3** cannot enter into such interactions, correlating with its reduced potency.

Against *S. aureus*, only compound **2** showed a markedly improved MIC relative to other analogs, suggesting that a hydroxyl substituent is particularly advantageous for the Gram-positive activity. The simpler peptidoglycan-rich envelope of Gram-positive bacteria may allow easier penetration of polar compounds, and the hydrogen bonding likely enhances binding to targets. While compound **1** did not improve the MIC in *S. aureus* to the same extent, both polar-substituted derivatives (**1**, **2**) achieved lower MICs than the phenyl analog. Nonetheless, identical MBCs across the series imply that high concentrations remain necessary for the bactericidal activity against *S. aureus*.

E. coli was uniquely susceptible to compound **1**. Its MIC of 31.25 μg mL^{-1} is four times lower than that of compounds **2** or **3**. This selectivity arises from the properties of the 4-pyridyl substituent: the pyridine nitrogen can be protonated under physiological conditions, imparting a positive charge and the hydrogen-bonding capacity that may enhance interactions with the negatively charged lipopolysaccharide layer and facilitate passage through porins. Furthermore, compound **1** has a lower log*P* (~2.6) and a moderate polar surface area (~35 $Å^2$) relative to compounds **2** and **3** (log*P* ≈ 3.1 and TPSA ~42/22 $Å^2$), suggesting a more balanced polarity-lipophilicity profile suited to the Gram-negative penetration. By comparison, 3-hydroxyphenyl compound **2** carries a neutral polar group which higher TPSA may impede transit across the hydrophobic outer membrane; phenyl compound **3** is more hydrophobic and may be sequestered in membrane lipids or effluxed before reaching its target. These differences rationalize why only compound **1** exhibits a strong activity against *E. coli,* while the others do not. Against *K. pneumoniae* and *P. aeruginosa*, however, none of the 2-substituents were sufficient to overcome the formidable permeability barriers and efflux mechanisms characteristic of these species, resulting in uniformly modest MIC values.

Thus, the SAR trends reveal that the polarity and hydrogen-bonding capacity in position 2 dramatically improve the antifungal and Gram-positive activity, whereas an optimal balance of polarity and basicity (exemplified by the 4-pyridyl group) is crucial for the potent *E. coli* activity. Hydrophobic 2-substituents can enhance uptake in certain Gram-negatives (e.g., the heptyl group in **5** [36]), but tend to compromise the Gram-positive efficacy and do not outperform the polar analogs overall. In general, the new aromatic compounds **1–3** in almost all cases correspond to or exceed the activity of aliphatic analogs. In particular, the 4-pyridyl and 3-hydroxyphenyl substitutions increase the activity against *C. albicans*, *S. aureus,* and *E. coli* relative to simple alkyl groups, while an optimally sized alkyl chain (heptyl) offers the intermediate activity, but fails to rival the broad-spectrum efficacy of aromatic analogs. These findings highlight the value of incorporating the polar or π-conjugated functionality in C-2 to improve the antimicrobial profile of this scaffold.

***In silico* ADMET analysis of compounds 1–3**

To complement the experimental evaluation, we used ADMETlab to predict the absorption, distribution, metabolism, excretion, and toxicity profiles of compounds **1–3**. These models integrate physicochemical descriptors and machine-learning algorithms to estimate pharmacokinetic and safety parameters [42–45], offering a comparative view of how the three 2-substituents influence drug-likeness. A radar-plot visualizing the predicted physicochemical spaces of compounds **1–3** is presented in **Figure 2**.

As summarized in **Table 2**, all three cations tested fulfill Lipinski's rule-of-five criteria with molecular weights below 325 Da, log*P* values between ~2.6 and 3.2, and hydrogen-bond donor counts ≤ 1, indicating classical drug-like characteristics [46]. Compound **1** (4-pyridyl) exhibits the highest predicted aqueous solubility and unbound fraction, while compound **2** (3-hydroxyphenyl) has the largest topological polar surface area due to its phenolic OH and is predicted to be the least soluble. Compound **3** (phenyl) is the least polar and slightly more hydrophobic than

ISSN 2308-8303 (Print) / 2518-1548 (Online)

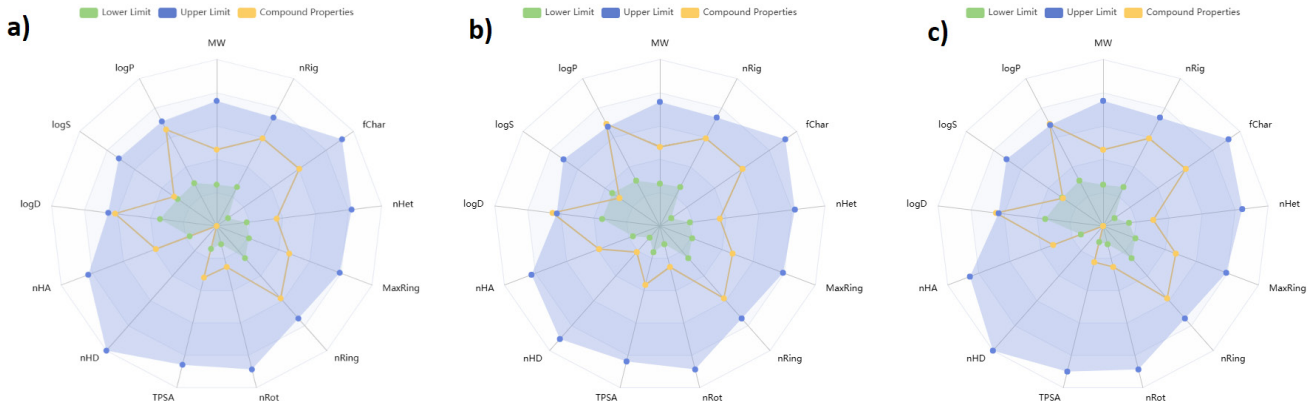

Figure 2. A radar-plot comparison of the predicted physicochemical profiles of thiazolo[3,2-*b*]triazol-7-ium cations **1**–**3** synthesized. Each panel illustrates the compound-specific descriptor values (orange) relative to the established lower (green) and upper (blue) thresholds associated with drug-likeness and acceptable oral bioavailability ranges. **(a)** Compound **1**. **(b)** Compound **2**. **(c)** Compound **3**.

Table 2. Physicochemical and absorption descriptors for compounds **1**–**3**

Descriptor	Compound			Comments
	1	**2**	**3**	
Molecular weight (MW, Da)	309.12	324.12	308.12	all below 500 Da, fulfilling the Lipinski's mass criterion
H-bond donors/acceptors (nHD/nHA)	0 / 4	1 / 4	0 / 3	introducing a phenolic OH in **2** increases the donor count and TPSA; the hydrogen-bond acceptor count includes hetero atoms of the fused thiazolotriazolium core (notably the N1 atom of the triazolium ring)
Topological polar surface area (TPSA, Å^2)	34.59	41.93	21.7	TPSA correlates with polarity; **2** is most polar due to the hydroxyl group
No rotatable bonds / rings / hetero atoms	2 / 4 / 5	2 / 4 / 5	2 / 4 / 4	a similar core rigidity across the series
Fraction of sp^3 carbons (Fsp3)	0.235	0.222	0.222	all highly aromatic cations (low Fsp3)
Predicted solubility logS	-3.73	-4.67	-4.07	negative values imply low aqueous solubility; **2** is least soluble
Predicted lipophilicity log*P*	2.61	3.15	3.06	**2** and **3** are more hydrophobic; **1** is more balanced
Caco-2 permeability (log cm s^{-1})	-5.19	-5.43	-5.02	values < −5 indicate poor intestinal permeability for all compounds
MDCK cell permeability (log cm s^{-1})	-4.53	-4.81	-4.63	consistent with the limited passive diffusion
Predicted human intestinal absorption (HIA)	≈ 0	≈ 0	≈ 0	extremely low (<10−5), reflecting the permanent cationic charge
Blood–brain barrier (BBB) permeability	0.114	0.006	0.181	probabilities < 0,5 indicate a negligible CNS penetration; only **3** shows a slightly higher score, but remains low
P-gp inhibition / substrate	inhibitor ≈1; substrate ≪1	inhibitor ≈1; substrate ≈0.01	inhibitor ≈1; substrate ≈0.0046	all three strongly inhibit P-gp while being poor substrates; this could the increase intracellular accumulation, but may cause drug–drug interactions
BCRP / BSEP	moderate BCRP (0.51–0.62) and strong BSEP inhibition (≈1) for all	similar for all	potential for the biliary transport inhibition	

compound **1**. All three cations exhibit very low predicted Caco-2 and MDCK permeabilities and negligible human intestinal absorption probabilities, consistent with their permanent positive charge and high polarity. The blood–brain barrier penetration is predicted to be minimal.

Table 3 shows that the compounds are predicted to have moderate volumes of distribution and strong plasma protein binding (> 90 %). Compound **1** has the highest unbound fraction (≈ 8 %), suggesting greater availability for the target engagement. Predicted elimination half-lives are short (< 0.5 h), implying rapid clearance although this may be offset by a high protein binding and potential transporter interactions. Bioconcentration factors are modest (≈ 2–3), indicating the limited environmental persistence.

Cations **1–3** differ in their predicted cytochrome P450 inhibition profiles. Compound **1** shows a strong inhibition of CYP2C19 and CYP2B6 and a moderate inhibition of CYP1A2, 2C9, 2D6, and 3A4, raising the possibility of drug–drug interactions. Compound **2** retains the strong CYP2C19 inhibition, but exhibits low probabilities of inhibiting other isoforms. Compound **3** shows an intermediate behavior, with the modest inhibition of CYP2B6 and CYP2C9 and the low inhibition of CYP1A2 and CYP2D6. None of the compounds are predicted to be CYP substrates.

ADMETlab predicts moderate to high probabilities of mutagenicity, carcinogenicity, drug-induced liver injury, and genotoxicity for all three compounds. Probabilities for nephrotoxicity, neurotoxicity, and hERG inhibition fall in the low to moderate range, suggesting some cardiotoxic and neurological risks. Skin sensitization probabilities are high. Among the three derivatives, compound **2** generally shows slightly lower toxicity scores.

The predicted ADMET profiles underscore both advantages and limitations of this scaffold. On the positive side, the cations satisfy fundamental drug-likeness criteria and exhibit a moderate lipophilicity, which can support the passive membrane diffusion. However, their predicted oral bioavailability is extremely low due to the poor permeability and permanent cationic charge, suggesting that the parenteral administration or prodrug strategies may be necessary. Compound **1** combines relatively better solubility with a higher risk of CYP-mediated interactions and toxicity; compound **2** has a lower solubility, but slightly reduced toxicity; compound **3** is the most hydrophobic and strongly protein-bound. Future optimization should therefore focus on enhancing the permeability and reducing the enzyme inhibition and toxicity while maintaining the beneficial aspects of the scaffold.

Molecular docking study

Taking into account the pronounced antifungal activity of compounds **1** and **2** against *Candida albicans* (**Table 1**), the molecular docking studies were primarily designed to investigate lanosterol 14-α-demethylase (CYP51, PDB ID: 5V5Z), a key enzyme in the ergosterol biosynthesis and a well-established molecular target of clinically used azole antifungals. The inhibition of CYP51 provides a direct and biologically plausible explanation for the antifungal effects of the thiazolotriazolium salts observed. The corresponding docking results and binding energy trends are summarized in **Table 4**.

For comparative and exploratory purposes only, docking calculations were additionally performed against two representative bacterial enzymes – MurB (PDB ID: 1MBT), involved in the bacterial cell wall biosynthesis, and DNA gyrase B (PDB ID: 4URO), a key enzyme in the DNA replication. These targets were selected as well-characterized, druggable antibacterial models supported by high-resolution crystal structures, allowing a preliminary assessment of potential antibacterial binding modes.

The docking against CYP51 revealed favorable binding affinities for compounds **2** and **3** (−8.6 kcal mol^{-1}), which moderately exceeded that of compound **1** (−8.0 kcal mol^{-1}). AutoDock Vina generated a single dominant binding pose for each

Table 3. Distribution, metabolism, and excretion for compounds **1–3**

Descriptor	Compound			Comments
	1	**2**	**3**	
Volume of distribution logVd	0.065	0.236	0.226	moderate volumes (0.1–0.3 L kg^{-1}) expected; **2** and **3** distribute slightly more than **1**
Fraction unbound (Fu, %)	8.16	4.15	1.54	compound **1** has the highest free fraction; **3** is almost completely protein-bound
Plasma protein binding (PPB, %)	90.2	94.9	98.1	all bind strongly to plasma proteins, particularly **3**
Elimination half-life (t1/2, h)	0.38	0.47	0.36	short predicted half-lives (<1 h) suggest rapid clearance
Bioconcentration factor (BCF)	2.18	2.12	2.85	slightly higher for **3**, but all are moderate

ISSN 2308-8303 (Print) / 2518-1548 (Online)

Table 4. The binding energies for compounds **1**–**3** with MurB (1MBT), DNA gyrase B (4URO), lanosterol 14-α-demethylase (5V5Z)

Protein (PDB ID)	Compound **1** (kcal mol^{-1})	Compound **2** (kcal mol^{-1})	Compound **3** (kcal mol^{-1})	Trend
Lanosterol 14-α-demethylase (5V5Z)	−8.0	−8.6	−8.6	2 ≈ 3 > 1
MurB (1MBT)	−8.9 (top pose)	−9.5 (strongest)	−9.3	2 > 3 > 1
DNA gyrase B (4URO)	−5.3	−5.7 (best)	−5.4	2 > 3 ≈ 1

ligand, suggesting a well-defined interaction mode within the enzyme active site.

All three compounds positioned their aromatic thiazolotriazolium core within a hydrophobic region of the CYP51 binding pocket. Compound **2** (3-hydroxyphenyl) adopted a particularly favorable orientation, in which the phenolic OH group formed a π-donor hydrogen bond / π-sulfur interaction with CYS470 (3.65 Å), accompanied by stabilizing π-alkyl interactions with ILE131 and ILE304 (**Figure 3**). This interaction pattern provides a clear structural rationale for the strong antifungal activity of compound **2** observed experimentally.

Compound **3** (phenyl) achieved a comparable binding energy through π–π stacking with TYR118 (≈ 3.80 Å) and hydrophobic contacts with CYS470 and ILE379, but lacked specific hydrogen-bonding interactions. In contrast, compound **1** (4-pyridyl) displayed a weaker binding, likely due to less optimal accommodation of the pyridyl substituent within the CYP51 pocket and the absence of strong directional hydrogen bonds.

The docking results against lanosterol 14-α-demethylase are fully consistent with the antifungal MIC data, supporting the CYP51 inhibition as a plausible molecular mechanism underlying the activity of compounds **1** and **2**, with the hydroxyl-substituted aromatic group in compound **2** conferring an additional binding advantage.

The complete interaction profiles and key contact distances for all protein–ligand complexes are summarized in **Table 5**.

The docking against MurB (PDB ID: 1MBT) yielded lower (more negative) binding energies than those obtained for DNA gyrase B. While compound **2** showed the strongest MurB affinity (−9.5 kcal mol^{-1}), this target did not directly explain the antifungal activity. Therefore, MurB is not considered the primary biological target in the present study.

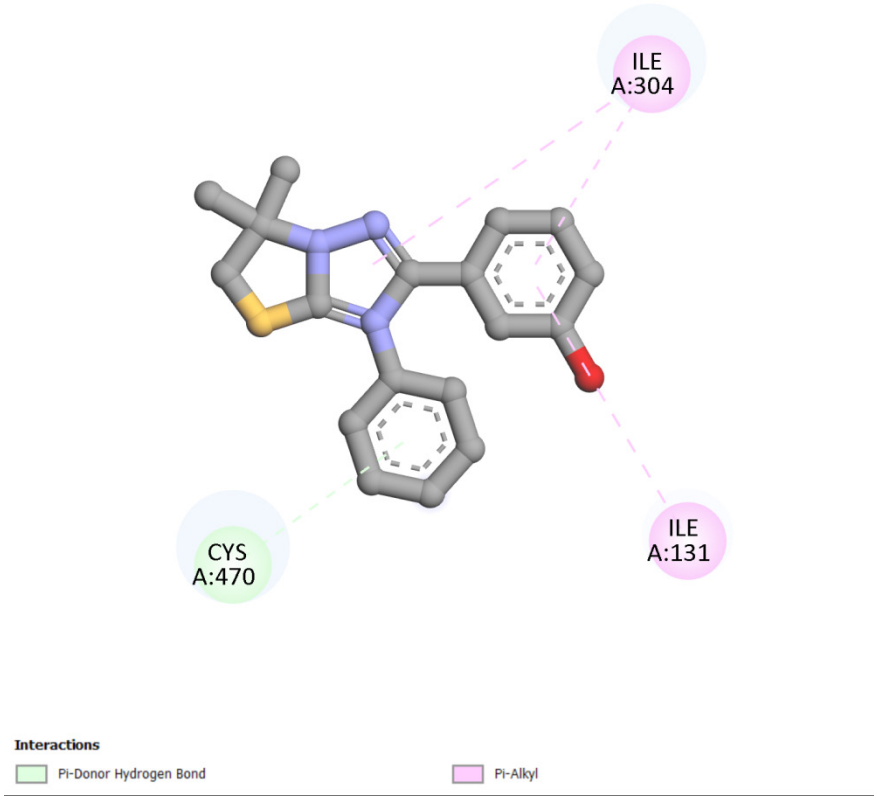

Figure 3. The predicted binding pose of compound **2** within the CYP51 active site (PDB ID: 5V5Z)

Table 5. The predicted protein–ligand interaction profiles of thiazolo[3,2-*b*]triazol-7-ium cations **1–3** with the key antimicrobial targets

Protein (PDB ID)	Compound	Key Interaction Type(s)	Interacting Residues (Protein)	Key Distances (A˚)
MurB (1MBT)	**1**	Conventional H-Bond, π-Alkyl	GLY47, VAL52, ILE119, ILE45, ILE173	H-Bond: 2.66
	2	2 Conventional H-Bonds, π-Cation, π-Alkyl	ASN65, ILE173, ARG327, ILE119, LEU46, ILE45	H-Bonds: 2.54, 2.52
	3	Conventional H-Bond, π-Alkyl	GLY47, VAL52, ILE45, ILE173, ILE119	H-Bond: 2.70
DNA Gyrase B (4URO)	**1**	π-Alkyl, Alkyl	LYS170	π-Alkyl: 4.14, 4.56
	2	π-Alkyl, Alkyl	LYS170	π-Alkyl: 4.15, 4.51
	3	Amide-π Stacked, π-Alkyl	LYS207, GLY208, ILE209	Amide-π: 3.94
Lanosterol 14-α-demethylase (5V5Z)	**1**	π-π Stacked, π-Alkyl, Alkyl	TYR118, CYS470, ILE379	π-π: 3.80
	2	π-Donor H-Bond/π-Sulfur, π-Alkyl	CYS470, ILE131, ILE304	H-Bond/π-Sulfur: 3.65
	3	π-π Stacked, π-Alkyl, Alkyl	TYR118, CYS470, ILE379	π-π: 3.80

All compounds exhibited poor binding to DNA gyrase B (−5.7 to −5.3 kcal mol^{-1}), with shallow, unstable binding modes and large RMSD values, indicating that the DNA gyrase inhibition was unlikely to contribute significantly to the biological effects observed.

The molecular docking results highlight lanosterol 14-α-demethylase (CYP51) as the most relevant molecular target for explaining the antifungal activity of thiazolotriazolium salts **1–3**. The favorable binding affinities and well-defined interaction patterns observed for compounds **2** and **3**, particularly the additional stabilizing interactions enabled by the phenolic OH group in compound **2**, are consistent with the experimentally determined antifungal MIC values.

■ Experimental part

General Information

All commercially available reagents and solvents were obtained from standard vendors and used without further purification unless otherwise stated. The starting methallyl thioethers were prepared according to the previously reported procedures [37]. ^{1}H NMR spectra were recorded using a Varian Mercury-400 instrument. Tetramethylsilane and deuterated dimethylsulfoxide were utilized in the NMR study as a standard and solvent, respectively. The elemental composition was determined with an Elementar Vario MICRO cube. Compounds **4, 5, 6** were previously reported (**4** – the sample **2a** [36]; **5** – the sample **2b** [36]; **6** – the sample **2d** [36]).

The General Procedure for the Synthesis of Compounds 1–3

The synthesis of thiazolo[3,2-*b*][1,2,4]triazol-7-ium hexabromotellurates was carried out *via* the electrophilic heterocyclization induced by tellurium(IV) species generated *in situ*. The mixture of 0.079 g of tellurium dioxide (TeO_2) in 1 mL acetonitrile, and 1 mL 48% hydrobromic acid (HBr) was stirred for 0.5 h until the formation of the H_2TeBr_6 complex. The corresponding methallyl thioether precursor (0.5 mmol) in 5 mL acetonitrile was subsequently added to the reaction mixture. The reaction mixture was heated for 1 h at 80–100 °C. Upon completion, the resulting orange colored precipitate was filtered, washed with a small amount of acetonitrile and ether, and dried to give the target hexabromotellurate salts **1–3** as crystalline solids.

6,6-Dimethyl-3-phenyl-2-(4-pyridyl)-5,6-dihydro-3H-[1,3]thiazolo[3,2-b][1,2,4]triazol-7-ium hexabromotellurate (**1**)

A bright orange-red solid. Yield – 0.39 g (64%) (55% [37]). M. p. 251–254 °C (decomp). Anal. Calcd for $C_{34}H_{34}Br_6N_8S_2Te$, %: C 33.31, H 2.80, N 9.14. Found, %: C 33.07, H 2.72, N 9.03. ^{1}H NMR (400 MHz, DMSO-d_6), δ, ppm: 1.78 (6H, s, $2CH_3$), 4.32 (2H, s, SCH_2), 7.54–7.65 (5H, m, Ph), 7.81 (2H, d, J = 4.5 Hz, Py-H), 8.56 (2H, d, J = 4.5 Hz, Py-H).

2-(3-Hydroxyphenyl)-6,6-dimethyl-3-phenyl-5,6-dihydro-3H-[1,3]thiazolo[3,2-b][1,2,4]triazol-7-ium hexabromotellurate (**2**)

A bright orange-red solid. Yield – 0.50 g (74%) (79% [37]). M. p. 262–263 °C (decomp). Anal. Calcd for $C_{36}H_{36}Br_6N_6O_2S_2Te$, %: C 34.43, H 2.89, N 6.69. Found, %: C 34.18, H 2.80, N 6.51. ^{1}H NMR (400 MHz, DMSO-d_6), δ, ppm: 1.76 (6H, s, $2CH_3$), 4.26 (2H, s, SCH_2), 6.80 (1H, d, J = 7.8 Hz, Ar-H), 6.85 (1H, s, Ar-H), 6.94 (1H, d, J = 8.0 Hz, Ar-H), 7.22 (1H, t, J = 8.0 Hz, Ar-H), 7.54–7.63 (5H, m, Ph).

6,6-Dimethyl-2,3-diphenyl-5,6-dihydro-3H-[1,3]thiazolo[3,2-b][1,2,4]triazol-7-ium hexabromotellurate (**3**)

A bright orange-red solid. Yield – 0.44 g (72%) (78% [37]). M. p. 256–258 °C (decomp). Anal. Calcd for $C_{36}H_{36}Br_6N_6S_2Te$, %: C 35.33, H 2.96,

ISSN 2308-8303 (Print) / 2518-1548 (Online)

N 6.87. Found, %: C 35.12, H 2.87, N 6.70. ^{1}H NMR (400 MHz, DMSO-d_6), δ, ppm: 1.76 (6H, s, 2CH_3), 4.24 (2H, s, SCH_2), 7.44–7.64 (10H, m, 2Ph).

Antimicrobial and Antifungal Activity Evaluation

The antimicrobial and antifungal activity of the compounds synthesized was evaluated in the Laboratory of the Research and Training Center for Molecular Microbiology and Immunology of Mucous Membranes, State Higher Educational Institution "Uzhhorod National University". Antibacterial and antifungal properties were determined by the serial dilution method to establish the minimum inhibitory concentration (MIC) and the minimum bactericidal concentration (MBC) values in accordance with CLSI M07 and EUCAST guidelines for *in vitro* antimicrobial testing [48].

For MIC and MBC testing, the contents of Eppendorf tubes with different dilutions of chemical compounds were re-inoculated onto solid nutrient media. The minimal concentration that completely inhibited the growth (no growth) was considered to be MBC. The minimal concentration that significantly inhibited the growth of microorganisms compared to the control was considered as MIC. Microbial test cultures included *Staphylococcus aureus*, *Candida albicans*, *Klebsiella pneumoniae*, *Escherichia coli*, and *Pseudomonas aeruginosa*. The strains of bacteria and fungi under research were clinical isolates collected from the parodontal pockets of patients with chronic generalized periodontitis who underwent treatment at the Uzhhorod University dental clinic. Microbial suspensions were prepared from 24-hour cultures on the appropriate media and adjusted to a 0.5 McFarland standard (≈ 1.5 × 10^8 CFU mL^{-1}). Each well of a sterile 96-well plate received 10 μL of the standardized microbial suspension and 100 μL of the compound solution prepared in the sterile broth. Control groups were: (1) the microbial growth control – inoculated medium without the compound (to verify viability); (2) the compound sterility control – the compound solution without the inoculum (to exclude contamination); (3) the solvent control – the medium with the solvent only in the working concentration (to eliminate the solvent antimicrobial effect). Plates were incubated at 37 °C for 24 h, followed by titration via serial 2-fold dilutions and reseeding onto selective agar media (MPA, Sabouraud, Endo, MRS, Enterococcus agar). After 24–48 h of incubation, the colony growth or the absence was visually assessed to determine MIC and MBC. All procedures were conducted under sterile conditions; sterility of the preparations was confirmed bacteriologically by plating 10 μL aliquots on the meat-peptone agar. Antimicrobial susceptibility tests with reference drugs were performed for all clinical isolates studied using the disc-diffusion Kirby-Bauer method [49] and the serial 2-fold dilution method to determine MIC and MBC. To compare the activity of the compounds studied with that of antibiotics, the latter were diluted to the same concentration range (250–15.625 μg mL^{-1}). Data about the susceptibility of the bacteria under research are given in **Table 6**.

Computational Methodology

ADMET Prediction

The pharmacokinetic properties and toxicity profiles of the compounds were predicted using the ADMETlab 3.0 web server [42]. Key parameters calculated included physicochemical descriptors (MW, TPSA, log*P*, logS), absorption (Caco-2 permeability, HIA), distribution (PPB, BBB penetration), metabolism (CYP450 inhibition), and toxicity endpoints (AMET test, hepatotoxicity).

Molecular Docking

Docking runs were performed with AutoDock Vina [50, 51] to evaluate how cations **1–3** interacted with MurB (UDP-*N*-acetylenolpyruvoylglucosamine reductase, PDB ID 1MBT), DNA gyrase B (ATPase subunit of bacterial topoisomerase, PDB ID 4URO), and lanosterol 14-α-demethylase (CYP51) from *Candida albicans* (PDB ID 5V5Z). Protein coordinates were downloaded from the Protein Data Bank and prepared using AutoDock Tools: water molecules

Table 6. Antimicrobial and antifungal susceptibility tests with reference drugs

Reference drug	MIC/MBC (μg mL^{-1})				
	C. albicans	*S. aureus*	*K. pneumoniae*	*E. coli*	*P. aeruginosa*
Fluconazol	<15.625	ND[a]	ND[a]	ND[a]	ND[a]
Levofloxacin	ND[a]	<15.625	<15.625	<15.625	<15.625
Lincomycin	ND[a]	<15.625	250 / >250	>250	>250
Amikacin	ND[a]	<15.625	31.25 / 62.5	31.25 / 31.25	62.5 / 62.5
Gentamicin	ND[a]	<15.625	61.5 / 125	31.25 / 125	125 / 250

Note: [a] ND – not determined. As the dilution range was 250-15.625 μg mL^{-1}, in some cases the MIC and MBC values were below (<15.625 μg mL^{-1}) or above (>250 μg mL^{-1}) the concentration range studied.

and any non-essential ligands were removed, polar hydrogens were added, and Gasteiger charges were assigned; essential cofactors were preserved. Each ligand was geometry-optimized and converted to *.pdbqt format before being docked individually into each receptor's active site. For MurB, the search grid was centered at X = 11.056, Y = 38.244 and Z = 18.464 with dimensions of 60 × 60 × 60 Å; DNA gyrase B used a center at X = 24.675, Y = –9.190 and Z = –26.488 with the same box size; the CYP51 enzyme employed a grid centered at X = –41.072, Y = –13.759 and Z = 25.140, and 60 Å per side. AutoDock Vina reports affinities in kcal mol^{-1}, with more negative scores indicating tighter predicted binding [52]; for each compound, the top-ranked pose was used for the subsequent analysis. The resulting complexes were visualized and their interactions examined in the BIOVIA Discovery Studio Visualizer [53].

Conclusion

An effective synthesis of a novel series of thiazolo[3,2-*b*]triazol-7-ium hexabromotellurates **1–3** has been successfully carried out. We have demonstrated the successful cyclization using the TeO_2/HBr electrophilic system under optimized reaction conditions. A systematic study of the structure–activity relationships has shown that substitutions in position 5 of the core heterocycle profoundly affect the antimicrobial efficacy – the introduction of a polar substituent with π-conjugated functionality in position 2 of the target [1,3]thiazolo[3,2-*b*][1,2,4]triazol-7-ium salts can improve the antimicrobial properties of the latter.

The high antifungal potency against *C. albicans* (MIC 15.625 μg mL^{-1}) was consistently observed for the derivatives containing polar groups, namely the 4-pyridyl (compound **1**) and the 3-hydroxyphenyl (compound **2**) derivatives. Crucially, the 4-pyridyl derivative (compound **1**) demonstrated the selective and potent activity against the Gram-negative bacterium *E. coli* (MIC 31.25 μg mL^{-1}), positioning it as the most promising lead candidate in this series.

Molecular docking studies support lanosterol 14-α-demethylase (CYP51) as a plausible molecular target underlying the antifungal activity observed. The enhanced binding affinities of compounds **2** and **3** are rationalized by favorable noncovalent interactions within the CYP51 active site, with the phenolic OH group of compound **2** enabling additional stabilizing contacts, while weaker binding of compound **1** reflects less optimal accommodation of the pyridyl substituent. In contrast, the docking against bacterial targets suggests that DNA gyrase B is unlikely to represent the primary mode of action.

These findings validate the strategy of combining a highly cationic thiazolotriazolium scaffold with a metal-complexed anion ($TeBr_6^{-2}$) to generate potent antimicrobial agents with a tunable selectivity. Future studies will focus on the structural optimization of lead compound **1**, elucidation of its precise cellular mode of action, and evaluation against clinically relevant multidrug-resistant strains.

References

1. Murray, C. J. L.; Ikuta, K. S.; Sharara, O. A., et al. Global burden of bacterial antimicrobial resistance 1990–2021: a systematic analysis with forecasts to 2050. *The Lancet* **2024**, *404* (10459), 1199–1226. https://doi.org/10.1016/S0140-6736(24)01867-1.
2. Tacconelli, E.; Carrara, E.; Savoldi, A., et al. Discovery, research, and development of new antibiotics: the WHO priority list of antibiotic-resistant bacteria and tuberculosis. *Lancet Infect. Dis*. **2018**, *18* (3), 318–327. https://doi.org/10.1016/S1473-3099(17)30753-3.
3. Ventola, C. L. The antibiotic resistance crisis: Part 1: Causes and threats. *P & T* **2015**, *40* (4), 277–283.
4. Cella, E.; Giovanetti, M.; Benedetti, F.; Scarpa, F.; Johnston, C.; Borsetti, A.; Ceccarelli, G.; Azarian, T.; Zella, D.; Ciccozzi, M. Joining Forces against Antibiotic Resistance: The One Health Solution. *Pathogens* **2023**, *12*, 1074. https://doi.org/10.3390/pathogens12091074.
5. Gattu, R.; Ramesh, S.S.; Ramesh, S. Role of small molecules and nanoparticles in effective inhibition of microbial biofilms: A ray of hope in combating microbial resistance. *Microb. Pathog*. **2024**, *188*, 106543. https://doi.org/10.1016/j.micpath.2024.106543.
6. Jampilek, J. Heterocycles in Medicinal Chemistry. *Molecules* **2019**, *24* (21), 3839. https://doi.org/10.3390/molecules24213839.
7. Łowicki, D.; Przybylsk, P. Piperidine-containing drugs and recently studied analogs – biological activity, mechanism of action and synthetic cascade access to their scaffolds. *Eur. J. Med. Chem.* **2025**, *302* (1), 118213. https://doi.org/10.1016/j.ejmech.2025.118213.
8. Manhas, N.; Kumar, G.; Dhawan, S.; Makhanya, T.; Singh, P. A Systematic Review of Synthetic and Anticancer and Antimicrobial Activity of Quinazoline/Quinazolin-4-one Analogues. *ChemistryOpen*. **2025**, *14* (7), e202400439. https://doi.org/10.1002/open.202400439.
9. Sousa, M. H. O.; Silva, C. H. L.; Silveira, M. V.; Godoi, M. Recent progress in 1-thioflavones and 4-thioflavones: Synthesis, applications and prospects. *Phosphorus Sulfur Silicon Relat. Elem.* **2025**, 1–34. https://doi.org/10.1080/10426507.2025.2578201.
10. Khidre, R. E.; Borik, R. M.; Behalo, M. S.; Elkarim, I. A. G.; Esam, A. Synthetic Methods and Pharmacological Potentials of Isothiocyanate Derivatives. *Mini-Rev. Org. Chem.* **2025**, *22* (6), 638–652. https://doi.org/10.2174/0118756298328213240904051112.
11. La Monica, G.; Bono, A.; Alamia, F.; Lauria, A.; Martorana, A. Bioisosteric heterocyclic analogues of natural bioactive flavonoids by scaffold-hopping approaches: State-of-the-art and perspectives in medicinal chemistry. *Bioorg. Med. Chem.* **2024**, *109*, 117791. https://doi.org/10.1016/j.bmc.2024.117791.
12. Morlion, F.; Magdalenic, K.; Van Camp, J.; D'hooghe, M. Heterocycle-substituted 1,5-benzothiazepines: biological properties and structure–activity relationships. *Monatsh Chem*. **2024**, *155*, 535–549. https://doi.org/10.1007/s00706-024-03195-3.

ISSN 2308-8303 (Print) / 2518-1548 (Online)

13. Khamitova, K.; Berillo, D.; Lozynskyi, A.; Konechnyi, Y.; Mural, D.; Georgiyants, V.; Lesyk, R. Thiadiazole and thiazole derivatives as potential antimicrobial agents. *Mini-Rev. Med. Chem*. **2024**, *24* (5), 531–545. https://doi.org/10.2174/1389557523666230713115947.
14. Korol, N.; Molnar-Babilya, D.; Slivka, M.; Onysko, M. A brief review on heterocyclic compounds with promising antifungal activity against Candida species. *Org. Commun*. **2022**, *15* (4), 304–323. https://doi.org/10.25135/acg.oc.141.2210.2609.
15. Slivka, M. V.; Korol, N. I. Condensed pyridopyrimidines and pyridopyrazines containing a bridgehead nitrogen atom: synthesis, chemical properties and biological activity. *Curr. Org. Chem*. **2021**, *25* (12), 1429–1440. https://doi.org/10.2174/1385272825666210525154330.
16. Hryhoriv, H.; Kovalenko, S.M.; Georgiyants, M.; Sidorenko, L.; Georgiyants, V. A. Comprehensive Review on Chemical Synthesis and Chemotherapeutic Potential of 3-Heteroaryl Fluoroquinolone Hybrids. *Antibiotics* **2023**, *12* (3), 625. https://doi.org/10.3390/antibiotics12030625.
17. Swathykrishna, C. S.; Amrithanjali, G.; Shaji, G.; Kumar R. A. Antimicrobial Activity and Synthesis of Thiazole Derivatives: A Recent Update. *J. Chem. Rev*. **2023**, *5* (3), 221–240. https://doi.org/10.22034/JCR.2023.383674.1211.
18. Korol, N. I.; Slivka, M. V. Recent progress in the synthesis of thiazolo [3,2-*b*][1,2,4]triazoles (microreview). *Chem. Heterocycl. Compd*. **2017**, *53* (8), 852–854. https://doi.org/10.1007/s10593-017-2136-3.
19. Slivka, M. V.; Korol, N. I.; Fizer, M. M. Fused bicyclic 1,2,4-triazoles with one extra sulfur atom: Synthesis, properties, and biological activity. *J. Heterocycl. Chem.* **2020**, *57* (9), 3236–3254. https://doi.org/10.1002/jhet.4044.
20. Farveen, M. D., Kalagara, S., Balraju, E., Jaysree, B., Shaik, A., Alia, B. Discovery of novel Quinazoline based Thiazolotriazole hybrids as potential EGFR inhibitor: Synthesis, anticancer evaluation and in silico studies. *Chem. Biol. Lett.* **2025**, *12* (2), 1261–1261. https://doi.org/10.62110/sciencein.cbl.2025.v12.1261.
21. Rostom, S. A.; Badr, M. H.; Abd El Razik, H. A.; Ashour, H. M. Structure-based development of novel triazoles and related thiazolotriazoles as anticancer agents and Cdc25A/B phosphatase inhibitors. Synthesis, *in vitro* biological evaluation, molecular docking and *in silico* ADME-T studies. *Eur. J. Med. Chem*. **2017**, *139*, 263–279. https://doi.org/10.1016/j.ejmech.2017.07.053.
22. Barbuceanu, S. F.; Draghici, C.; Barbuceanu, F.; Bancescu, G.; Saramet, G. Design, synthesis, characterization and antimicrobial evaluation of some heterocyclic condensed systems with bridgehead Nitrogen from thiazolotriazole class. *Chem. Pharm. Bull.* **2015**, *63* (9), 694–700. https://doi.org/10.1248/cpb.c15-00379.
23. Almasirad, A.; Sani, P. S. V.; Mousavi, Z.; Fard, G. B.; Anvari, T.; Farhadi, M.; Vosooghi, M.; Azizian, H. Novel thiazolotriazolone derivatives: design, synthesis, in silico investigation, analgesic and anti-inflammatory activity. *ChemistrySelect*. **2022**, *7* (28), e202103228. https://doi.org/10.1002/slct.202103228.
24. Slivka, M.; Onysko, M. The use of electrophilic cyclization for the preparation of condensed heterocycles. *Synthesis*. **2021**, *53* (19), 3497–3512. https://doi.org/10.1055/s-0040-1706036.
25. Kut, D.; Kut, M.; Komarovska-Porokhnyavets; O., Kurka; M., Onysko, M.; Lubenets, V. Antimicrobial activity of halogen-and chalcogen-functionalized thiazoloquinazolines. *Lett. Drug Des. Discovery*. **2024**, *21* (13), 2490–2496. https://doi.org/10.2174/1570180820666230726160348.
26. Pantyo, V. V.; Haleha, O. V.; Kut, D. Z.; Kut, M. M.; Onysko, M. Y.; Danko, E. M.; Koval G.M.; Pantyo V.I.; Haza K.V.; Bulyna, T. B. The effect of low-intensity laser radiation on the sensitivity of *Staphylococcus aureus* to some halogen-containing azaheterocycles. *Regulatory Mechanisms in Biosystems*. **2024**, *15* (2), 230–234. https://doi.org/10.15421/022434.
27. Kut, M. M.; Onysko, M. Y. Aryltellurium trihalides in the synthesis of heterocyclic compounds (microreview). *Chem. Heterocycl. Compd.* **2020**, *56* (5), 503–505. https://doi.org/10.1007/s10593-020-02688-3.
28. Sabti, A.B.; Al-Fregi, A.A.; Yousif, M.Y. Synthesis and antimicrobial evaluation of some new organic tellurium compounds based on pyrazole derivatives. *Molecules* **2020**, *25* (15), 3439–3456. http://dx.doi.org/10.3390/molecules25153439.
29. Al-Fregi, A.A.; Al-Salami, B.K.; Al-Khazragie, Z.K.; Al-Rubaie, A.Z. Synthesis, characterization and antibacterial studies of some new tellurated azo compounds. *Phosphorus Sulfur Silicon Relat. Elem.* **2019**, *194*, 33–38. http://dx.doi.org/10.1080/10426507.2018.1470179.
30. Halpert, G.; Halperin Sheinfeld, M.; Monteran, L.; Sharif, K.; Volkov, A.; Nadler, R.; Schlesinger, A.; Barshak, I.; Kalechman, Y.; Blank, M.; Shoenfeld, Y.; Amital, H. The tellurium-based immunomodulator, AS101 ameliorates adjuvant-induced arthritis in rats. *Clin. Exp. Immunol.* **2021**, *203*(3), 375–384. http://dx.doi.org/10.1111/cei.13553.
31. Cabrera, N.; Mora, J.R.; Márquez, E.; Flores-Morales, V.; Calle, L.; Cortés, E. QSAR and molecular docking modelling of anti-leishmanial activities of organic selenium and tellurium compounds. *SAR QSAR Environ. Res.* **2021**, *32*(1), 29–50. http://dx.doi.org/10.1080/1062936X.2020.1848914.
32. Ba, L. A.; Döring, M.; Jamier, V.; Jacob, C. Tellurium: An element with great biological potency and potential. *Org. Biomol. Chem.* **2010**, *8* (19), 4203–4216. https://doi.org/10.1039/C0OB00086H.
33. Vávrová, S.; Struhárňanská, E.; Turňa, J.; Stuchlík, S. Tellurium: A Rare Element with Influence on Prokaryotic and Eukaryotic Biological Systems. *Int. J. Mol. Sci.* **2021**, *22* (11), 5924. https://doi.org/10.3390/ijms22115924.
34. Slivka, M.; Fizer, M.; Mariychuk, R.; Ostafin, M.; Moyzesh, O.; Koval, G.; Holovko-Kamoshenkova, O.; Rusyn, I.; Lendel, V. Synthesis and Antimicrobial Activity of Functional Derivatives of thiazolo [2,3-*c*][1,2,4] triazoles. *Lett. Drug Des. Discovery* **2022**, *19* (9), 791–799. https://doi.org/10.2174/1570180819666220110145659.
35. Slivka, M.; Korol, N.; Pantyo, V.; Baumer, V.; Lendel, V. Regio-and stereoselective synthesis of [1,3]thiazolo[3,2-*b*][1,2,4]triazol-7-ium salts via electrophilic heterocyclization of 3-*S*-propargylthio-4*H*-1,2,4-triazoles and their antimicrobial activity. *Heterocycl. Commun.* **2017**, *23* (2), 109–113. https://doi.org/10.1515/hc-2016-0233.
36. Slivka, M.; Sharga, B.; Pylypiv, D.; Aleksyk, H.; Korol, N.; Fizer, M.; Fedurcya, O.; Pshenychnyi, O.; Mariychuk, R. [1,3]Thiazolo[3,2-*b*]-[1,2,4]triazolium Salts as Effective Antimicrobial Agents: Synthesis, Biological Activity Evaluation, and Molecular Docking Studies. *Int. J. Mol. Sci.* **2025**, *26* (14), 6845. https://doi.org/10.3390/ijms26146845.
37. Fizer, M., Slivka, M., Baumer, V. (2021). Efficient synthesis of substituted [1,3] thiazolo [3,2-b][1,2,4]triazol-7-ium hexabromotellurates. *J. Organomet. Chem.* **2021**, *952*, 122044. https://doi.org/10.1016/j.jorganchem.2021.122044.
38. Biot, N.; Romito, D.; Bonifazi, D. Substituent-Controlled Tailoring of Chalcogen-Bonded Supramolecular Nanoribbons in the Solid State. *Crystal Growth & Design*. **2021**, *21* (1), 536–543. https://doi.org/10.1021/acs.cgd.0c01318.
39. Ungureanu, D.; Tiperciuc, B.; Nastasă, C.; Ionuț, I.; Marc, G.; Oniga, O.; Oniga, I. An Overview of the Structure–Activity Relationship in Novel Antimicrobial Thiazoles Clubbed with Various Heterocycles (2017–2023). *Pharmaceutics* **2024**, *16*, 89. https://doi.org/10.3390/pharmaceutics16010089.
40. Mohanty, P.; Jena, S.; Rout, L.; et al. Antibacterial Activity of Thiazole and Its Derivatives: A Review. *Biointerface Res. Appl. Chem.* **2021**, *11*, 2172–2187. https://doi.org/10.33263/BRIAC122.21712195.
41. Goyal, A.; Bhandari, M. Synthetic and therapeutic review of triazoles and hybrids. *Heterocycl. Commun.* **2024,** *30* (1), 20220174. https://doi.org/10.1515/hc-2022-0174.

42. Fu, L.; Shi, S.; Yi, J.; Wang, N.; He, Y.; Wu, Z.; Cao, D. ADMETlab 3.0: An Updated Comprehensive Online ADMET Prediction Platform. *Nucleic Acids Res.* **2024**, *52* (W1), W422–W431. https://doi.org/10.1093/nar/gkae236.
43. Xiong, G.; Wu, Z.; Yi, J.; Fu, L.; Yang, Z.; Hsieh, C.; Cao, D. ADMETlab 2.0: An Integrated Online Platform for Accurate and Comprehensive Predictions of ADMET Properties. *Nucleic Acids Res.* **2021**, *49* (W1), W5–W14. https://doi.org/10.1093/nar/gkab255.
44. Guan, L.; Yang, H.; Cai, Y.; Sun, L.; Di, P.; Li, W.; Liu, G.; Tang, Y. ADMET-score - a comprehensive scoring function for evaluation of chemical drug-likeness. *Medchemcomm* **2019**, *10* (1), 148–157. https://doi.org/10.1039/c8md00472b.
45. Dulsat, J.; Lopez, A.; Fuguet, E.; et al. Evaluation of Free Online ADMET Tools for Academic or Commercial Use. *Molecules* **2023**, *28* (2), 776. https://doi.org/10.3390/molecules28020776.
46. Klimoszek, D.; Ziecik, A.; Kowalska, J.; et al. Study of the Lipophilicity and ADMET Parameters of New Compounds. *Pharmaceuticals* **2024**, *17* (6), 725. https://doi.org/10.3390/ph17060725.
47. Yakobi, S.; Zuckerman, O.; Cohen, S.; et al. Molecular Docking and Structure-Activity Relationship of Novel Heterocyclic Scaffolds. *ChemistrySelect* **2024**, *9*, e202303341. https://doi.org/10.1002/slct.202303341.
48. European Committee on Antimicrobial Susceptibility Testing. EUCAST Reading Guide for Broth Microdilution. Version 5.0 (January 2024). https://www.eucast.org/fileadmin/eucast/pdf/MIC/Reading_guide_BMD_v_5.0_2024.pdf.
49. European Committee on Antimicrobial Susceptibility Testing. EUCAST Disk Diffusion Method for Antimicrobial Susceptibility Testing. Version 13.0 (January 2025). https://www.eucast.org/fileadmin/eucast/pdf/disk_test_documents/2025/Manual_v_13.0_EUCAST_Disk_Test_2025.pdf.
50. Ubaid, A.; Shakir, M.; Ali, A.; Khan, S.; Alrehaili, J.; Anwer, R.; Abid, M. Synthesis and SAR Studies on New 4-Aminoquinoline-Hydrazones and Isatin Hybrids. *Molecules* **2024**, *29* (23), 5777. https://doi.org/10.3390/molecules29235777.
51. Trott, O.; Olson, A. J. AutoDock Vina: Improving the Speed and Accuracy of Docking with a New Scoring Function, Efficient Optimization, and Multithreading. *J. Comput. Chem.* **2010**, *31* (2), 455–461. https://doi.org/10.1002/jcc.21334
52. Eberhardt, J.; Santos-Martins, D.; Tillack, A.F.; Forli, S. AutoDock Vina 1.2.0: New Docking Methods, Expanded Force Field, and Python Bindings. *J. Chem. Inf. Model.* **2021**. https://doi.org/10.1021/acs.jcim.1c00203
53. BIOVIA, Dassault Systèmes. *BIOVIA Discovery Studio Visualizer*; Dassault Systèmes: San Diego, CA, **2019**.

Information about the authors:
Nataliya I. Korol, Candidate of Chemistry, Associate Professor of the Organic Chemistry Department, Uzhhorod National University; https://orcid.org/0000-0001-7155-1676.
Valeriy V. Pantyo, Candidate of Biology, Associate Professor of the Microbiology, Virology, Epidemiology, with the Course Infectious Department, Uzhhorod National University; https://orcid.org/0000-0002-0207-3372.
Victoriia O. Bestritska, Engineer of the Organic Chemistry Department, Uzhhorod National University; https://orcid.org/0009-0009-2437-8773.
Kamila A. Avdeeva, Master's Degree Student of the Pharmaceutical Disciplines Department, Uzhhorod National University.
Dzhosiya I. Molnar-Babilya, Candidate of Chemistry, Associate Professor of the Hotel and Restaurant Business Department, Ferenc Rákóczi II Transcarpathian Hungarian Institute; Associate Professor of the Department of Hotel and Restaurant Business, Mukachevo State University; https://orcid.org/0000-0003-1063-013X.
Maksym M. Fizer, Candidate of Chemistry, Associate Professor, Research Assistant Professor of the Department of Chemistry, University of Nevada Reno; https://orcid.org/0000-0001-6583-3159.
Mykhailo V. Slivka (*corresponding author*), Dr.Sci. in Chemistry, Professor, Professor of the Organic Chemistry Department, Uzhhorod National University; https://orcid.org/0000-0003-4788-0511; e-mail for correspondence: mikhailo.slivka@uzhnu.edu.ua.

ISSN 2308-8303 (Print) / 2518-1548 (Online)

Journal of Organic and Pharmaceutical Chemistry

Original Research

OPEN ACCESS
Freely available online on
http://ophcj.nuph.edu.ua

UDC 547.382.2 + 547.382.3 + 579.66 + 542.943

V. Shah[1], V. Nikitenkova[2], Yu. Kurtash[1], T. Krupodorova[3], T. Zhuk[1,2]

[1] Faculty of Chemical Technology, National Technical University of Ukraine "Igor Sikorsky Kyiv Polytechnic Institute", 37 Beresteiskyi ave., 03056 Kyiv, Ukraine
[2] Institute of Food Chemistry and Food Biotechnology, Justus Liebig University Giessen, Heinrich-Buff-Ring 17, 35392 Giessen, Germany
[3] Department of Plant Food Products and Biofortification, Institute of Food Biotechnology and Genomics, National Academy of Sciences of Ukraine, 2A Baidy-Vyshnevetskoho str., 04123 Kyiv, Ukraine

Biocatalytic Approach to Aldehydes Using Lyophilisates of *Bjerkandera adusta* Fungus

Abstract

An optimized biocatalytic oxidation protocol has been developed for the efficient conversion of benzylic and allylic alcohols into their corresponding aldehydes. The sustainable method uses lyophilized mycelia of *Bjerkandera adusta* white-rot fungus as a catalyst in the aqueous medium with 2-propanol (10 % *v*/*v*) as a co-solvent, and operates under mild conditions to give high yields for a wide range of substrates. On a preparative scale, the approach allowed the synthesis of important aldehydes, including benzaldehyde, piperonal, cinnamaldehyde, cuminaldehyde, methoxybenzaldehydes, and citral.

Keywords: biocatalytic oxidation; benzylic alcohols; allylic alcohols; fungal biocatalysis; mild oxidation

В. Шах[1], В. Нікітенкова[2], Ю. Курташ[1], Т. Круподьорова[3], Т. Жук[1,2]

[1] Хіміко-технологічний факультет, Національний технічний університет України «Київський політехнічний інститут імені Ігоря Сікорського», Берестейський проспект, 37, м. Київ, 03056, Україна
[2] Інститут харчової хімії та харчової біотехнології, Університет Юстуса Лібіха, Гіссен, Кільце Генріха-Баффа, 17, м. Гіссен, 35392, Німеччина
[3] Відділ рослинних харчових продуктів та біофортифікації, Інститут харчової біотехнології та геноміки НАН України, вул. Байди-Вишневецького, 2А, Київ, 04123, Україна

Біокаталітичний підхід до синтезу альдегідів з використанням ліофілізатів гриба *Bjerkandera adusta*

Анотація

Розроблено оптимізований протокол біокаталітичного окислення для ефективного перетворення бензилових та алілових спиртів на відповідні альдегіди. Цей екологічно безпечний метод використовує ліофілізований міцелій гриба білої гнилі *Bjerkandera adusta* як каталізатор у водному середовищі з 2-пропанолом (10 % *v*/*v*) як розчинником і працює в м'яких умовах, забезпечуючи високий вихід продукту для широкого спектра субстратів. У препаративному масштабі цей підхід дозволив здійснити синтез важливих альдегідів, зокрема бензальдегіду, піпероналю, цинамальдегіду, кумінальдегіду, метоксибензальдегідів та цитралю.

Ключові слова: біокаталітичне окислення; бензилові спирти; алілові спирти; грибний біокаталіз; м'яке окислення

Citation: Shah, V.; Nikitenkova, V.; Kurtash, Yu.; Krupodorova, T.; Zhuk, T. Biocatalytic Approach to Aldehydes Using Lyophilisates of *Bjerkandera adusta* Fungus. *Journal of Organic and Pharmaceutical Chemistry* **2025**, *23* (4), 57 – 63.
https://doi.org/10.24959/ophcj.25.340347
Received: *29 September 2025*; **Revised:** *3 December 2025*; **Accepted:** *5 December 2025*.

Funding: The authors received no specific funding for this work.
Conflict of interests: The authors have no conflict of interests to declare.

Introduction

Flavor aldehydes represent the pivotal components in the food, fragrance, and pharmaceutical industries. However, their production remains constrained by factors, including their inherently low natural abundance and the limitations of the conventional chemical synthesis and biotechnological approaches. Aldehydes are most commonly produced by oxidizing primary alcohols using toxic and costly reagents, such as chromium(VI), manganese compounds, or other strong inorganic oxidants [1, 2]. Industrial aerobic oxidations typically employ transition-metal catalysts [3–6], while emerging photocatalytic methods also rely on transition metals [7–9]. Consequently, the food, beverage, and cosmetic industries are increasingly exploring microbial and enzymatic alternatives for aldehyde production [10, 11].

Biocatalysis is a powerful tool for a sustainable chemical synthesis, yet its broader industrial implementation is often constrained by economic and technical challenges. Current research in this field primarily focuses on the development of recombinant expression systems for the production of target enzymes. However, isolation and purification of these enzymes remain economically demanding, limiting their large-scale applicability. Recent analyses of manufacturing costs for biocatalysts revealed that industrial-grade (non-purified) enzymes are priced between 250 and 1000 € per kg, whereas whole-cell preparations are significantly more cost-effective, ranging from 35 to 100 € per kg [12]. Efforts in whole-cell biocatalysis, therefore, focus on engineering modified host organisms to enhance the productivity and stability of the enzymes they express and on using these organisms directly without further enzyme purification. Nevertheless, the use of genetically modified living systems can pose regulatory, safety, and operational challenges, making them less desirable for certain industrial applications. To address these limitations, we recently reported an alternative approach employing the *Bjerkandera adusta* white-rot fungus lyophilisate for the selective oxidation of alcohols to the corresponding aromatic aldehydes [13, 14]. This strategy avoids the recombinant expression and enzyme purification while preserving the principal advantages of whole-cell catalysts, namely, low cost, robustness, and cofactor independence. The high catalytic performance of the *B. adusta* lyophilisate is due to the presence of aryl-alcohol oxidases (AAO), which retain activity even after freeze-drying and extended storage, thereby offering a practical and scalable biocatalytic solution. AAOs are FAD (flavin adenine dinucleotide)-dependent oxidoreductases that use only molecular oxygen for the substrate oxidation, producing hydrogen peroxide as a by-product, without requiring additional cofactors (**Scheme 1**).

One of the main drawbacks of biocatalytic approaches is their limited scalability. The aim of this study was to evaluate the scalability of the *B. adusta* lyophilisate-based approach as a safe and sustainable strategy for the production of aldehydes with prospective applications in beverages, food, and cosmetics.

Results and discussion

The present work is based on our previous study, in which we demonstrated the catalytic

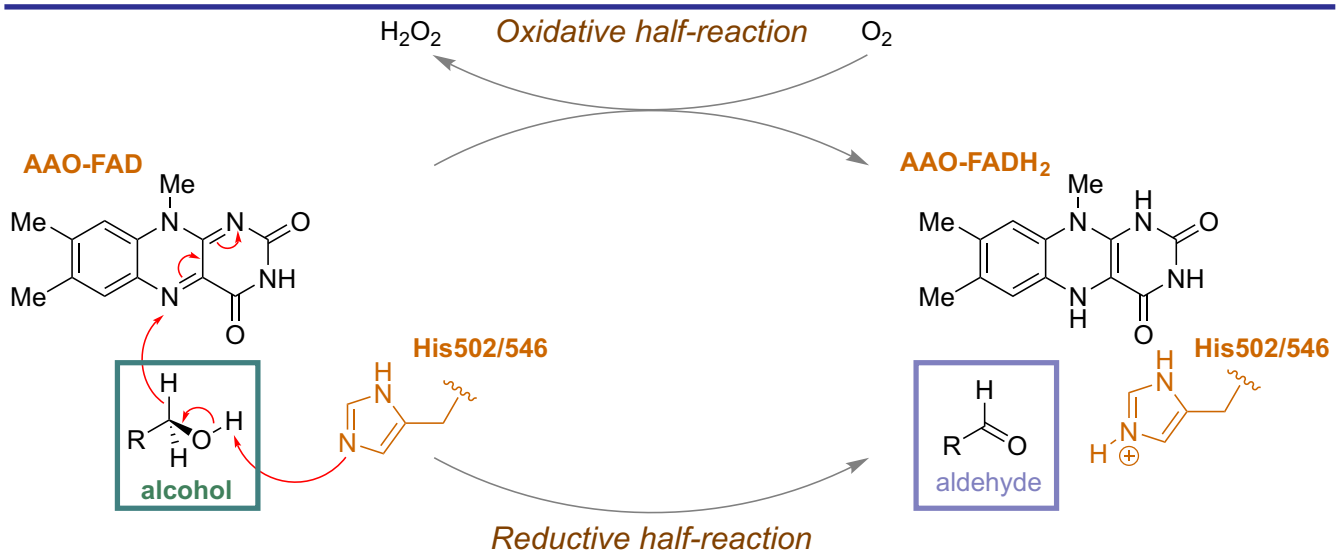

Scheme 1. The mechanism of the alcohol oxidation with aryl-alcohol oxidase (AAO) (FAD – Flavin Adenine Dinucleotide)

ISSN 2308-8303 (Print) / 2518-1548 (Online)

activity of lyophilisates in relation to aromatic and allylic alcohols [13], extending this concept to a,b-unsaturated substrates. While our previous works [13, 14] are mainly method-oriented, this study is anchored in specific high-value compounds that define the aromas of almonds, cinnamon, cumin, and citrus, which directly addresses industrial relevance. It should also be noted that *Babkina et al.* [13] focused on aromatic substrates, whereas *Calza et al.* [14] investigated allylic substrates. In contrast, this study integrates both substrate classes within a single methodology, using the same lyophilisate preparation. This demonstrates that the catalyst system is not limited to one narrow substrate family.

The preparation of lyophilisates is summarized in **Figure 1**. Initially, *B. adusta* was cultivated as a surface culture, followed by the submerged cultivation to enhance mycelial the biomass production. The collected mycelia were subsequently frozen at –80 °C and freeze-dried. The resulting lyophilisates can be stored at –20 °C for extended periods without the loss of the catalytic activity.

Our previous studies demonstrated that 2-propanol, at 10% (*v*/*v*), was the most effective co-solvent for this procedure. This observation is notable given the presence of its hydroxyl functional group, which in principle could undergo oxidation to yield acetone. Nevertheless, under the reaction conditions developed, secondary alcohols, such as 2-propanol, were shown to be resistant to oxidation, thereby preserving their role as a benign co-solvent without introducing competing side reactions. In addition to solvent effects, the substrate concentration was identified as a decisive parameter influencing the reaction efficiency. At 20 mM, the product formation was consistently reduced, whereas 10 mM gave markedly higher yields, frequently exceeding 90%. Furthermore, the stirring intensity was found to be equally critical as the stirring rates below 500 rpm resulted in lower reproducibility and yields. Collectively, these findings highlight the intricate interplay between the solvent composition, the substrate concentration, and hydrodynamic conditions in determining the success of the procedure. Our study consolidates previously scattered optimization insights from earlier work [13, 14] and integrates them into a coherent and practical protocol, including the defined lyophilizate loading, buffer volume and pH, 2-propanol fraction, 10 mM substrate, stirring rate, reaction time, workup, and purification procedures. This level of detail and consolidation is new and directly useful for practitioners.

The optimized methodology was subsequently applied to a series of alcohol substrates serving as precursors to valuable flavor aldehydes and was tested at a preparative scale. Benzaldehyde (**1**), the principal compound responsible for the characteristic aroma of bitter almonds, was obtained in the yield of 88% (**Scheme 2**). Piperonal (**2**), a perfume agent with a sweet, floral, heliotrope-like odor, was isolated in the yield of 92%. Both 3- and 4-methoxybenzyl alcohols were subjected to the optimized procedure, giving the corresponding aldehydes **3** and **4**. 3-Methoxybenzaldehyde (**3**) is characterized by a sweet, floral, and slightly spicy aroma, whereas 4-methoxybenzaldehyde (**4**) possesses a similar but more intense fragrance, reminiscent of anise or hawthorn. Responsible for the characteristic warm, sweet, and spicy aroma of cinnamon, the cinnamic aldehyde (**5**) was produced in the yield of 95%. Similarly, cuminaldehyde (**6**) known for its spicy, green odor was produced in the yield of 92%. In addition, a mixture of isomeric geranial and neral known as citral (3,7-dimethyl-2,6-octadienal, **7**) [15] and distinguished by its fresh, lemon-like aroma was obtained as the oxidation product of geraniol in the yield of 96%. It should be noted that for all six target aldehydes and a mixture of two additional aldehydes, we report isolated yields close to the quantitative ones. In contrast, *Calza et al.* [14] reported similarly high yields for model allylic substrates, but not specifically for this flavor portfolio.

No traces of carboxylic acids were detected in the reaction mixtures for any of the flavor aldehydes,

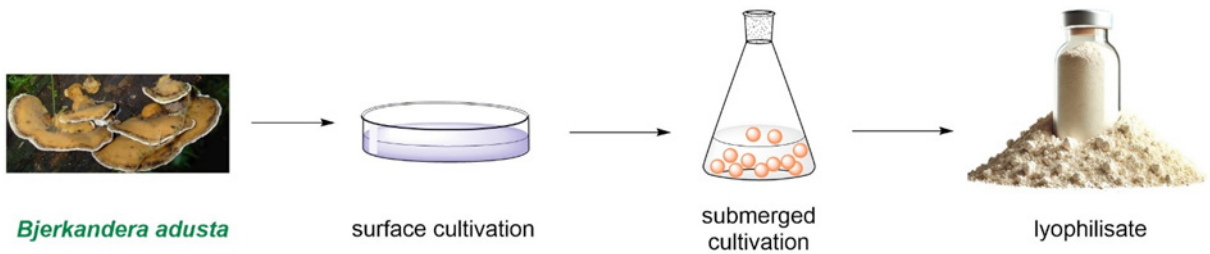

Figure 1. The process of the lyophilisate production

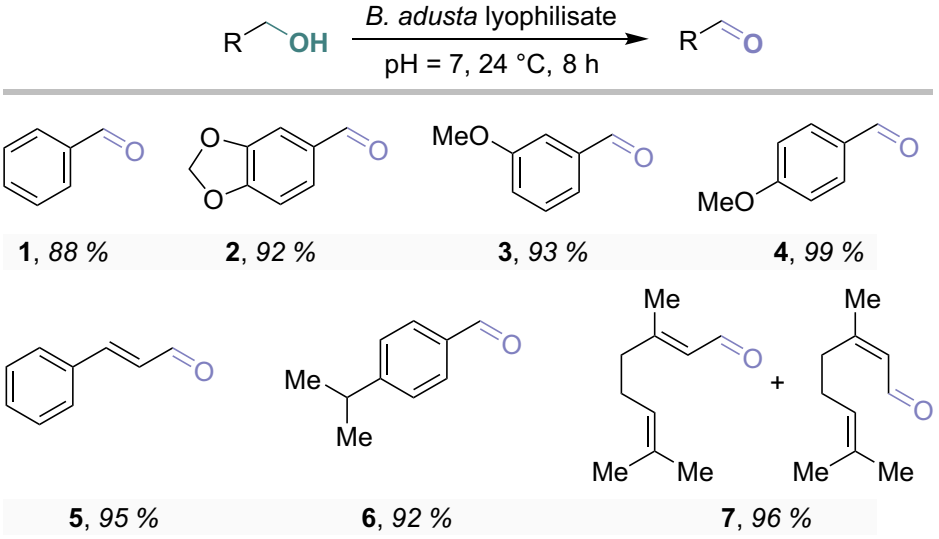

Scheme 2. The general scheme of the biocatalytic oxidation of aromatic and allylic alcohols to the corresponding aldehydes and the structures of the products and their respective yields

indicating the selective formation of aldehydes under mild conditions. Compared to our results, *Calza et al.* [14] demonstrated that lyophilisates gave a selective oxidation of primary benzylic and allylic alcohols to aldehydes, with the overoxidation suppression under optimized conditions. Also, these researchers upscaled a model allylic substrate to about ten millimolar in 90 mL buffer with 1.6 g of lyophilisate, mainly to confirm that the reaction remained selective. In our study, the general protocol was applied to hundreds of milligrams of structurally diverse substrates without the loss of selectivity or formation of detectable carboxylic acids.

The biocatalytic transformations were performed on a 300–500 mg scale, and the results clearly demonstrated the potential for upscaling of the approach. This shows that the protocol works on a scale and with solvents acceptable for the flavor and fragrance development. *Babkina et al.* [13] mostly reported smaller-scale experiments in the DMSO-containing medium, which was less attractive for food applications. *Calza et al.* [14] later demonstrated that 10% (*v*/*v*) 2-propanol gave very good performance for α,β-unsaturated alcohols. Our study adopts 2-propanol universally, confirms its chemical inertness under the oxidative conditions, and demonstrates that it remains effective at a preparative scale for a realistic set of flavor precursors. This is a genuine improvement in terms of safety.

Compared to conventional oxidation protocols, the *B. adusta*-lyophilisate method offers significant improvements in both efficiency and mildness of conditions. Traditional chemical oxidations of benzylic or allylic alcohols typically rely on stoichiometric inorganic oxidants (e.g. chromates, permanganates or nitric acid) and elevated temperatures, which often lead to poor selectivity, overoxidation to carboxylic acids, and hazardous waste generation [16]. For example, the benzyl alcohol oxidation by ferric nitrate in aqueous nitric acid reaches ~85% yield of benzaldehyde [17], but requires careful control of corrosive reagents. In stark contrast, our biocatalytic process employs a freeze-dried fungal mycelium in a simple H_2O / 2-propanol medium under ambient air. This benign setup cleanly converts primary aromatic and allylic alcohols to the corresponding aldehydes with no detectable overoxidation (no acids formed) and without additional co-oxidants [14]. For instance, 3,4-dimethozybenzyl alcohol (veratryl alcohol) was oxidized to veratraldehyde in the isolated yield of 84% under our conditions, and geraniol/nerol were selectively oxidized to citral (a mixture of (*E*)- and (*Z*)-isomers) in a high yield, with no side-products from further oxidation or double-bond reduction [14]. These outcomes illustrate the excellent chemoselectivity of the *B. adusta* catalyst, which contrasts with many chemical oxidants and even some enzymatic systems (e.g. the aryl-alcohol oxidase from *P. ostreatus* can overoxidize alcohols beyond the aldehyde stage to acids [18]). Notably, fungal laccases are also known to oxidize benzylic alcohols to aldehydes, but laccase reactions typically require artificial mediators and can nonselectively oxidize a broad range of phenolics [18], making them less ideal for the preparative flavor synthesis.

Equally important are the practical and green engineering advantages of our approach.

ISSN 2308-8303 (Print) / 2518-1548 (Online)

The freeze-dried *B. adusta* mycelium serves as a readily accessible, whole-cell oxidase catalyst that obviates the need for the extensive enzyme purification or cofactor addition. *In situ*, the fungus own aryl-alcohol oxidase (AAO) uses molecular oxygen (from air) as the terminal oxidant, producing only water (*via* H_2O_2) as a benign by-product [16]. This differs from many isolated enzyme systems, which may require expensive cofactors and regeneration systems. For example, while a recombinant AAO from *Pleurotus eryngii* showed a high catalytic turnover (over 2 million for trans-2-hexen-1-ol oxidation), it had to be obtained via the inclusion body refolding and could not be used in whole-cell form. Engineered microbial approaches achieved complete conversion of allylic alcohols to aldehydes, but only through complex cascade designs: *Qiao et al.* [16] co-expressed an NAD^+-dependent alcohol dehydrogenase and an NADPH oxidase in *E. coli*, and further introduced a hemoglobin for oxygen uptake, to boost the yield of 3-methyl-2-butenal from 21% to 51%. Even then, pure oxygen and a fused multi-enzyme construct were required to attain >80% yield within 8 hours. In contrast, our single-organism, freeze-dried catalyst achieves high yields in similar or shorter timeframes under air without genetic modifications or intensive process controls. Typical reactions in this study went to completion within hours to a day, whereas traditional submerged fungal fermentations for flavor aldehydes often require several days to weeks. For instance, *B. adusta* cultures produce benzaldehyde from *L*-phenylalanine or benzyl alcohol over multiple days of growth, reaching titers of only a few hundred mg L^{-1} [19] and necessitating tricks like the product adsorption to mitigate toxicity [20, 21]. By using the non-growing (lyophilized) mycelium, we circumvent such limitations: the enzymatic activity is harnessed directly in a controlled batch reaction, decoupled from the slower kinetics and complexities of the microbial growth. Additionally, the stability of the freeze-dried catalyst is an asset – we have found that *B. adusta* lyophilisate retains full activity for at least 7 months when stored dry [18], which is advantageous for the consistent performance and potential reusability in a process setting.

We also studied alternative fungal lyophilisates to ensure that the efficiency observed was unique to *B. adusta*. Lyophilized mycelia of *Pleurotus sapidus* and *P. eryngii* (basidiomycetes known to produce oxidative enzymes) were tested in the model oxidation of cinnamyl alcohol. These preparations yielded significantly less aldehyde than *B. adusta* under identical conditions. According to the literature, *B. adusta* is an especially potent source of aryl-alcohol oxidase [14]. The choice of *B. adusta*, a non-toxic white-rot fungus, is particularly relevant for the flavor synthesis. *Babkina et al.* [13] have highlighted that *B. adusta* lyophilisate is a safe, metal-free oxidation catalyst suitable for food, beverage, and cosmetic applications. In our process, the fungal biomass is removed by a simple filtration after the reaction, and the resulting aldehyde product can be classified as nature-derived. This has important regulatory implications: flavors produced via biocatalysis from natural precursors may be labeled as "natural flavorings", whereas the same compounds made by synthetic chemical routes would be considered artificial [22]. The ability to market benzaldehyde, cinnamaldehyde, and other aroma aldehydes as natural products adds significant value in the flavor and fragrance industry. Moreover, the mild aqueous reaction conditions and avoidance of toxic reagents mean that the process complies with the principles of green chemistry and sustainability. Scalability is also favorable as the fungus can be cultivated on inexpensive media (including agro-industrial residues) and easily preserved by lyophilization, enabling a robust supply of a biocatalyst. In summary, this innovative method distinguishes itself by combining high yields and selectivity (no overoxidation) with milder, greener conditions and a straightforward, scalable setup. These advances underscore the novelty and applicability of using *B. adusta* lyophilisates for the synthesis of flavor aldehydes, offering a sustainable alternative to both traditional chemical oxidation and other biocatalytic systems [16].

■ Conclusions

This sustainability-focused study incorporates renewable feedstocks and minimizing environmental impact in accordance with the principles of green chemistry. The results underscore the versatility and scalability of the protocol, highlighting its potential for applications in the fragrance and flavor production. An optimized biocatalytic oxidation protocol was developed using 2-propanol (10% *v*/*v*) as a "green" co-solvent, with the reaction efficiency strongly dependent on the substrate concentration (10 mM optimal) and the stirring intensity (>500 rpm). The method was applied to a variety of alcohols serving as

precursors to valuable flavor aldehydes. It still provides high isolated yields and clean product mixtures without overoxidation. High yields were obtained for benzaldehyde (*88%*), piperonal (*92%*), methoxybenzaldehydes (*96%*), cinnamaldehyde (*95%*), cuminaldehyde (*92%*), and citral (*96%*). The results highlight the broad applicability of the protocol and its potential for the preparative-scale and industrial upscaling.

■ Experimental part

This section contains protocols for preparing the compounds described in the paper. All starting compounds were obtained from commercial sources and used without additional purification. All solvents were purified according to the standard procedures. Experimental data comply with the referenced samples. ^{1}H NMR and ^{13}C NMR spectra were recorded at 298 K on a Bruker Avance II 400 MHz WB instrument (Billerica, Massachusetts, USA) at 400 MHz for ^{1}H nuclei and 100 MHz for ^{13}C nuclei. The NMR chemical shifts are referenced using the solvent signals at 7.26 and 77.1 ppm for ^{1}H and ^{13}C nuclei, respectively, in $CDCl_3$.

Lyophilisates

Lyophilisates from submerged cultures of *Bjerkandera adusta* fungus were produced following the procedure described in [14].

The general procedure for biotransformation

The *B. adusta* lyophilisate (4.5 g) was rehydrated in 270 mL of the potassium phosphate buffer (100 mM, pH 7) while stirring at 800 rpm and 24 °C for 20 min. The corresponding alcohol dissolved in 30 mL 2-propanol was added to the final concentration of 10 mM. The reaction mixture was stirred at 24 °C and 800 rpm for 8 h. Subsequently, sodium chloride (7 g) was added, and the mixing continued for 10 min. The mixture was extracted with diethyl ether (3 × 60 mL), the suspension was centrifuged, and the combined organic phases were dried over Na_2SO_4. After evaporation of the organic phase to dryness, the products were purified by column chromatography on silica gel using a gradually changing pentane/diethyl ether eluent (10:1 → 7:3 → 1:1). The identity of the products was confirmed by comparing their ^{1}H and ^{13}C NMR spectra with those of an authentic reference compound.

Benzaldehyde (1)

A colorless liquid. Yield – 279 mg (88%). ^{1}H NMR (400 MHz, $CDCl_3$), δ, ppm: 10.02 (1H, s), 7.87 (2H, m), 7.64 (1H, m), 7.56 (2H, m). ^{13}C NMR (100 MHz, $CDCl_3$), δ, ppm: 192.6, 136.4, 134.6, 129.9, 129.1.

Piperonal (2)

A colorless solid. Yield – 414 mg (92%). ^{1}H NMR (400 MHz, $CDCl_3$), δ, ppm: 9.79 (1H, s), 7.37 (1H, dd, J = 7.9, 1.8 Hz), 7.28 (1H, d, J = 1.8 Hz), 6.89 (1H, d, J = 7.8 Hz), 6.05 (2H, s). ^{13}C NMR (100 MHz, $CDCl_3$), δ, ppm: 190.31, 153.14, 148.81, 131.92, 128.54, 108.40, 107.18, 102.32.

3-Methoxybenzaldehyde (3)

A colorless liquid. Yield – 380 mg (93%). ^{1}H NMR (400 MHz, $CDCl_3$), δ, ppm: 9.93 (1H, s), 7.46–7.39 (2H, m), 7.36–7.33 (1H, m), 7.16–7.10 (1H, m), 3.83 (3H, s). ^{13}C NMR (100 MHz, $CDCl_3$), δ, ppm: 192.11, 160.09, 137.61, 129.95, 123.65, 121.60, 112.07, 55.52.

4-Methoxybenzaldehyde (4)

A colorless liquid. Yield – 405 mg (99%). ^{1}H NMR (400 MHz, $CDCl_3$), δ, ppm: 9.89 (1H, s), 7.84 (2H, d, J = 8.8 Hz), 7.01 (2H, d, J = 8.7 Hz), 3.89 (3H, s). ^{13}C NMR (100 MHz, $CDCl_3$), δ, ppm: 191.10, 164.71, 132.05, 130.00, 114.25, 55.72.

Cinnamic aldehyde (5)

A pale-yellow liquid. Yield – 377 mg (95%). ^{1}H NMR (400 MHz, $CDCl_3$), ppm: 9.68 (1H, d, J = 8.0 Hz), 7.63–7.54 (2H, m), 7.51–7.42 (4H, m), 6.73 (1H, dd, J = 16.0, 8.0 Hz,). ^{13}C NMR (100 MHz, $CDCl_3$), δ, ppm: 193.78, 152.90, 134.07, 131.33, 129.14, 128.67, 128.53.

Cuminic aldehyde (6)

A pale-yellow liquid. Yield – 409 mg (92%). ^{1}H NMR (400 MHz, $CDCl_3$), δ, ppm: 10.00 (1H, s), 7.82 (2H, d, J = 8.0 Hz), 7.39 (2H, d, J = 8.0 Hz), 3.03–2.96 (1H, m), 1.29 (6H, s, J = 7.9 Hz). ^{13}C NMR (100 MHz, $CDCl_3$), δ, ppm: 192.05, 156.25, 134.56, 130.02, 127.15, 34.49, 23.64.

Citral (7)

A pale-yellow liquid. Yield – 444 mg (96%). ^{1}H NMR (400 MHz, $CDCl_3$), δ, ppm: 9.96-9.87 (1H, m), 5.85 (1H, m), 5.06 (1H, m), 2.56 (1H, t, J = 7.5 Hz), 2.21 (3H, m), 2.14 (d, J = 1.4 Hz, 2H), 1.96 (1H, d, J = 1.4 Hz), 1.66 (3H, s), 1.57 (3H, d, J = 6.5 Hz). ^{13}C NMR (100 MHz, $CDCl_3$), δ, ppm: 191.22, 190.68, 163.77, 133.61, 132.83, 128.61, 127.38, 122.59, 122.28, 40.55, 32.57, 27.05, 25.71, 25.59, 25.03, 17.65, 17.53.

■ Acknowledgement

The authors are grateful to Professor Dr. Holger Zorn and Dr. Marco Fraatz for their helpful scientific advice.

ISSN 2308-8303 (Print) / 2518-1548 (Online)

References

1. Strazzolini, P.; Runcio, A. Oxidation of Benzylic Alcohols and Ethers to Carbonyl Derivatives by Nitric Acid in Dichloromethane. *Eur. J. Org. Chem.* **2003**, *2003* (3), 526–536. https://doi.org/10.1002/ejoc.200390090.
2. Gunchenko, P. A.; Li, J.; Liu, B.; Chen, H.; Pashenko, A. E.; Bakhonsky, V. V.; Zhuk, T. S.; Fokin, A. A. Aerobic Oxidations with N-Hydroxyphthalimide in Trifluoroacetic Acid. *Mol. Catal.* **2018**, *447*, 72–79. https://doi.org/10.1016/j.mcat.2017.12.017.
3. Besson, M.; Gallezot, P. Selective Oxidation of Alcohols and Aldehydes on Metal Catalysts. *Catal. Today* **2000**, *57* (1-2), 127–141. https://doi.org/10.1016/S0920-5861(99)00315-6.
4. Biella, S.; Rossi, M. Gas Phase Oxidation of Alcohols to Aldehydes or Ketones Catalysed by Supported Gold. *Chem. Commun.* **2003**, 3, 378–379. https://doi.org/10.1039/b210506c.
5. Minisci, F.; Punta, C.; Recupero, F.; Fontana, F.; Pedulli, G. F. A New, Highly Selective Synthesis of Aromatic Aldehydes by Aerobic Free-Radical Oxidation of Benzylic Alcohols, Catalysed by n-Hydroxyphthalimide under Mild Conditions. Polar and Enthalpic Effects. *Chem. Commun.* **2002**, 7, 688–689. https://doi.org/10.1039/b110451a.
6. Miao, C.-X.; Wang, J.-Q.; Yu, B.; Cheng, W.-G.; Sun, J.; Chanfreau, S.; He, L.-N.; Zhang, S.-J. Synthesis of Bimagnetic Ionic Liquid and Application for Selective Aerobic Oxidation of Aromatic Alcohols under Mild Conditions. *Chem. Commun.* **2011**, *47* (9), 2697. https://doi.org/10.1039/c0cc04644b.
7. Ding, J.; Xu, W.; Wan, H.; Yuan, D.; Chen, C.; Wang, L.; Guan, G.; Dai, W.-L. Nitrogen Vacancy Engineered Graphitic C3N4-Based Polymers for Photocatalytic Oxidation of Aromatic Alcohols to Aldehydes. *Appl. Catal., B* **2018**, *221*, 626–634. https://doi.org/10.1016/j.apcatb.2017.09.048.
8. Xu, C.; Yang, F.; Deng, B.; Zhuang, Y.; Li, D.; Liu, B.; Yang, W.; Li, Y. Ti_3C_2/TiO_2 Nanowires with Excellent Photocatalytic Performance for Selective Oxidation of Aromatic Alcohols to Aldehydes. *J. Catal.* **2020**, *383*, 1–12. https://doi.org/10.1016/j.jcat.2020.01.001.
9. Dai, Y.; Ren, P.; Li, Y.; Lv, D.; Shen, Y.; Li, Y.; Niemantsverdriet, H.; Besenbacher, F.; Xiang, H.; Hao, W.; Lock, N.; Wen, X.; Lewis, J. P.; Su, R. Solid Base $Bi_{24}O_{31}Br_{10}(OH)_\delta$ with Active Lattice Oxygen for the Efficient Photo-Oxidation of Primary Alcohols to Aldehydes. *Angew. Chem. Int. Ed.* **2019**, *58* (19), 6265–6270. https://doi.org/10.1002/anie.201900773.
10. Schober, L.; Dobiašová, H.; Jurkaš, V.; Parmeggiani, F.; Rudroff, F.; Winkler, M. Enzymatic Reactions towards Aldehydes: An Overview. *Flavour & Fragrance J.* **2023**, *38* (4), 221–242. https://doi.org/10.1002/ffj.3739.
11. Kazimírová, V.; Rebroš, M. Production of Aldehydes by Biocatalysis. *Int. J. Mol. Sci.* **2021**, *22* (9), 4949. https://doi.org/10.3390/ijms22094949.
12. Tufvesson, P.; Lima-Ramos, J.; Nordblad, M.; Woodley, J. M. Guidelines and Cost Analysis for Catalyst Production in Biocatalytic Processes. *Org. Process Res. Dev.* **2011**, *15* (1), 266–274. https://doi.org/10.1021/op1002165.
13. Babkina, V. V.; Albuquerque, W.; Haiduk, Y. M.; Michalak, W.; Ghezellou, P.; Zorn, H.; Zhuk, T. S. Fungal Lyophilisates as Catalysts for Organic Synthesis: Preparative Oxidations with the White-Rot Fungus *Bjerkandera adusta*. *Mol. Catal.* **2023**, *549*, 113451. https://doi.org/10.1016/j.mcat.2023.113451.
14. Calza, L.; Nikitenkova, V.; Albuquerque, W.; Zorn, H.; Zhuk, T. Selective Oxidation of α,β-Unsaturated Alcohols With Lyophilisates of *Bjerkandera adusta*. *Chem. Biodiversity* **2025**, *22* (12), e01127. https://doi.org/10.1002/cbdv.202501127.
15. Paoli, M.; Maroselli, T.; Casanova, J.; Bighelli, A. A Fast and Reliable Method to Quantify Neral and Geranial (Citral) in Essential Oils Using ^{1}H NMR Spectroscopy. *Flavour & Fragrance J.* **2023**, *38* (6), 476–482. https://doi.org/10.1002/ffj.3760.
16. Qiao, Y.; Wang, C.; Zeng, Y.; Wang, T.; Qiao, J.; Lu, C.; Wang, Z.; Ying, X. Efficient Whole-Cell Oxidation of α,β-Unsaturated Alcohols to α,β-Unsaturated Aldehydes through the Cascade Biocatalysis of Alcohol Dehydrogenase, NADPH Oxidase and Hemoglobin. *Microb. Cell Fact.* **2021**, *20* (1), 17. https://doi.org/10.1186/s12934-021-01511-8.
17. Xu, S.; Wu, J.; Huang, P.; Lao, C.; Lai, H.; Wang, Y.; Wang, Z.; Zhong, G.; Fu, X.; Peng, F. Selective Catalytic Oxidation of Benzyl Alcohol to Benzaldehyde by Nitrates. *Front. Chem.* **2020**, *8*, 151. https://doi.org/10.3389/fchem.2020.00151.
18. Marino, I.; Pignataro, E.; Danzi, D.; Cellini, F.; Cardellicchio, C.; Biundo, A.; Pisano, I.; Capozzi, M. A. M. A Comparative Screening of Laccase-Mediator Systems by White-Rot Fungi Laccases for Biocatalytic Benzyl Alcohol Oxidation. *Sci. Rep.* **2022**, *12* (1), 21602. https://doi.org/10.1038/s41598-022-24839-6.
19. Lapadatescu, C.; Feron, G.; Vergoignan, C.; Djian, A.; Durand, A.; Bonnarme, P. Influence of Cell Immobilization on the Production of Benzaldehyde and Benzyl Alcohol by the White-Rot Fungi *Bjerkandera adusta*, Ischnoderma Benzoinum and Dichomitus Squalens. *Appl. Microbiol. Biotechnol.* **1997**, *47* (6), 708–714. https://doi.org/10.1007/s002530050999.
20. Lomascolo, A.; Lesage-Meessen, L.; Labat, M.; Navarro, D.; Delattre, M.; Asther, M. Enhanced Benzaldehyde Formation by a Monokaryotic Strain of *Pycnoporus cinnabarinus* Using a Selective Solid Adsorbent in the Culture Medium. *Can. J. Microbiol.* **1999**, *45* (8), 653–657. https://doi.org/10.1139/w99-056.
21. Lomascolo, A.; Asther, M.; Navarro, D.; Antona, C.; Delattre, M.; Lesage-Meessen, L. Shifting the Biotransformation Pathways of L-Phenylalanine into Benzaldehyde by *Trametes suaveolens* CBS 334.85 Using HP20 Resin. *Lett. Appl. Microbiol.* **2001**, *32* (4), 262–267. https://doi.org/10.1046/j.1472-765X.2001.0873a.x.
22. Sandes, R. D. D.; Dos Santos, R. A. R.; De Jesus, M. S.; Araujo, H. C. S.; Leite Neta, M. T. S.; Rajkumar, G.; Narain, N. Agro-Industrial Residues Used as Substrates for the Production of Bioaroma Compounds with Basidiomycetes: A Comprehensive Review. *Fermentation* **2023**, *10* (1), 23. https://doi.org/10.3390/fermentation10010023.

Information about the authors:

Vladislav Shah, M.Sci. in Chemistry, Faculty of Chemical Technology, National Technical University of Ukraine "Igor Sikorsky Kyiv Polytechnic Institute", Ukraine.

Valeriia Nikitenkova, M.Sci. in Chemistry; PhD student of the Institute of Food Chemistry and Food Biotechnology, Justus Liebig University Giessen, Germany, https://orcid.org/0000-0002-8229-457X.

Yuliia Kurtash, M.Sci. in Chemistry, Faculty of Chemical Technology, National Technical University of Ukraine "Igor Sikorsky Kyiv Polytechnic Institute", Ukraine.

Tetiana Krupodorova, Dr.Sci. in Biotechnology, Leading Researcher of the Department of Plant Food Products and Biofortification, Institute of Food Biotechnology and Genomics of the National Academy of Sciences of Ukraine, https://orcid.org/0000-0002-4665-9893.

Tetiana Zhuk (*corresponding author*), Ph.D. in Chemistry, Associate Professor of the Department of Physical Chemistry, Faculty of Chemical Technology, National Technical University of Ukraine "Igor Sikorsky Kyiv Polytechnic Institute", Ukraine; Alexander von Humboldt Fellow of the Institute of Food Chemistry and Food Biotechnology, Justus Liebig University Giessen, Germany, https://orcid.org/0000-0001-5184-704X; e-mail for correspondence: t.zhuk@xtf.kpi.ua.

CONTENTS / ЗМІСТ

ISSN 2308-8303 (Print) / 2518-1548 (Online)